HYPERSPECTRAL ENDOSCOPY IMAGING: SYSTEM DEVELOPMENT, CLINICAL EVALUATION, AND FURTHER APPLICATION

A Thesis
Presented to
The Academic Faculty

by

Zhimin Han

In Partial Fulfillment
of the Requirements for the Degree
Doctor of Philosophy in the
Department of Biomedical Engineering

Georgia Institute of Technology
May 2016

HYPERSPECTRAL ENDOSCOPY IMAGING: SYSTEM DEVELOPMENT, CLINICAL EVALUATION, AND FURTHER APPLICATION

Approved by:

Professor Shuxiang Dong,
Committee Chair
Department of Materials Science and Engineering
Peking University

Professor Peng Xi
Department of Biomedical Engineering
Peking University

Professor Tianyu Xie, Advisor
Department of Biomedical Engineering
Peking University

Professor Changhui Li
Department of Biomedical Engineering
Peking University

Professor May D. Wang
Department of Biomedical Engineering
Georgia Institute of Technology and Emory University

Date Approved: 10 December 2015

To my parents,

I have the greatest parents in the world. They have always put their child's interests ahead of their own, and have given me more love than I could have asked for, or deserved. My parents have always been my biggest support all along the way to accomplish my PhD career, and got my back for every major decision I made. I love my parents, and will love them more in future.

ACKNOWLEDGEMENTS

I would like to thank my advisor at PKU, Prof. Tianyu Xie, for leading directions during my PhD career. I learned so much from him on how to be a contributive engineer, and at the same time, how to be a responsible man.

I would like to thank my co-advisor at GT, Dr. May D. Wang, for her kindly guidance and help. I learned from her on how to make effective communication. Those experiences studying at US are the most valuable and cherished memory for me.

I wish to thank all my colleagues and friends: Xiguang Wang, Shenghou Ma, Mingda Chen, Zongzhou Li, Aoyu Zhang, Qingxiao Chen, Zongxiao Sun, Ye Fu, Yishu Hu, Wanchen Sun, Lianwang Dong, at PKU; and John Phan, Leo Wu, James Cheng, Chanchala Kaddi, Janani Venugopalan, Aiswaria Nair, Ryan Hoffman, Cheng Yang, Li Tong, Hang Wu, at GT, for their kindly help and encouragement. We spent days and nights together, we shared joys and frustrations. They made it easier for me to fit in new environments. And we are and will always be a family.

Last but not least, I also want to thank the cooperation institutions: Shanghai Zhongshan Hospital, 3rd Hospital of Peking University, Haidian Hospital, and Aohua Co. Ltd, for their support and help regarding this thesis.

TABLE OF CONTENTS

LIST OF TABLES

LIST OF FIGURES

SUMMARY

HSI originated from remote sensing field combines spectral measurement of a pixel with 2-D imaging technology. It is capable to provide a series of images containing both spectral and spatial information, and has been widely used in medical domain for diagnosis and surgery guidance. However, most researches on medical HS imaging are focused on ex-vivo biopsy or skin and oral mucosa. The study on HS imaging regarding in-vivo disease lags far behind. Especially, cancers on esophagus, stomach, and colon lead to many deaths. In-vivo HS imaging applied on digestive diseases provides opportunities for early-detection and early-therapy, which could increase survival rate significantly. In this thesis, we did some research on in-vivo HS imaging regarding GI tract diseases.

In this thesis, we developed a novel flexible HS endoscope system. It is capable to acquire a series of HS images in vivo in a non-contact way among the wavelength range of 405 - 665 nm. Twenty-eight sequential narrow-band interference filters are mounted in two motorized filter wheels positioned in the optical path of light source, and generates narrow-band illumination. The filter wheels are driven by Geneva Mechanism, and this dispersive device is the major innovative part for this system, with two authorized patents. At the same time, many printed circuit boards, hardware programs, and software programs were designed to drive the motors and process the acquired HS images. After a lot of time-consuming modifying and debugging work, this new system has high stability and convenience to be applied in clinic now.

We evaluated this system in clinic. First, we got ethics approval for clinical trials. Then, we obtained HS images regarding GI diseases inside patients using this system. As far as we know, there is no such in-vivo image data reported in previous literatures.

Thus based on these HS images, we built a database for GI mucosa, including both normal tissues and disease tissues on different organs. Next, we analyzed some typical HS images tentatively. The method of Contrast Calculation, Dependence of Information, and Recursive Divergence are implemented to extract valuable and diagnostic information from HS images. All these results prove the effect and applicability of this new HS endoscope system, and show its great potential to be used as a platform and guidance for further medical studies.

To further apply these analysis results, we proposed a novel endoscopy imaging technique that could enhance the display of valuable information on images. This technique is named as Adaptive Narrow-Band Imaging (ANBI) based on band selection of HS images of a specific type of disease. It is expected that it has higher accuracy, sensitivity, and specificity compared to conventional Narrow-Band Imaging (NBI).

In this thesis, we also discussed the future directions of the new system. There is still a lot of work to be done so that HS endoscopy could help more in clinical disease diagnosis, or even endoscopy therapy. Especially, to improve light intensity and signal-noise-ratio of HS images in wide-field view, we proposed a new imaging method using broad- and overlapped-band filters. Although this method only performs greatly on the foundation of accurate image registration, we hope to apply it in our system in the future.

In conclusion, we succeeded in combining HS imaging technique with flexible endoscope, and did some researches on in-vivo HS imaging regarding digestive tract diseases. These researches enlarge the application of HS imaging in medical domain, and provide a platform for further clinical studies.

CHAPTER I

INTRODUCTION

Section 1.1 describes briefly concepts and background knowledge relating to this thesis. It is aimed primarily at readers who are not familiar with the field that my

It is also intended to serve as a navigational aid for the rest of the thesis.

1.1 Background

In practical clinical terms, "diagnosis" is recognizing the cause and knowing the cure of a disease, with or without interfering with the patients. In reality, a number of diagnostic tools have been applied, from excisional biopsy (invasive) to venopuncture (minimal-invasive) to medical imaging (non-invasive). In general, "the less invasive a diagnostic procedure the less damage and discomfort it will cause"[41]. However, every diagnostic tool or method has its own limitations. For example, radiologic imaging that has the ability to exactly outline the anatomical margins of a lesion is non-specific and could not give the exact diagnosis. Up until now, histopathological examination is the gold standard of making diagnosis. Even for histopathological examination, there are severe concerns on intra- and inter-observer variability, and generally a tissue biopsy always has to be taken in order to definitely pinpoint the diagnosis[38, 71]. Thus development of diagnosis tools and methods is necessary.

Gastrointestinal (GI) tract is a well studied anatomical area with a wide variety of diseases. Stomach and colon ulcers are common, and GI cancers are among the diseases with high death rate. Barrett's Esophagus (BE) has strong association with esophageal cancer, while gastric cancer is the second most frequent cause of cancer-related death worldwide[68]. And colorectal cancer is the third leading cause[123].

Moreover, "more than 59,000 patients in United States manifest hepatic metastases from digestive tract cancers each year"[34, 67]. Early detection offers opportunity to perform early-stage therapies, and could increase survival significantly[67, 80].

Endoscope systems are widely being applied in clinical practical examination and therapy of GI and bronchial diseases. Surveillance endoscopy is convenient and less invasive being used to detect early-stage GI diseases. Compared to fiber endoscopes, video endoscopes could show an electrically captured and enhanced image and provide it to doctors for diagnosis and storage. They are with higher image resolution, higher light intensity, and better stability. Their application as indispensable devices for diagnosis and treatment has been spreading fast[49]. Nevertheless, standard white light endoscopy combining with random biopsies may miss some lesion regions[23].

To detect and monitor early progression of various diseases, spectral measurement and analysis providing accurate quantification of mucosa micro-vascular and morphological properties are helpful. However, as point spectroscopy detects light from a single point, it does not account for tissue spatial heterogeneity, which makes it ineffective for mapping a lesion area. Spectral imaging, on the other hand, could provide spatial mapping of tissue morphology and physiology, and account for tissue spatial heterogeneity. It involves the acquisition and analysis of series of reflected 2D images sampled at different wavelengths[108].

1.1.1 Tissue Optics for Spectral Endoscopy

The transmission of light within tissue is important for the development of diagnostic methods. This section gives a brief description on the mechanisms of light and tissue interaction , optical processes involved in hyperspectral imaging, and some helpful diagnostic information that can be provided by spectral endoscopy.

Photons delivered to biological tissue undergoes multiple scattering as it propagates within the tissue[109]. As biological tissues are heterogeneous in composition

with spatial variations in optical properties, scattering occurs everywhere, especially where there is a spatial variation in the refractive index such as nuclear crowding or the increased nuclear/cytoplasmic ratio as diseases progress[99]. In cellular media, subcellular organelles with their size running from 100 nm to 6 um are important scatters, together with cells whose shape and size vary among different types of tissue with diameters of a few microns and larger[87, 99].

Within mucosal tissues, the penetration depth of light depends on wavelength (scattering) and how strongly the tissue absorbs light[87]. The interaction of photons with cellular structures results in elastic scattering. "Scattering is a process of photon absorption and re-emission without loss of energy but possibly associated with a change in photon direction. For biological structures, the re-emission has a high probability to be in the forward direction for each scattering event. Despite this, the accumulation of multiple scattering events results in a gradual randomization of the propagation direction"[104]. The mean free path (MFP) for photons propagating within tissue is defined as $\frac{1}{\mu_t}$, where μ_t is the transport coefficient. This coefficient typically is expressed as a sum of the tissue's absorption coefficient μ_a and the tissue's scattering coefficient μ_s, that is, $\mu_t = \mu_a + \mu_s$[104]. Traditionally, we believe the maximum penetration depth in mucosa tissue positively correlated to MFP.

Most mucosal tissues are so sufficiently weak absorbers ($\mu_s \gg \mu_a$) that they permit significant light penetration among visible (VIS) and near-infrared (IR) regions[99]. Within these regions, scattering may be largely over absorption, so the wavelength defines the penetration depth. For a typical person, the optical penetration depth in digestive tract mucosa is 3.57 mm at 850 nm, 0.24 $\sim$ 0.48 mm at 550 nm, and 0.17 mm at 415 nm[87, 107].

Under some other cases, for example, for vessels and capillaries in superficial mucosa layer, absorption is significantly over scattering[105]. Tissue absorption is related to molecular composition[87]. When photons' energy fits an interval between

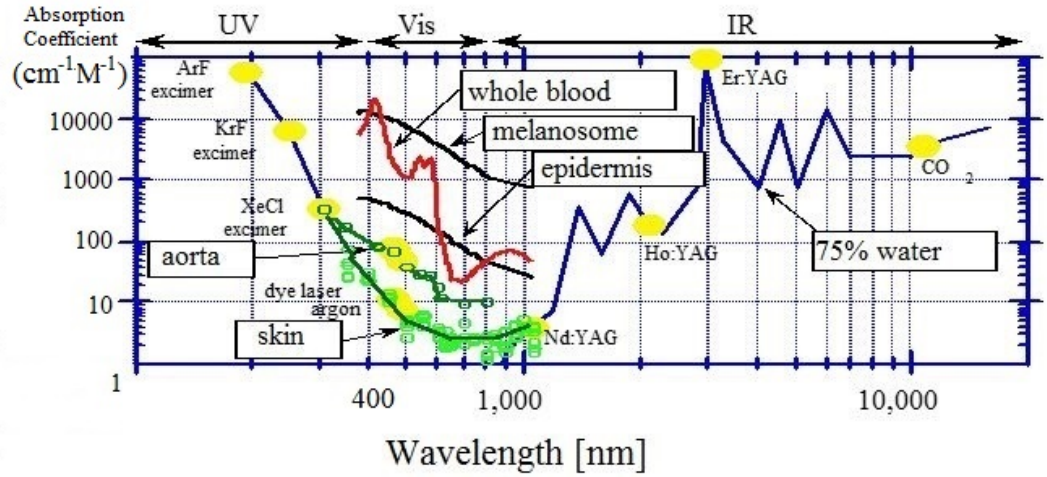

Figure 1: Absorption coefficients of some typical chromophores for human body

internal energy states, molecules absorb these photons, and the transition between quantum states obeys the selection rules for the species[87]. Thus these transitions that are well defined at specific wavelength could serve as a spectral fingerprint of the molecule for diagnostic purposes[99, 157]. These tissue components that absorb light are called chromophores. Protein and amino acids are the primary absorbers for ultraviolet (UV) and Near-IR wavelengths, while water is an important chromophore for mid-IR wavelengths[87, 148]. Procedural digestive endoscopes usually work in visible region, and Hemoglobin in blood is among the most important chromophores in visible wavelength region for GI tract disease imaging. Figure 1 shows absorption coefficients of some common chromophores.

Incident light may be directly reflected on the surface of the mucosa tissue or be scattered due to random spatial variations in tissue density and then be remitted to the tissue surface[118]. The measured reflectance signal contains information from a variety of depths within the mucosa and is, therefore, an average measurement of the properties over a certain volume of tissue[9]. These reflectance data helps us model and interpret the scattering and absorption inside mucosa layer. Thus the reflectance signal measured from epithelial tissue is determined by the structural and biochemical properties of the mucosa, and changes in optical properties can be used

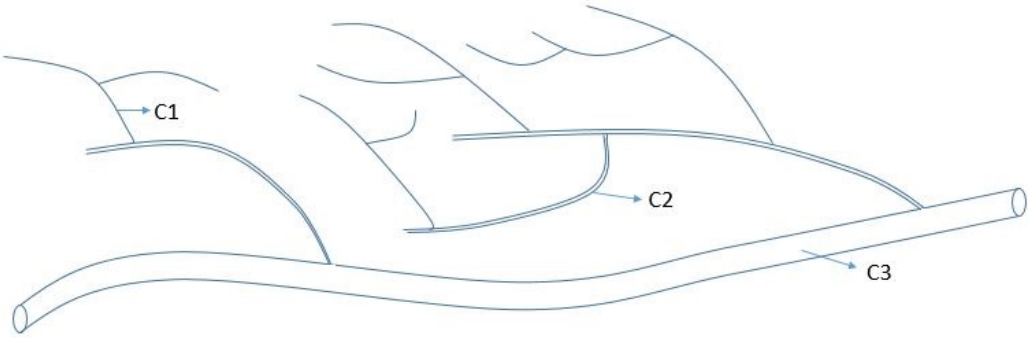

Figure 2: Structure of blood vessels in mucosa. C1 indicates the fine capillaries in the superficial mucosa. C2 indicates the thick capillaries in deeper regions. C3 indicates thick veins in regions deeper than C1 and C2

to non-invasively probe the tissue's micro-environment[9].

For instance, oxy- and deoxy-hemoglobin absorption spectra can characterize the oxygen saturation and concentration. This reveals two hallmarks of cancer on mucosa surface layer: angiogenesis and hypermetabolism[147]. Figure 2 shows the schema of vascular patterns of blood vessels[105]. A dense capillary bed is typically found in superficial layers of the mucosa, and thicker blood vessels run in deeper layers. These vascular patterns are classified into three classes by thickness and depth in the mucosa. The capillaries found in the superficial mucosa are classified as class 1 (C1 pattern). The thicker vasculature in deeper layers is classified as class 2 (C2 pattern), while thick veins are classified as class 3 (C3 pattern). The thickness of C1, C2 and C3 patterns are about 10 to 20, 20 to 50, and 200 to 500 um, respectively. The difference in blood vessel depth may enhance the contrast and distinguishability of the image, and display the angiogenesis and hypermetabolism better. Figure 3 shows the absorption and scattering coefficients of vessels, together with the penetration depth of light at each wavelength and the corresponding spectral images on vessels. Figure 4[89] shows the contrast enhancement effect of narrowband imaging (NBI) on a colon adenocarcinoma . We can see that C1 pattern can be distinguished significantly from C2 and C3 pattern.

Moreover, light absorbed by tissue constituents, typically in the UV or VIS region,

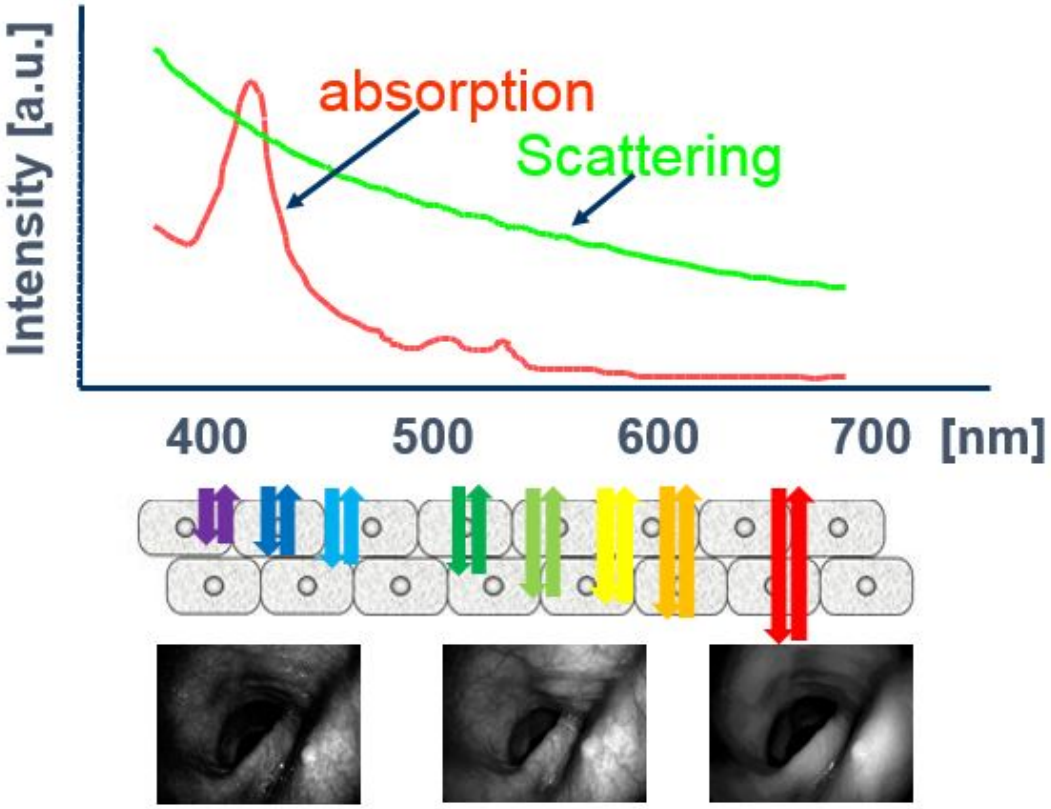

Figure 3: Absorption and scattering coefficients of vessels together with the penetration depth of light at each wavelength and the corresponding spectral images on vessels

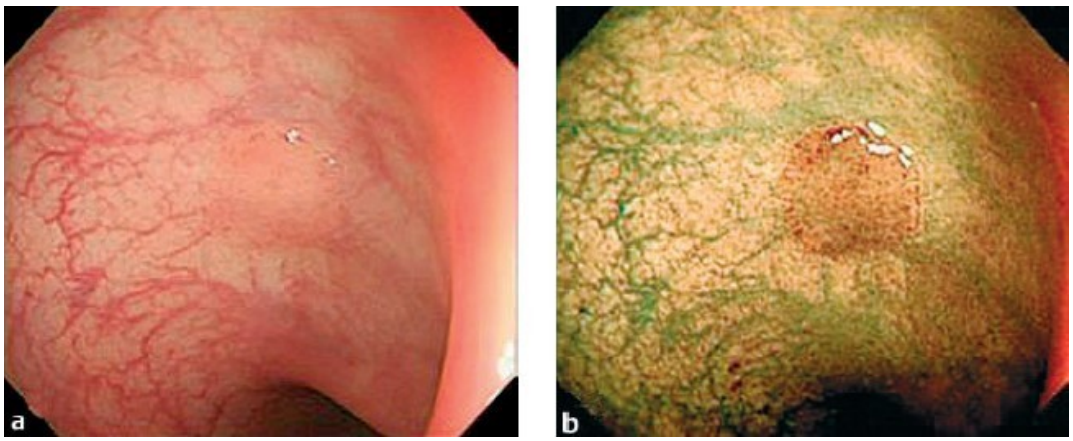

Figure 4: comparison of conventional endoscopic imaging and NBI. (a). Conventional view of a 0-IIa lesion, 7 mm in diameter, in the normal sigmoid colon. Faint redness, in an oval shape. It is difficult to identify the lesion. (b). NBI colonoscopy findings: the lesion was brownish in color. The contrast and visualization of lesions against mucosa around it was better. This picture is cited from literature[89]

may be either converted to heat or radiated in the form of luminescence, including fluorescence and phosphorescence[99, 118, 139]. The majority of the fluorophores are associated with various cellular metabolic pathways or with the structural matrix of tissue[37, 99]. The most common endogenous fluorophores in the structural matrix are collagen and elastin, while the predominant fluorophores involved in cellular metabolism are the nicotinamide adenine dinucleotide (NADH), lipopigments, and flavin adenine dinucleotide (FAD)[138]. There are also many types of exogenous tumor-specific fluorescence imaging agents[111]. Cells in different disease stages often have different structures or undergo different rates of metabolism and result in different fluorescence emission spectra. Therefore, fluorescence imaging makes it possible to investigate tissues for disease diagnosis[99, 138, 139]. Hyperspectral (HS) endoscopy systems can be applied to extract this kind of fluorescence information on mucosa of digestive tract.

1.1.2 Anatomy of GI Mechanisms

The vascular patterns and mucosa structure of GI mucosa on different organs are similar with each other[88]. Figure 5 shows the anatomic and histologic properties of esophageal wall[54]. Basically, there are epithelium layer, mucosa layer, submucosal layer, and propria layer. At the same time, there are some differences within each layer, for instance, the difference between squamous and columnar cells on esophagus and stomach epithelium layer , or the serosa of small intestine.

Most of cancers on surface of GI tract begin from epithelium of the mucosa layer thus mucosa layer is the focus of our attention when making early-stage cancer detection throughout digestive tract[89]. Figure 6 shows the development of esophageal cancer and its 5year survival rate at each stage[54]. We can find that early-stage detection and therapy offer great opportunity to increase survival[67]. The anatomic layer of colon mucosa and staging evaluation of colon cancer show similarity with that

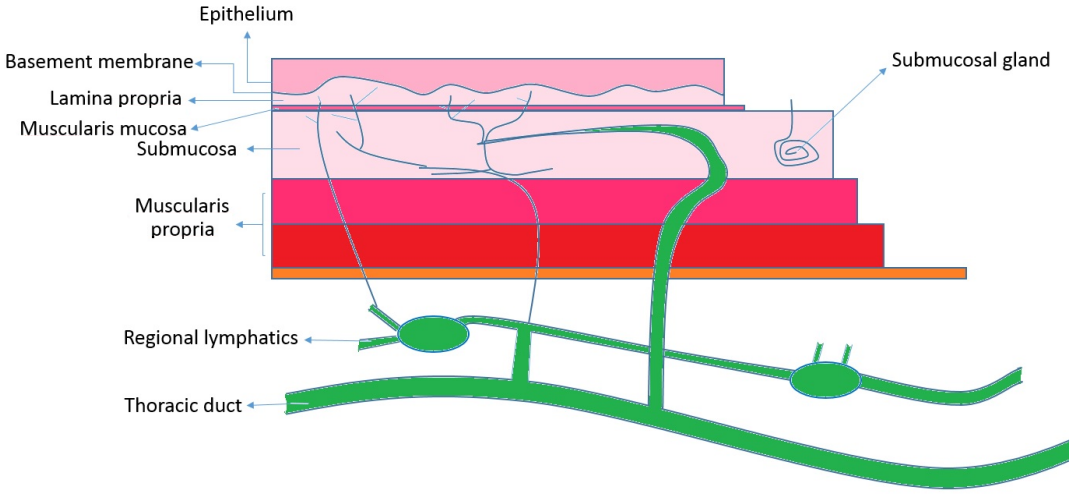

Figure 5: Anatomic and histologic properties of esophagus

of esophageal cancer.

American Joint Commission on Cancer (AJCC) gives a staging criterion with name of tumor-node-metastasis (**TNM**) classification[45]. Table 1 and Table 2 give the details on it.

1.1.3 Digestive Endoscopy

Endoscopy is necessary for patients with digestive tract diseases. In this part, we describe the pipeline tailored to make spectral endoscopy imaging. In previous literatures, a model of the spectral reflection estimation for paint has been proposed which could also be used in spectral endoscopy modeling[10]. Figure 7 shows the diagram of spectral endoscopy system. It consists of five units: light source unit (including illumination part, lens, and spectral filters), optical fibers, high quality charged-couple-device (CCD) camera sensor, image processing part, and monitor. Light source unit contains a lamp, which has an integrated parabolic reflector collecting light from the light bulb and producing a collimated output beam. Filters are positioned in the path of the collimated beam. In conventional white light illumination mode, RGB color filters are switched in the illumination beam path. An optical fiber bundle directs the beams to the object inside body after the optical taper focuses the light onto the

Table 1: AJCC definitions for tumor-node-metastasis (**TNM**) classification

<table>
<tr><th colspan="5">**TNM** Definitions</th></tr>
<tr><td>Primary Tumor(T)</td><td>Regional Lymph Nodes(N)</td><td colspan="3">Distant Metastasis(M)</td></tr>
<tr><td>**TX**: Primary tumor cannot be assessed</td><td>**NX**: Regional lymph nodes cannot be assessed</td><td colspan="3">**MX**: Distant metastasis cannot be assessed</td></tr>
<tr><td>**T0**: No evidence of primary tumor</td><td>**N0**: No regional lymph node metastasis</td><td colspan="3">**M0**: No distant metastasis</td></tr>
<tr><td>**Tis**: Carcinoma in situ</td><td rowspan="5">**N1**: Regional lymph node metastasis **N1a**: One to three nodes involved **N1b**: Four to seven nodes involved **N1c**: More than seven nodes involved</td><td colspan="3">**M1**: Distant metastasis</td></tr>
<tr><td>**T1**: Tumor invades lamina propria (T1a) or submucosa (T1b)</td><td rowspan="4">Tumors of the lower thoracic esophagus: **M1a**: Metastases in celiac lymph nodes **M1b**: Other distant metastases</td><td rowspan="4">Tumors of the midthoracic esophagus: **M1a**: Not applicable **M1b**: Nonregional lymph nodes and/or other distant metastases</td><td rowspan="4">Tumors of the upper thoracic esophagus: **M1a**: Metastases in cervical nodes **M1b**: Other distant metastases</td></tr>
<tr><td>**T2**: Tumor invades muscularis propria</td></tr>
<tr><td>**T3**: Tumor invades adventitia</td></tr>
<tr><td>**T4**: Tumor invades adjacent structures</td></tr>
</table>

Table 2: AJCC Stage Grouping

<table>
<tr><td rowspan="2">Stage 0</td><td rowspan="2">Stage I</td><td colspan="2" rowspan="2">Stage II</td><td rowspan="2">Stage III</td><td colspan="2">Stage IV</td></tr>
<tr><td colspan="2">Any T, any N, M1</td></tr>
<tr><td rowspan="2">Tis, N0, M0</td><td rowspan="2">T1, N0, M0</td><td>Stage IIA</td><td>Stage IIB</td><td rowspan="2">(T3, N1, M0) or (T4, any N, M0)</td><td>Stage IVA</td><td>Stage IVB</td></tr>
<tr><td>T2 or T3, N0, M0</td><td>T1 or T2, N1, M0</td><td>Any T, any N, M1a</td><td>Any T, any N, M1b</td></tr>
</table>

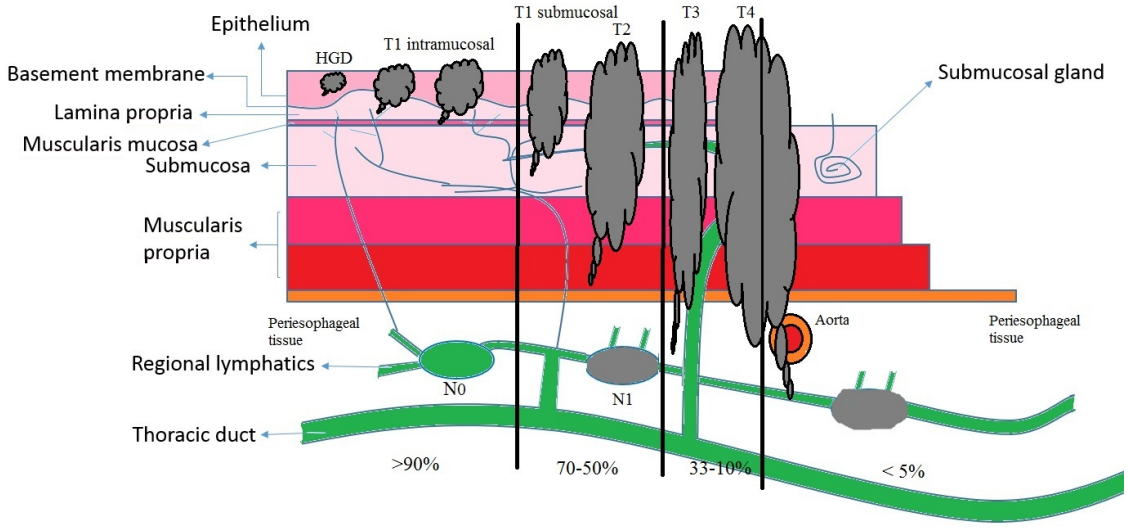

Figure 6: The staging evaluation of esophageal cancer and 5-year survival ratio at each stage

bundle. A combination of lenses is attached to the distal end of the fiber bundle to generate illumination. A monochromatic CCD positioned at the distal end of the optical fiber bundle is used to spectrally resolve the reflectance images from the mucosa. Analog signals read from the CCD are sequentially transformed into digital signals in the image processing unit. A cable is used to connect the image processing unit to the medical monitor, which is used to display the reflectance images from the mucosa. A lot of endoscopy systems in clinic apply color CCD without the RGB filters. This is a fixed-filter-mask imaging mode locating the filter in front of the CCD instead of in the illumination path. Figure 8 shows an endoscopy system that is applied in clinic.

The response ν at position (x, y) of the CCD sensor with the i^{th} spectral filter is expressed as Equation 1[50].

$$\nu_i(x,y) = \int t_i(\lambda)E(\lambda)S(\lambda)\gamma(x,y,\lambda)\,d\lambda + n_i(x,y), i = 1, ..., m \tag{1}$$

where $t_i(\lambda)$, $E(\lambda)$, $S(\lambda)$, and $\gamma(x, y, \lambda)$ are the spectral transmittance of the i^{th} spectral filter, the spectral radiance of the illuminance, the spectral sensitivity of the camera, and the spectral reflectance of an object, respectively. $n_i(x, y)$ denotes

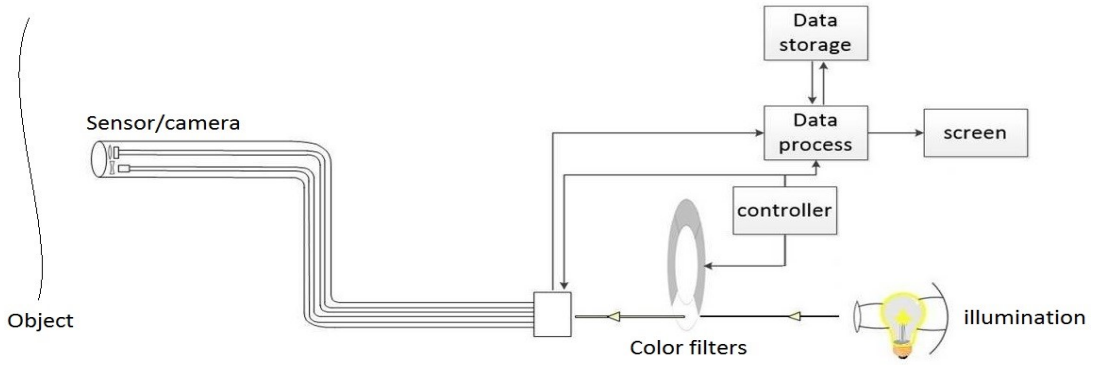

Figure 7: Diagram of spectral endoscopy systems

additive noise in the i^{th} channel image and m denotes the total number of channels. Given $E(\lambda)$, $S(\lambda)$, and $t_i(\lambda)$, $\gamma(x, y, \lambda)$ of the object can be evaluated through $\nu_i(x, y)$ through a lot of methods[135]. The working principle of HS imaging is regarding design of $t_i(\lambda)$.

1.1.4 Hyperspectral Imaging

Hyperspectral imaging (HSI), also called imaging spectrometer[149], offers a hybrid modality of optical diagnostics that obtains spectral information and renders the information in image form. In the field of earth observation, HS detector systems have been developed decades ago. They allow precise measurement of an object from remote sensing platforms such as satellites. This enables the object's electromagnetic properties to be identified without the physically travelling to the areas which need examination, same as the non-invasive diagnostic method in the medical field. Figure 9 shows an diagram of HSI image cube from AVIRIS database targeted at Terrain, with two spatial dimensions (x,y) and one spectral dimension (λ). The spectral information at each pixel on the image is also called "spectral signature"[87]. Based on these spectral signatures, researchers could make image classification, and distinguish targeted areas from surrounding regions.

Moreover, there are two main classes of spectral imaging techniques: multi- and

Figure 8: An endoscopy system applied in clinic

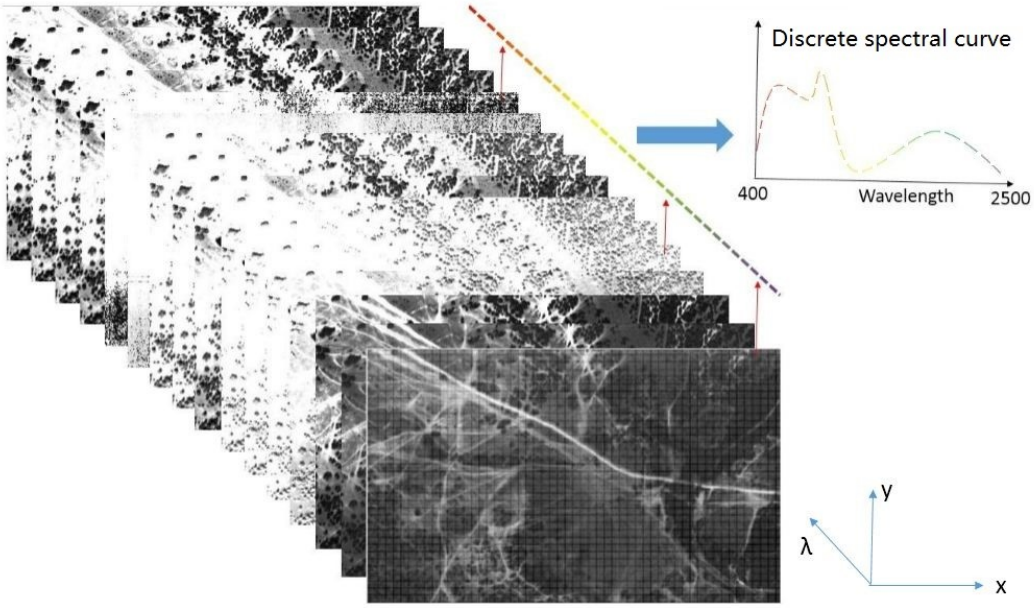

Figure 9: HSI image cube. There are three dimensions: two for spatial information (x,y), and one for spectral information (λ). The spectral curve at each pixel is spectral signature

hyper-spectral imaging (MSI/HSI). The most commonly used for in-vivo applications now is multi-spectral one, as it is easier to implement the technology with the use of 5 to 10 filters[65]. For MSI, $\frac{\delta\lambda}{\lambda} \sim 0.1$, in which λ is center wavelength, and $\delta\lambda$ indicates Full Width at Half Maximum (FWHM). It collects increased spectral information hoping to yield improved early cancer detection. Researchers now are also actively pursuing HSI devices which can provide 10 to 100 spectral channels per image pixel. For HSI, $\frac{\delta\lambda}{\lambda} \sim 0.01$. Hypercube with higher spectral and spatial resolution may potentially contain more diagnostic information while at the same time they make it difficult to perform manual or automatic analysis of HS data. In particular, it is complex in many aspects: (1) variability of HS signatures, (2) high data redundancy due to high correlation in the adjacent bands, (3) curse of dimensionality, and (4) object drift among in-vivo images[74]. Although HS image analysis methods have been intensively investigated in the remote sensing area, their development and application in medical domain, especially in digestive tract imaging

1.2 Research Overview

This research has goal of combining the HS imaging technology with flexible endoscopy, hoping to help make diagnosis for digestive tract diseases, especially early-stage ones. This thesis has several specific aims: 1) Develop a flexible HS endoscope system, and apply it in clinic; 2) Obtain HS images on mucosa diseases inside digestive tract using this system; 3) Analyze these HS images and prove that spectral imaging endoscopy has potential to help make diagnosis; 4) Propose novel algorithms further applying HS image analysis results in clinic.

This section aims to briefly describe the overview of my research design and is intended to serve as a navigational aid for the rest of the thesis.

First, literature survey relating to this thesis is introduced in Chapter 2. In the beginning section, HSI in medical domain is introduced from two aspects: HSI hardware, and HSI application. Then, most endoscopy imaging technologies relating to spectral imaging including conventional RGB sequential imaging, NBI, Fujinon Intelligence Color Enhancement (FICE), I-scan (Pentax, Japan), and Auto-Fluorescence Imaging (AFI) are summarized. In the following section, existing HSI endoscope systems are summarized. In the last section, HS image processing algorithms are presented briefly, including common procedure, pre-processing, feature extraction, image classification, and image enhancement.

Second, the development of flexible HS endoscope system is introduced in Chapter 3 focusing on the dispersive method. We use filter wheels to select light wavelength. Then Geneva mechanism that is used to drive the filter wheels is described. Then the differences and innovations of this system are described compared to other similar systems. At last, the stability of the prototype machine is tested.

Third, clinical evaluation is described in Chapter 4. This chapter includes four

parts: ethical approval, protocol of clinical trials, clinical trial results, and tentative image analysis. For the image analysis part, some interesting information and spectral image differences at first glance are presented. Then, HS images are tentatively analyzed applying some methods from previous literatures, including Contrast Calculation, Dependence of Information, and Recursive Divergence. These methods and algorithms are employed on the data we obtained, and we get some useful results.

Fourth, a new application further applying HS analysis results is introduced in Chapter 5. This new application, named adaptive narrowband imaging (ANBI) is the extension of conventional NBI and based on band selection of HS images of a specific disease. One case study proves that ANBI gives higher accuracy, sensitivity, and specificity in specific-object detection than conventional NBI.

Finally, discussion on future study is presented in Chapter 6. Clinical evaluation for the results of HS image analysis and ANBI will be made after acquiring and analyzing large mount of data. Some work still needs to be done to improve the system stability and light efficiency. Especially, we propose a new HS imaging method applying broad- and overlapped-band filters to improve the light intensity and Signal-Noise-Ratio (SNR). Simulation shows exciting results. Although this method only performs greatly on the foundation of accurate soft image registration, we hope to apply it in our system in the future. Moreover, the system needs more accurate calibration methods, together with targeting analysis methods on medical HS images.

CHAPTER II

STATE OF ART

This chapter reviews the thesis-relating technologies in this research field. In the beginning section, HSI is introduced from two aspects: HSI hardware, and HSI application in medical domain. Then, spectral-related endoscopy imaging technologies including conventional red-green-blue (RGB) sequential imaging, Chromoendoscopy (including NBI, Fujinon Intelligence Color Enhancement (FICE), and I-scan (Pentax, Japan)), and Auto-Fluorescence Imaging (AFI) are summarized. In the next section, existing HSI endoscope systems are summarized. In the last section, existing HS image processing algorithms in remote sensing field are presented briefly.

2.1 Hyperspectral Imaging in Medical Domain

HSI endoscopy is able to deliver images containing bio-marker information, and provide pathophysiology assessment based on spectral properties of disease tissue[108]. Compared to MSI, HSI with higher spectral and spatial resolution potentially contains more diagnostic information while they also make it difficult to perform manual or automatic analysis of large amount of HS data. Although HS image analysis methods have been intensively investigated in the remote sensing area, their development and application in medical domain, especially in digestive tract imaging domain lag far behind. And the relationships between spectral features and underlying physiological or pathological mechanisms are not well understood by now[87]. In this section, HSI applied in medical domain is overviewed briefly in two aspects: hardware, and applications.

Table 3: Summary of classification methods for HSI endoscope systems

System Classification Methods	Examples
Acquisition mode	Spatial/Spectral Scanning
Dispersive device	Monochromator/Optical Filter/Singleshot Imager/Fourier Transformation Infrared Imaging
Spectral region and resolution	UV/VIS/IR, Broadband/Narrowband
Measurement mode	Reflectance, Scattering and Fluorescence
Endoscope manufacture	Rigid/Flexible/Capsule

2.1.1 Hardware

Spectral endoscope system is a hybrid modality that combines spectral imaging and endoscopy. With spatial information, the origin of each spectrum on samples can be located, which makes it possible to probe the light interactions with pathology more completely. The spectral signature of each pixel on the images enables HSI to identify various pathological conditions. HSI has the potential to capture the subtle spectral changes under different pathological conditions. Conventionally, HS endoscope systems are composed of light source, wavelength dispersion devices, and detectors, similar as previous model. There are different ways of classifying these systems, and these classification methods are discussed in this part. Table 3 shows some of them.

Acquisition Mode

The fundamental classification of spectral endoscopy systems is based on the acquisition mode, which means how spectral and spatial information is acquired[121]. The typical spectral endoscopy systems involve two imaging methods[87]: spatial scanning and spectral scanning. Table 4 summaries the working principles, advantages, and challenges of both methods.

Table 4: Summary of spatial scanning and spectral scanning methods

Method	Description	Advantages	Challenges
Spatial Scanning	Acquire a spectrum for each pixel or line of pixels, and spatially scan through the scene	Collect accurate spectral information, and always be applied in spectrum analysis	It cannot provide live display of spectral images
Spectral Scanning	Capture the whole scene with 2-D detector arrays in a single exposure, and then change wavelengths	Display live spectral images, which is essential for aiming and focusing	It needs image registration methods to compensate the image translation and deformation

These image-acquiring systems must trade off critical parameters, such as speed, spectral resolution, image size, and signal-to-noise ratio (SNR)[63]. This trade-off has led to the development of image mapping spectroscopy (IMS)[31, 32, 63, 64], which captures the whole data cube in a single snapshot without compromising image resolution or speed. It is one of real-time, non-scanning endoscopic techniques. But the spectral resolution among the image cube is low for this technology.

Dispersive Devices

Dispersive device is the key element for spectral imaging systems. They are either located between the light source and the object, or between the object sample and the image sensor. There are many types of optical and electro-optical dispersive devices, which can perform spectral dispersion or wavelength selection for spectral endoscopy systems. The commonly used devices can be divided into three types[87]: monochromators, optical filters, and single-shot imagers.

Monochromator Monochromators can separate white light into its constituent spectrum of colors. Prism and diffraction grating are two commonmonochromators[87].

The change of the refractive index of the prism material, which varies with the wavelength of incident light, enables prism to disperse light and causes the incident lights of different wavelengths to leave the prism at different angles. A diffraction grating consists of reflecting or transmitting elements with lines or grooves ruled on the surface. It is able to diffract incident light, and modify the electric field amplitude or phase or both, of the incident electromagnetic wave[106]. Prism has low scatter over the spectral range of VIS and NIR, and is free from overlapping spectral orders that cause complications in grating, though it needs long light path to separate wavelengths if used in light beam with large aperture. Moreover, optical designs based on prism tend to be more complex than grating because of the nonlinear scanning dispersion of the prism.

Prisms and gratings deal with a lot of wavelengths, thus they are always used in multi-band spectral imaging systems, such as MSI and HSI. TILL Corporation at Germany developed a commercialized spectral light source, called Polychrome IV/V, based on grating. It has spectral tuning period of around 1 ms with bandwidth of 10 nm. However, as grating is based on slit, light throughput is around 10 mW, which is not enough for wide-view imaging. Lindsley et al.[84] developed a HSI bronchoscope based on Polychrome IV. It takes 0.5 seconds to collect 45 bands of image within range from 350 nm to 800 nm. Gerstner et al.[41] developed a laryngoscope system based on Polychrome V. It takes 25s to collect 30 bands of image with 15 nm bandwidth, from 390 nm to 680 nm. Although these systems are prototype with low light output, they prove that HSI has great potential in digestive tract disease examination.

Optical Filter Optical band-pass filters, including fixed ones and tunable ones, are widely used in multi- and hyper-spectral endoscopy systems. Fixed color filters, such as interference filters are convenient. Color mask of CCD is a type of fixed filter application, and can be applied in conventional real-time colorful imaging[130].

Fixed filters can also be placed in a filter wheel rotating to switch wavelengths[12]. The wheel can locate in optical path of light source, or in front of sensors. Although filter wheels are easy to use and with low cost, they suffer from slow speed of switching wavelengths, mechanical vibration from moving parts, and image dis-registration due to object movement. Thus these fixed filters are usually implemented in real-time imaging system with filter number less than 5, such as conventional color imaging and NBI, or MSI systems with no more than 10 filters[59, 115].

Tunable filters which can be electronically controlled without moving mechanical parts and at high tuning speeds, are also frequently used in spectral endoscopy systems. Liquid crystal tunable filter (LCTF), acoustic-optical tunable filter (AOTF), and Fabry-Perot interference filter (FPIF) are predominantly utilized in most HSI systems. Table 5 summaries these techniques on working principle descriptions, advantages, and challenges. As they can deal with a lot of wavelengths, tunable filters are commonly applied in non-real-time MSI and HSI endoscopy systems. Clancy et al.[21] developed a laparoscope HSI system based on LCTF. Martin et al.[92, 93] developed a HSI system working with fluorescence based on LCTF. Leitner et al.[81] developed a HSI laryngoscope system based on AOTF, which is capable to collect 51 images with FWHM of 5 nm in 1.25s. I. Shimoyama et al.[28] developed a micro FPIF for wavelength-adjustable spectral endoscope at the tip of a flexible endoscope.

Single Shot Imager Single shot imagers, such as a computer-generated hologram (CGH) which consists of arrayed cells of square pixels to form a 2-D grating, are used to disperse light in snapshot imaging systems[32, 48, 51, 58, 87]. CGH enables capturing both spatial and spectral information in a single frame. Tkaczyk et al.[63] developed a real-time HSI endoscope based on image snapshots and mapping technology. As for this method, the high speed is an advantage while the spatial resolution is a challenge.

Table 5: Summary of tunable filters

Tunable Filter	LCTF	AOTF	FPIF
Description	Commonly be built by tunable retardation liquid crystal plates and a stack of polarizers	Consist of a crystal in which a single wavelength can be accurately separated from incident light by radio frequency acoustic waves, based on acoustic-optical effect and Bragg Diffraction[60]	Be typically made of a transparent plate with two reflecting surfaces, or two parallel highly reflecting mirrors, with adjustable distance or refractive index
Advantage	They work from VIS to NIR region, without changing the direction of light path. High speed and having no moving parts, and can be used in light beam with large aperture	They can operate at a broad wavelength range from UV to IR, with faster tuning speed and higher throughput than LCTFs	They can be applied in light beam with large aperture, and have high tuning speed. And they can be made on a tiny chip combining with micro-electromechanical systems (MEMS) technology
Challenge	They are based on polarization effect and birefringence effect of crystal[61, 151], thus the output light is polarized with low intensity. And they have low thermal threshold and liquid crystal materials cannot stand light with high power	AOTFs separate light based on output angle and polarization[16]. It requires system design with high accuracy	The transmission rate is not high enough at selected wavelength, while not low enough at gap regions

Fourier Transform Infrared Imaging Fourier transform infrared imaging (FTIR) is another type of method to make spectral imaging. It collects a series of images as a function of interferometer optical path difference. A lot of mid-infrared HSI systems in medical domain are based on FTIR[5, 22, 120]. Some Fourier transform methods are employed together with HSI to separate depth information regarding object samples[19]. Yellin et al.[153] developed a spectrally-encoded endoscopy method which has the ability to make 3-D biomedical imaging.

Spectral Range and Resolution

Spectral range indicates the wavelength regions covers by spectral endoscopy systems, generally including UV (200-400 nm), VIS (400-780 nm), NIR (780-2500 nm) and mid-IR (2500-25,000 nm) based on different applications[7]. The most widely used spectral range in literatures on digestive diseases diagnosis falls in VIS and NIR regions[87]. Visible light penetrates only 1$\sim$2 mm below mucosa and obtains information regarding veins and capillaries[103]. NIR penetrates deeper into tissue than VIS and mid-IR as water absorbs mid-IR light strongly and covers absorption of other molecules such as proteins within the sample.

Spectral resolution of a spectral imaging system refers to the limit of the ability to separate two adjacent monochromatic features among the spectrum[132]. High spectral resolution allows accurate reconstruction of the spectral profile of the reflected light from tested sample. Spectral bandwidth is also an important parameter for a spectral endoscopy system[132]. It is defined as the FWHM of transmission. Systems with higher spectral resolution and narrower bandwidth could provide more accurate description of spectral properties of the observed sample. Actually, the ambiguity problem among the applications of MSI and HSI is mainly related to spectral resolution[87]. The more accurate the spectral sampling is, the higher spectral resolution HSI has, and the less possibly the ambiguity problem occurs.

Measurement Mode

According to the optical properties of biological tissue, spectral endoscopy systems work on reflectance, scattering and fluorescence modes. The majority of these systems work on the reflectance mode. Absorption and depth information could influence the reflected light. In many cases, fluorescence and reflectance modes are combined together[8, 33], and spectral imaging techniques are employed to separate fluorescence information from the reflectance information. In recent years, scattering under illumination with specific wavelength is also applied in depth-resolved imaging on biological tissue[119] which has great potential to be employed combining with endoscopy.

Endoscopes Manufacture

Spectral endoscopes are developed on foundation of conventional white light endoscope platforms, which have three types: rigid endoscope, flexible one and capsule one[141]. Each of them has specific working zone and corresponding organs along digestive tract, as Table 6 shows. Rigid endoscopes are usually applied on mouth, larynx, and rectum. And these endoscopes are similar with those applied ex vivo. Flexible endoscope systems fit the applications along esophagus, stomach, and large bowel. They are much deeper inside than rigid ones, and play an important role in early-stage cancer detection and non-invasive examination. Recently, capsule endoscopes are widely developed while there is no specific spectral technique combining with them nowadays, except for the conventional wide-band color imaging. We believe that wireless capsule endoscopes are now developed mainly for making non-invasive examination of small intestine[42, 82].

2.1.2 Applications

HSI is able to deliver images containing bio-marker information, and provide assessments of tissue pathophysiologies based on the spectral characteristics of different tissues[108]. Therefore, HSI is increasingly being used for medical diagnosis and

Table 6: Summary of endoscopes and targeting organs

Endoscopes	Targeting organs in digestive tract
Rigid	Mouth, Larynx, Rectum
Flexible	Esophagus, Stomach, Large Bowel
Capsule	Whole digestive tract, especially Small Intestine

image-guided surgery. For instance, HSI has been applied to the diagnosis of hemorrhagic shocks[14, 15], the detection of laryngeal disorders[93], the early detection of dental caries[142], the fast characterization of kidney stone types[143], the assessment of peripheral artery disease[56], and so on. Especially, HSI studies on cancers have been performed in the following four major aspects[87]: 1) recognizing protein bio-markers and genomic alterations on tumor cells in vitro[140]; 2) analyzing the structural and morphological properties of cancer histological specimens to classify the cancer margins and stages; 3) examining the tissue surface to identify malignant lesions in vivo; 4) measuring the tissue blood oxygenation and blood volume to quantify the tumor angiogenesis and tumor metabolism. In the following part, we just focus on the HSI applications of diagnosing GI diseases. Other applications, such as cardiac disease, retinal disease, diabetic foot, shock, tissue pathology, and image-guided surgery, please refer to literature for details[87].

In – Vitro Diagnosis

Pathological analysis is the basis of cancer diagnosis and treatment. Malignant tumor leads to considerable variations in nuclei size and shape. Traditionally, pathologists examine the specimens under microscopes and make judgments based on the deviations in the cell structures and changes in the distribution of the cells. However, this process is subjective, time-consuming, and inconsistent due to inter- and intra-observer variation[55]. To overcome these problems, Medical HSI has been developed to discriminate different cell types and tissue patterns on pathology slides. Studies

from previous literature have shown that the spectral characteristics of nucleus and interstitial are different from each other[26].

At the same time, many researchers classify the colon biopsy samples into benign and malignant classes based on the HS information. Masood et al.[94] explored a series of research problems for classification of HS colon biopsy images and conclude that HSI has enough discriminatory power to distinguish normal and malignant biopsy tissues. Kiyotoki et al.[68] developed a HS camera microscope and Leiter et al.[81] made classification of biopsy tissues.

Most of these studies are on HS microscope platforms. These systems implement dispersive devices in the illumination optical path, or in front of CCD sensor. Compared to clinical in-vivo applications, these systems do not have the limitations of data-acquisition time, working space, clinical stability, and volume of cooled CCD which enables the working wavelength range from UV to IR. On the other hand, as the biopsies are processed ex vivo and many components may change such as hemoglobin oxygen contents, these ex-vivo studies may be inaccurate.

In – Vivo Diagnosis

With the establishment of expedient procedures, HSI could provide a in-vivo, non-invasive and reliable diagnostic method that allows accurate classification and determination of pathological tissues. Lu et al.[158] builds an HS system to measure and analyze the spectral property and detect human tongue tumor. Using the system, a recognition rate of 96.5% is achieved.

Besides studies on tongue tumor, there are a lot of in-vivo HS applications on other locations, for instance, cervical cancer, skin cancer, head and neck cancer, retinal diseases, diabetic foot, etc[87].

2.2 Endoscopy Imaging Technologies

As described in previous section, reflected and transmitted light from tissue captured by spectral endoscopy carries quantitative diagnostic information on tissue pathology. In recent years, a variety of spectral endoscopic imaging technologies have revolutionized the non-invasively diagnostic approaches for patients with digestive diseases. Thus spectral endoscopy is now increasingly being used in GI disease diagnosis and treatment. In this part, we will introduce several typical and spectra-related imaging endoscopic techniques, such as NBI, FICE, and AFI, together with their applications.

2.2.1 Conventional Color Imaging

Conventional color imaging is actually a typical application of spectral imaging. The spectral information is separated by different fixed filter with broad band (80 - 100 nm). Usually, this conventional color imaging contains 3 or 4 filters: RGB or CMYK (Cyan-Magenta-Yellow-blacK)[53, 110]. Figure 10 and 11 show the transmission curve of these filters. Doctors make diagnosis according to these colors together with their combined visualizations that extract and enhance color (rough spectral) information display. There are also two types of color imaging endoscopy referring to the location of filters: one implements monochromatic sensor and rotating color filter wheel, while the other is based on fixed color mask in front of sensors[42]. The former has an advantage of high spatial resolution, with the loss of temporal resolution. The real-time display of conventional color imaging will drift under the case of movement, and image registration is needed to compensate it. The latter method does not have color drift problem, as it could get several colorful images at the same time, trading off the spatial resolution. Both types of color imaging endoscopy have been widely used in practical GI endoscopy examination nowadays.

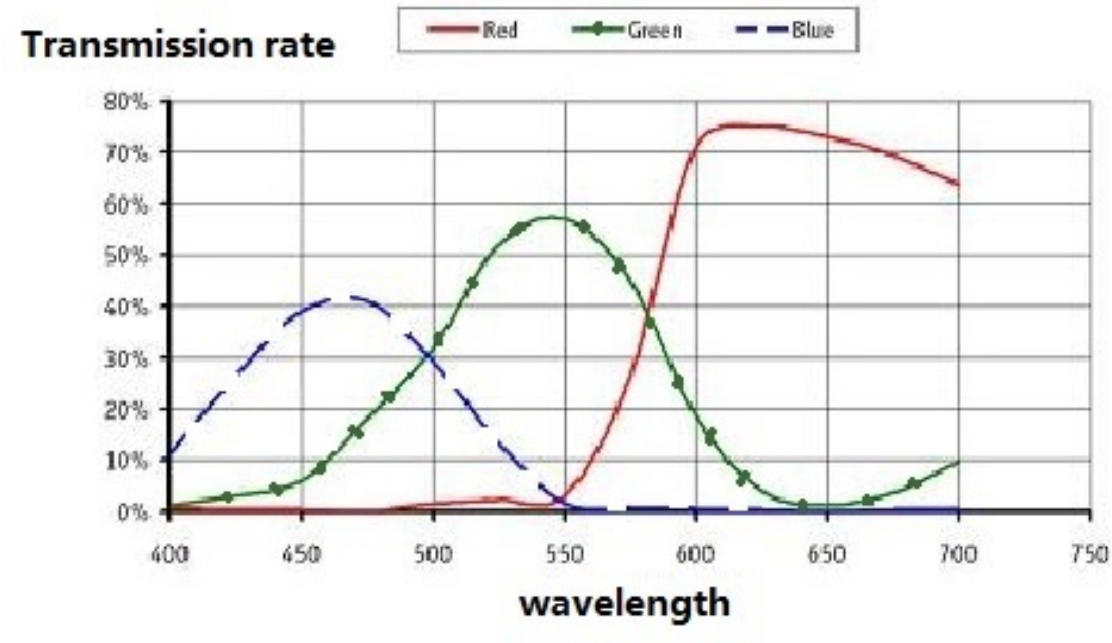

Figure 10: Transmission rate curve of RGB filters for conventional color imaging

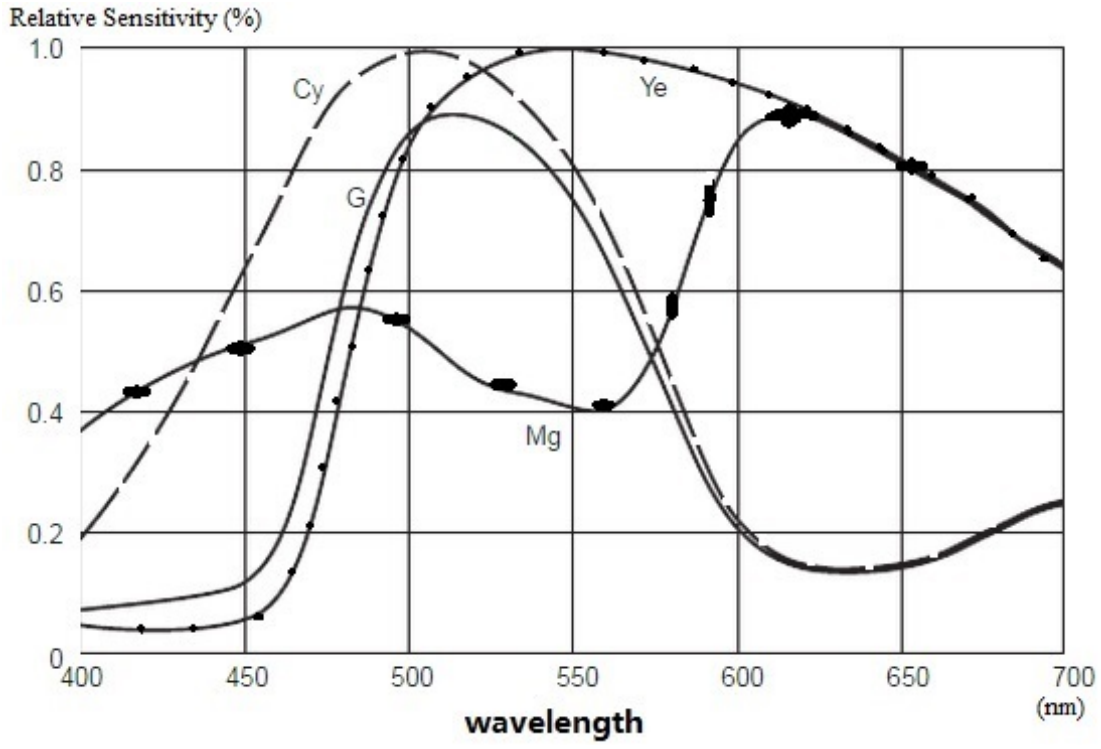

Figure 11: Transmission rate curve of CMYK filters for conventional color imaging. This picture is cited from Datasheet of CCD whose model number is Sony ICX239

2.2.2 Chromoendoscopy

In the past decade, chromoendoscopy including dye-based chromoendoscopy (DBC) and dye-less chromoendoscopy (DLC, also called virtual chromoendoscopy) is also widely commercialized and used in the examination of digestive tract[39, 102, 113, 126, 131]. Chromoendoscopy is based on dye such as methylene blue (0.1% - 0.5%), which is absorptive stain and identifies specific epithelial cell types across the cell membrane, and indigo carmine (0.2% - 0.4%), which is contrast stain and seeps through mucosal crevices highlighting surface topography[102]. DBC yields a 3-4% additional diagnostic and detection rate of intra-epithelial neoplasia[52, 66] on digestive tract. However, DBC has some limitations. It is time-consuming, with additional costs for dye spraying equipment, and the possibility of uneven spraying of the dye. Moreover, the DBC does not allow for sub-epithelial capillary analysis.

DLC includes NBI (Olympus, Japan), Fujinon intelligent color enhancement (FICE; Fujinon, Japan), and I-Scan (Pentax, Japan)[102]. NBI applies two optical filters with narrow band centered at 415 nm and 540 nm. Under this narrow band illumination, blood vessels are enhanced and thus seen more clearly and easily. FICE and I-Scan are based on similar physical principle as NBI, but they are dependent on some computed spectral estimation technology, other than the presence of optical filters[96, 102, 122]. They could reconstruct virtual images in real time. By increasing blue component and decreasing red and green components on the image so as to improve the contrast of capillary patterns, I-Scan is effective to predict neoplasia as precisely as DBC[102]. However, recent studies shows that FICE could not improve the delineation of diseases, such as ulcers and erosions in Crohn's disease[20].

NBI

Technology Description NBI is a representative technology of DLC[102]. A rotating filter wheel is interposed after the light source. Most NBI systems contain two

optical filters with narrow band centered at 415 nm (FWHM = 40 nm) and 540 nm (FWHM = 20 nm). Some also apply a third band centered at 600 nm (FWHM = 20 nm)[43, 44, 105]. Through these filters, the spectral characteristics of the incident light are changed. At the same time, these incident light differ for the depth of penetration, with average penetration depth for 415 nm is 0.17 mm, 0.24 mm for 540 nm, and 0.28 mm for 600 nm[116]. The photons with a shorter wavelength in the blue part re-produce a morphologic image of the mucosal surface and the superficial network of capillaries. The scatter with a minimal depth of penetration and selectively absorption by hemoglobin, give a good contrast for small vessels, while images obtained with a broadband filter will dilute all these information. The photons in green and red part of spectrum, less scattered, penetrate more deeply and give large vessels a good contrast from the adjacent tissues[116].

As blood vessels at different depths are enhanced and seen more clearly and easily under these narrow band illuminations, NBI is increasingly being used in clinic. It is believed that the outline of disease area and the capillary patterns could be enhanced. This is especially helpful in diagnosis of some specific diseases such as Barrett's Esophagus (BE)[125].

There have been a lot of studies on NBI in clinic in the past decade. Some studies showed that NBI could improve the detection rate of early-stage digestive disease from 85% to 92%, while some other showed that NBI could not improve the detection rate significantly[27, 43, 89]. American Society for Gastrointestinal Endoscopy concludes that: "(1) NBI itself could not improve neoplasia detection rate; (2) NBI could help margin disease region, thus is useful in targeting biopsy and diagnosing some disease such as Barrett's Esophagus; (3) NBI combining with magnifying endoscopy could improve the diagnosis of intra-epithelial neoplasia in ulcerative colitis"[72]. When combined with magnifying endoscopy, NBI could show microvascular density and pit pattern more clearly, and it is also called "optical biopsy"[25].

NBI is convenient to realize and could be applied in real time. It causes no additional damage and pain to patients. However, NBI implements only two or three fixed wavelengths, and chooses only hemoglobin as disease bio-marker. NBI studies regarding other bio-marker and wavelengths are required.

Moreover, the magnifying endoscope which can be used in vivo to observe the micro-patterns is similar with ex-vivo microscopes in working principle. Hence the research conclusion that spectral imaging combined with microscopes ex vivo is helpful in diagnosis also indicates HSI in vivo combining magnifying endoscope has great potential and bright future in clinical application domain.

Relationship between NBI and MSI/HSI Both NBI and MSI/HSI are typical techniques on spectral endoscopy. The former is commercialized and widely used, while the latter has great potential for future application in digestive examination and disease diagnosis. Actually, MSI/HSI originating from remote sensing field has similar working principle with NBI, which means HSI can also derive from NBI by adding band numbers and narrowing filter bandwidth. Sometimes, NBI is considered as a kind of MSI when applied together with conventional color imaging. However, the focus of NBI technique is different with that of MSI/HSI. In fact, both of the bands employed by NBI are around absorption peaks of hemoglobin, and are capable to enhance the contrast between veins and background, while the difference between the two bands indicates the veins' depth information – veins enhanced by illumination at 540 nm are deeper than those at 415 nm. On the other hand, MSI/HSI makes image classification based on reflected spectra curve at each pixel. The curve integrates absorption information, depth information, and even scattering information. Wavelength bands selected through band selection algorithm as a result of MSI/HSI processing can be applied into NBI. Thus NBI can be considered as a distinguished-wavelength-specific MSI/HSI, with broader FWHM and fewer bands.

FICE

FICE (Fujinon, Japan)[97, 98] is a typical technology of virtual spectral endoscopy, and also is a typical type of DLC. It is based on principle component analysis (PCA) and Wiener estimation[97]. Principle components are calculated for spectral curves at each pixel based on many priori single-point spectral measurements. Then based on these principle components and the real-time conventional RGB color images, we can reconstruct the spectral curve at each pixel using spectral estimation methods. After spectral estimation, specific spectral images are assigned as new R, G, and B components for the displayed image which will enhance the spectral information on color image.

Although widely applied in clinic, studies showed that FICE could not improve detection rate for adenomatous polyp significantly[25]. However, the use of magnification combining with FICE did improve its performance[25]. And similar with NBI, FICE helps a lot in margining the outlines of disease area.

Virtual Spectral Endoscopy Virtual spectral endoscopy is a type of Dye-less Chromoendoscope (DLC) which is now increasingly being applied in clinic instead of DBC. Most virtual spectral endoscopies implement spectral estimation technologies (SET). They take an ordinary endoscopic image from video processor and arithmetically process, estimate, and produce an image centered at a dedicated wavelength of light. They could also enhance the image color using spectral information for better visual observation of tissue disorder and blood vessel or capillaries structure, and make image analysis more efficient. A lot of popular SET methods have been proposed, such as PCA and Wiener estimation.

Compared to those spectral endoscopies on the foundation of dispersive devices, virtual spectral endoscopy technologies are with high processing speed and could show spectral images in real time. However, they rely on large sets of priori training

data. If the environment of application changes or noise affects the RGB images, SET will give inaccurate spectral reconstruction. Especially, nowadays there are lots of new SET methods which need small amount of training sets, such as partial least-squares regression[11]. This enlarges the influence of environment consistency between training and working.

PCA PCA can identify key discriminative features, highlight the relative distributions of different component mixtures, and estimate spectrum in spectral endoscopy data[6, 33, 41, 117, 160, 161]. Although PCA transforms the original data into a subspace spanned by eigenvectors, which makes it difficult to interpret the biological meaning after transformation, PCA performs quite well in SET[98] and helps a lot in virtual spectral endoscopy. Miyake et al.[97] studied 310 spectral reflectance cases on digestive tract including stomach, duodenum, small intestine, and colon. They found that three principle components allowed accurate estimation of the spectral reflectance on the gastric mucosa and skin.

Wiener Estimation Wiener estimation has been widely studied and applied in virtual endoscopy. The model that is represented by Equation 1 can be briefly described as following:

$$\boldsymbol{\nu} = \boldsymbol{H}\boldsymbol{\gamma} \tag{2}$$

where $\boldsymbol{\nu}$ indicates vector of ν_i, and $\boldsymbol{H}$ is system function which should be computed to obtain $\boldsymbol{\gamma}$ from $\boldsymbol{\nu}$. To determine $\boldsymbol{H}$, an endoscope should capture sample color charts corresponding to spectral radiance $\boldsymbol{\gamma}$, and the camera output $\boldsymbol{\nu}$ should be measured, as shown in Figure 12[98]. The Wiener estimation method is to find the estimation of $\boldsymbol{H}$ that minimizes the error between the actual spectral radiance and the estimation for all sample data obtained[98, 136], as shown in Equation 3[57].

$$\boldsymbol{E}\{\parallel \boldsymbol{\gamma} - \hat{\boldsymbol{\gamma}} \parallel^2\} \rightarrow min \tag{3}$$

where $\hat{\gamma}$ represents estimated reflected spectrum vector. Then we assume $\boldsymbol{G}$ as the estimated pseudo-inverse matrix of $\boldsymbol{H}$, and

$$\hat{\gamma} = \boldsymbol{G\nu} \tag{4}$$

As

$$\| \gamma - \hat{\gamma} \|^2 = trace\{(\gamma - \hat{\gamma})(\gamma - \hat{\gamma})^{\boldsymbol{T}}\} \tag{5}$$

according to Wiener estimation, combining Equation 5 with 2 and 4, we have

$$\begin{aligned} &\frac{\partial trace}{\partial \boldsymbol{G}}\{\boldsymbol{E}\left[\gamma\gamma^{\boldsymbol{T}} - \hat{\gamma}\gamma^{\boldsymbol{T}} - \hat{\gamma}\gamma^{\boldsymbol{T}} + \hat{\gamma}\hat{\gamma}^{\boldsymbol{T}}\right]\} \\ &= \frac{\partial trace}{\partial \boldsymbol{G}}\{\boldsymbol{E}\left[\gamma\gamma^{\boldsymbol{T}} - \gamma\gamma^{\boldsymbol{T}}\boldsymbol{H}^{\boldsymbol{T}}\boldsymbol{G}\boldsymbol{T} - \boldsymbol{G}\boldsymbol{H}\gamma\gamma\boldsymbol{T} + \boldsymbol{G}\boldsymbol{H}\gamma\gamma^{\boldsymbol{T}}\boldsymbol{H}^{\boldsymbol{T}}\boldsymbol{G}^{\boldsymbol{T}}\right]\} \\ &= 0 \end{aligned}$$

Then we have

$$\boldsymbol{E}\left[-\gamma\gamma^{\boldsymbol{T}}\boldsymbol{H}^{\boldsymbol{T}} - \gamma\gamma^{\boldsymbol{T}}\boldsymbol{H}^{\boldsymbol{T}} + \boldsymbol{G}\boldsymbol{H}\gamma\gamma^{\boldsymbol{T}}\boldsymbol{H}^{\boldsymbol{T}} + \boldsymbol{G}\boldsymbol{H}\gamma\gamma^{\boldsymbol{T}}\boldsymbol{H}^{\boldsymbol{T}}\right] = 0 \tag{6}$$

So,

$$\boldsymbol{G} = \boldsymbol{E}(\gamma\gamma^{\boldsymbol{T}}\boldsymbol{H}^{\boldsymbol{T}})\boldsymbol{E}(\boldsymbol{H}\gamma\gamma^{\boldsymbol{T}}\boldsymbol{H}^{\boldsymbol{T}})^{-1} = \boldsymbol{E}(\gamma\boldsymbol{n}\boldsymbol{u}^{\boldsymbol{T}})\boldsymbol{E}(\boldsymbol{\nu}\boldsymbol{n}\boldsymbol{u}^{\boldsymbol{T}})^{-1} \tag{7}$$

Then we could obtain the estimated $\hat{\gamma}$ from ν through 4.

2.2.3 I – Scan

I-Scan (Pentax, Japan)[122] actually contains three functions: Surface Enhancement (SE), Contrast Enhancement (CE), and Tone Enhancement (TE). SE is actually a function of high-pass filter and not spectral-related. CE individually filters RGB components of a pixel corresponding to the luminance area of this pixel. With low luminance, the pixel will be slightly bluish white after CE. Minute irregularities on mucosal surface are enhanced through CE. With TE, on the other hand, RGB components of an ordinary endoscope image are converted independently along the tone curve, followed by a re-synthesis of the three components to yield a reconstructed image. The tone curve can be divided roughly into S and J types.

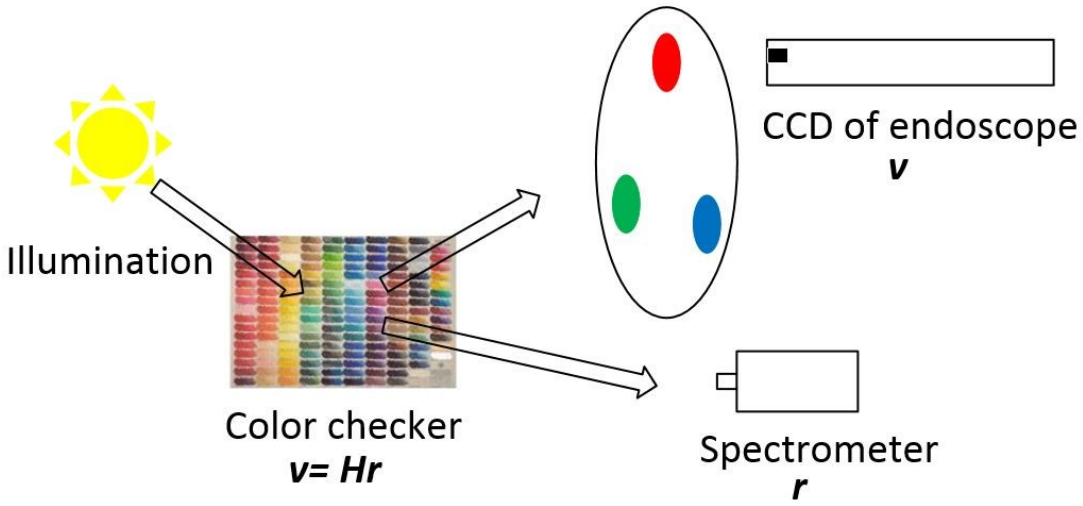

Figure 12: Measurement of spectral reflectance by the Wiener estimation

2.2.4 Auto – Fluorescence Imaging Endoscopy

As described above, fluorescence-based spectral signature is an important endogenous early cancer bio-marker. Multi- and hyper-spectral approaches are always applied on illumination and collection pathways to separate the fluorescence information. Actually, a large portion of existing multi- and hyper-spectral endoscopy systems are based on auto-fluorescence imaging (AFI), due to the low light throughput after light dispersion on spectrum. Kester[65], Martin[92], Vo-Dinh[146], developed several HSI endoscope systems combining with fluorescence, to help make early cancer detection. Ferris et al.[33] performed a clinical study on a diverse population of women with varying disease and non-disease states with a medical HSI system covering the UV and VIS regions, and measured tissue fluorescence and reflectance of the cervical epithelium on the ectocervix.

2.2.5 Combination with Other Imaging Techniques

Spectral endoscopy can be combined with many other techniques, such as optical coherence tomography (OCT)[124], magnifying endoscopy, high-resolution endoscope[131], and compressive sensing (CS)[40]. Studies[154] as presented above have shown that

narrow-band spectral imaging[44] combining with magnifying endoscope has ability to enhance pattern of disease mucosa surface, identify tiny structure of colon disease mucosa, and improve early-stage disease detection rate significantly. In recent years, CS technique is also being developed with potential to combining with spectral endoscopy imaging techniques.

2.3 HS Endoscope Systems

Table 7 summarizes some typical multi- and hyper- spectral endoscopy systems. We can see from this table that most HS endoscope systems are on the foundation of rigid endoscopes. There are three flexible spectral endoscope systems. However, the one built by Dohi[28] is based on Fabry-Perot Interference Filter which is not accurate enough for wavelength dispersion. The FWHM of the select light for this machine is around 60-80 nm, and the block gap is not low enough among stop wavelength region. For the system built by Kester[63], it trades off spatial resolution (350 pixels $\times$ 350 pixels) for high imaging speed. This spatial resolution is too low to provide useful diagnostic information. For the system presented by Fawzy[152], the FWHM is 20 nm and the targeted organ is lung.

2.4 HS Image Analysis

In remote sensing field, there has already been a lot of algorithms and methods proposed to analyze HS images. Generally, as Figure 13 shows, the basic procedure for spectral image analysis involves preprocessing, feature extraction and selection, image classification, and image enhancement. As there are many review papers on spectral image analysis in this area, we introduce this part in brief. Detailed description of these algorithms is beyond this thesis and interested readers may check related references to identify them.

Table 7: Summary of some typical multi- and hyper-spectral imaging systems

Reference	Spectral Range (nm)	Rigid or flexible	Dispersive device	Application	Bandwidth (nm) × band number
[81]	400 - 650	Rigid	AOTF	Oral, larynx, parotid	5 × 51
[92]	720 - 700	Ex vivo	LCTF	Fluorescence	7 × 40
[41]	390 - 680	Rigid	Polychrome V	Larynx	15 × 30
[3]	400 - 1000	Ex vivo	Prism and grating	Intestine	5 × 121
[4]	1000 - 2500	Ex vivo	Prism and grating	Gastric	6.29 × -
[63]	450 - 650	Rigid	Prism	-	(4 - 10) × 48
[68]	400 - 800	Ex vivo	HS camera	Gastric	5.6 × 72
[28]	400 - 1000	Flexible	FPIF	Colon and gastric	-
[63]	400 - 700	Flexible	“Snapshot”	-	(5 - 7) × 48
[152]	400 -760	Flexible	Filter wheel	Lung	20 × 18

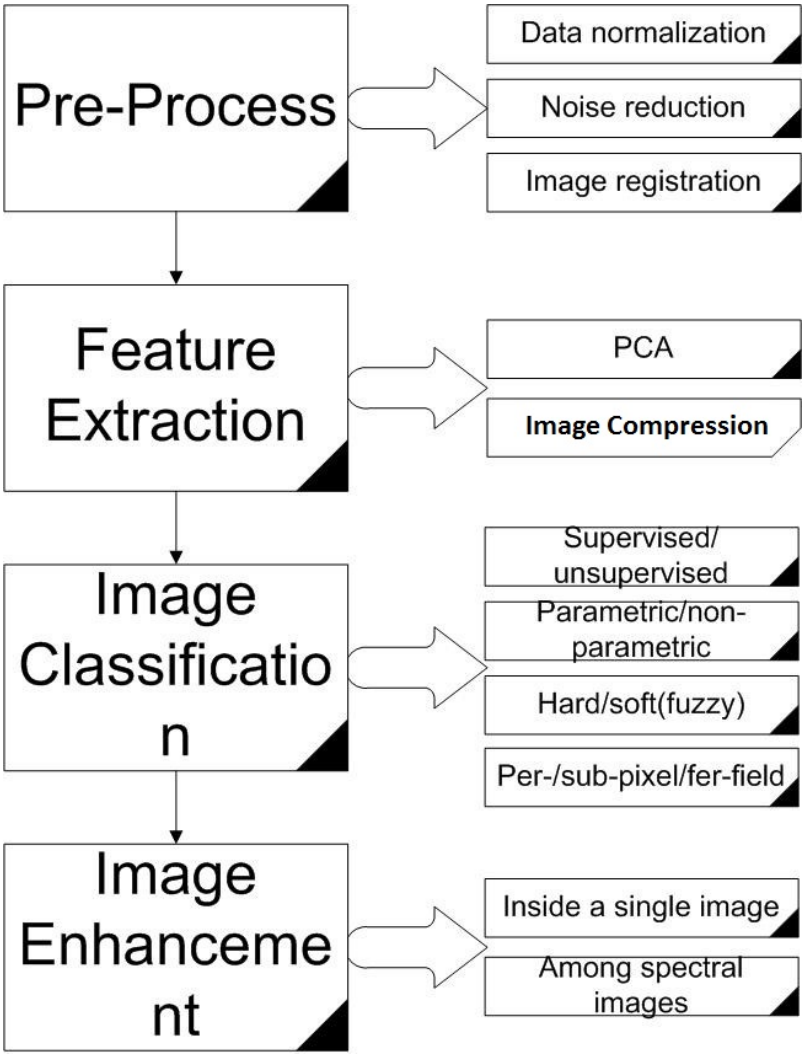

Figure 13: Procedures of image processing

2.4.1 Pre – processing

Spectral image pre-processing mainly involves data normalization, noise-reduction, and image registration. Data normalization normalizes spectral radiance observations to values that describe the intrinsic characteristics of biological samples, and better prepares images for further analysis. Under uneven surface illumination, the differences among the objects may be greater on different locations. One of the most commonly used normalization method is background estimation and homogenization[36, 91]. Such normalization could reduce system noise at the same time. Gaussian filters could also be used to smooth spectral and spatial features and reduce the noise influence[69].

Object translation, deformation, and sensor movement could lead to image dis-alignment. Image registration is commonly applied when there is dis-alignment among images on the same object and it will help to obtain accurate spectral information for each pixel[87]. The major difficulty for registration lies on the limited resemblance of features between images, and soft (elastic) tissue movement[73] which can be reduced by improving image acquisition speed. A lot of work has been done in image registration domain and those algorithms can be classified by many methods, such as rigid, semi-rigid, and non-rigid methods, feature-based and non-feature-based methods, and sub-pixel-, pixel-, and feature-based methods[13, 24, 36, 85, 91, 144, 145, 159]. Kybic[73] summarized a lot of image registration methods and proposed a fast elastic image registration algorithm, based on which Lange et al.[75] developed an new elastic registration method to match reflectance and fluorescence images to compensate for soft tissue movement during the image acquisition.

2.4.2 Feature Extraction

The most widely used methods for feature extraction is PCA. It can highlight the relative distributions of different molecular component mixtures[160, 161], identify key

discriminative features[33, 41], and estimate spectrum in the spectroscopic data[6]. PCA is to minimize the mean square error[117]. There are also several PCA variants, such as minimum noise fraction (MNF)[76] and independent component analysis (ICA)[156]. However, PCA transforms the original data to a subspace spanned by eigenvectors, which makes it difficult to interpret the biological meaning after transformation.

2.4.3 Image Classification

Image classification methods applied in imaging of digestive tract mucosa is similar with those in remote sensing and medical domain. Users' need, scale of the study data, economic condition, and analyst's skills are important factors influencing the selection of data, design of classification procedure, and the quality of classification results[86]. There are many ways to classify algorithms on image classification. Generally, they can be grouped as supervised and unsupervised, parametric and non-parametric, hard and soft (fuzzy)[56], or per-pixel, sub-pixel and per-field approaches[86]. In digestive tract domain, non-parametric per-pixel[35, 77, 79, 90, 100, 155] and sub-pixel[150] methods based on the type of pixel information are most widely applied. Support vector machines (SVMs), artificial neural networks (ANN), and spectral information divergence (SID) are among the most commonly used methods.

SVM

SVM has been proven to be suitable for classifying multiple spectral data. Kong[69] chose Gaussian radial-basis function (RBF) kernel as the kernel function for SVM and learned SVM parameters from 100 training samples chosen randomly from each of the normal and tumor classes, showing that spatial filtering enhanced classification accuracy from 83% to 86%. Akbari[2] constructed a library of spectral signatures from HS images of abdominal organs, arteries, and veins, and SVMs were used to differentiate between them.

SID

To measure the distance of probable behaviors between two spectra, SID models the spectrum of a pixel at same location among images as a probability distribution. Based on this, Guan[46] segmented pathological white blood cells into four components: background, nucleus, erythrocytes, and cytoplasm.

ANN

Neural network has been adopted by many researchers due to its nonparametric nature, arbitrary decision boundary, etc[1, 59, 86, 143]. It is a supervised method that needs large amount of training data. Nowadays, deep learning (DL)[18, 70], convolutional neural network (CNN)[70, 78] and auto-encoder (AE)[83] has been incorporated to analyze spectral images. Although hidden features extracted by neural network have no biological meaning, the accuracy of classification is high.

2.4.4 Visualization and Image Enhancement

Image enhancement methods aim to help make diagnostic feature more obvious. Some of these methods are based on feature selection on a single image. Marin[91] and Foracchia[36] made blood vessel selection and segmentation, and helped diagnosis. Some other image enhancement methods are based on the relationship among spectral images, and band selection is needed before the image enhancement, especially for multi- or hyper-spectral images analysis. For instance, based on two selected bands – 415nm and 540nm, NBI technique[44] makes higher image contrast and help margin disease region. Xie[49] also proposed a hemoglobin enhancement method based on the relationship between two broadband spectral images.

Band selection methods find a subset of spectral bands significant in information content, and remove the bands of less importance. All the spectral bands do not carry the same types of information[30]. Many criteria such as distance measures, information-theoretic approaches, and eigen-analysis have been proposed to

make band selection for HS image-cubes[30]. Kehsava[62] developed a band selection method based on the spectral angle mapper (SAM) metric. Tu[137] proposed a band selection algorithm based on canonical analysis. Du[29] used divergence for band de-correlation and high-order moments for band ranking. Kong[30] made band selection for HS images based on recursive calculation of divergence with an additional band. With a small number of optimal spectral bands selected from HS image data, we could build fast classification system with multi-spectral image sensors or even real-time HS image processing system.

2.5 Summary on State of Art

As presented above, we conclude the research state in related field here. On one hand, HS imaging has been widely used in medical domain. There are many types of medical HS systems developed. The applications in the whole medical field are also with high variety. On the other hand, the HS applications in endoscopy domain lag far behind. First, most HS endoscope systems are reported in the past 5 years. The research in this field just begins. Second, most HS endoscope systems are prototype machines. Few are being used in clinic. There is a lot of work to be done before these systems capable to be used in procedural medical examination. Third, Most reported HS endoscope systems are on the foundation of rigid endoscopes. The few flexible systems have their own limitations. Thus most HS images in this research field now are regarding skin, oral cavity, tongue, and larynx. There are few in-vivo HS images on esophagus, stomach, and colon diseases reported now. Fourth, HS image analysis on in-vivo GI images lags far behind. The most frequent analysis is classifying disease areas from normal tissues. Nevertheless, these systems and the pilot studies show the bright future of HSI endoscope being applied in standard clinical diagnosis.

CHAPTER III

SYSTEM DEVELOPMENT

In this chapter, we introduce how the novel flexible HS endoscope system is developed and tested. The dispersive device is the major part for our system, and this part will be described in detail together with how the device is driven. The most time-consuming part for this thesis is the PCB design, system modification and program debugging work in order to meet the stability and convenience requirements for clinical application. However, as this time-consuming part is about engineering, it is only presented briefly in this chapter.

3.1 Platform

This system is modified based on a commercialized endoscope system (model number AQ-100) donated by Shanghai Aohua Photoelectric Endoscope CO. LTD, and Figure 14 shows the system.

3.2 Dispersive Methods

Dispersive method is the major part in an HS system. We take several methods into account, such as AOTF, LCTF, grating and prism, FPIF, tunable laser, and filter wheels. Table 8 shows advantages and limitations of these methods.

AOTF, LCTF, FPIF and tunable laser have a common advantage that they have no mechanical moving part. This could increase stability of the system and make the wavelength output easy to control. However, they also have a common limitation that the optical throughout is too low to make wide-field-view imaging, the same as grating and prism.

The filter wheel method has the advantages of low-cost, high optical transmission,

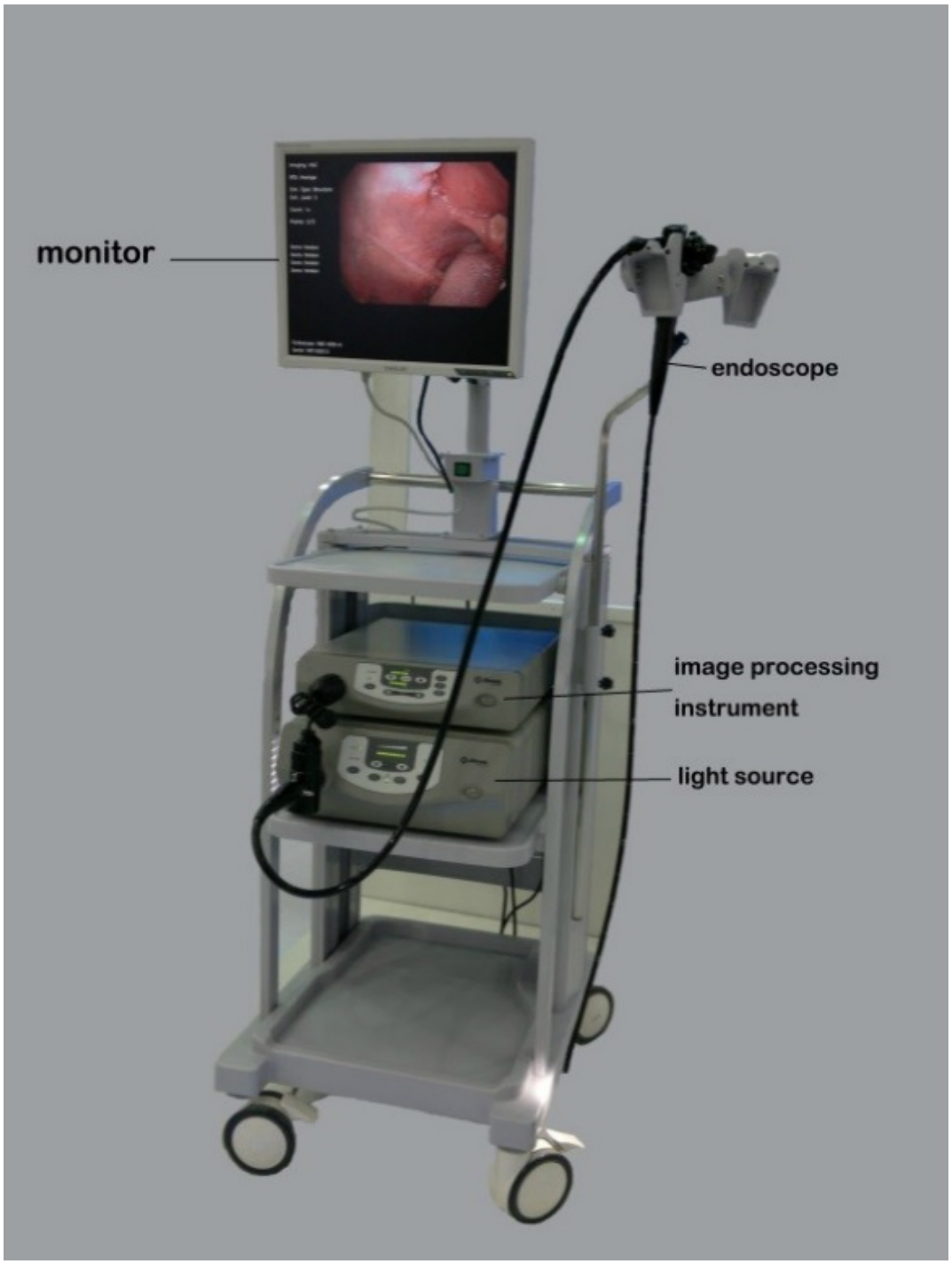

Figure 14: AQ-100 endoscope system based on which we develop the HS endoscope system

Table 8: Advantages and limitations of different dispersive methods

Methods	Advantages	Limitations
AOTF	There is no moving part; Fast switching speed (∼us)	Low optical throughout; High cost ($20K)
LCTF	There is no moving part; Fast switching speed (∼ms); Low cost	Low optical throughout; Low safety thermal threshold; Low transmission rate among 400-430nm
Grating and prism	Low cost	Low optical throughout
FPIF	There is no mechanical moving part	Low accuracy for wavelength selection; Large diameter for endoscope distal end
Tunable or white light laser	Wavelength selection is accurate; Optical path is easy to design	Low optical energy (FWHM is too narrow); High cost ($200K)
Single Filters (Filter wheel)	Low cost; Large diameter for light beam; High transmission rate	The selected wavelength is fixed and non-continuous; It needs mechanical switching part

and being easy for optical design. The limitations for this method are that the wavelength is fixed and non-continuous, and that it needs mechanical part to switch wavelengths, which will decrease the stability of the system. As for our research, FWHM of filters is 10 nm which is accurate enough for HSI and we can design a precise and stable controlling part to drive the filter wheels.

After overall consideration, we implement filter wheels to make dispersive illumination. Figure 15 shows the diagram of the HS system. The reason why we use two wheels instead of one wheel is that the wheel would be too large if we fix all filters in one wheel, and that the size of the platform machine could not fit the wheel diameter.

Figure 16 shows the wheels that contain narrow-band filters and all-pass holes. All filters are interference filters. The two filter wheels in maximum could fix 32 filters and 2 all-pass holes. For the selection of filters, we have two series. At first, we employ 32 filters centered from 400 nm to 700 nm with incremental and FWHM of 10 nm, plus one filter centered at 425 nm with FWHM of 25 nm. There is some

HS image data implementing this series of filters in later parts. However, the light intensity for images among 400-440 nm and 660-700 nm is too low to provide useful information. Thus we modified the light source, optical design, and series of filters aiming to resolve this problem. And in clinic, we just employ 28 filters, including 27 narrow-band filters centered from 405 nm to 665 nm with both incremental and FWHM of 10 nm, together with a filter centered at 680 nm with FWHM of 25 nm. Maximum transmission rate for these filters applied in clinic are around 60%. All clinical HS images are obtained using this series of filters.

This filter wheel design used to disperse light - together with the Geneva Mechanism used to drive the wheels - has been authorized with two Chinese patents.

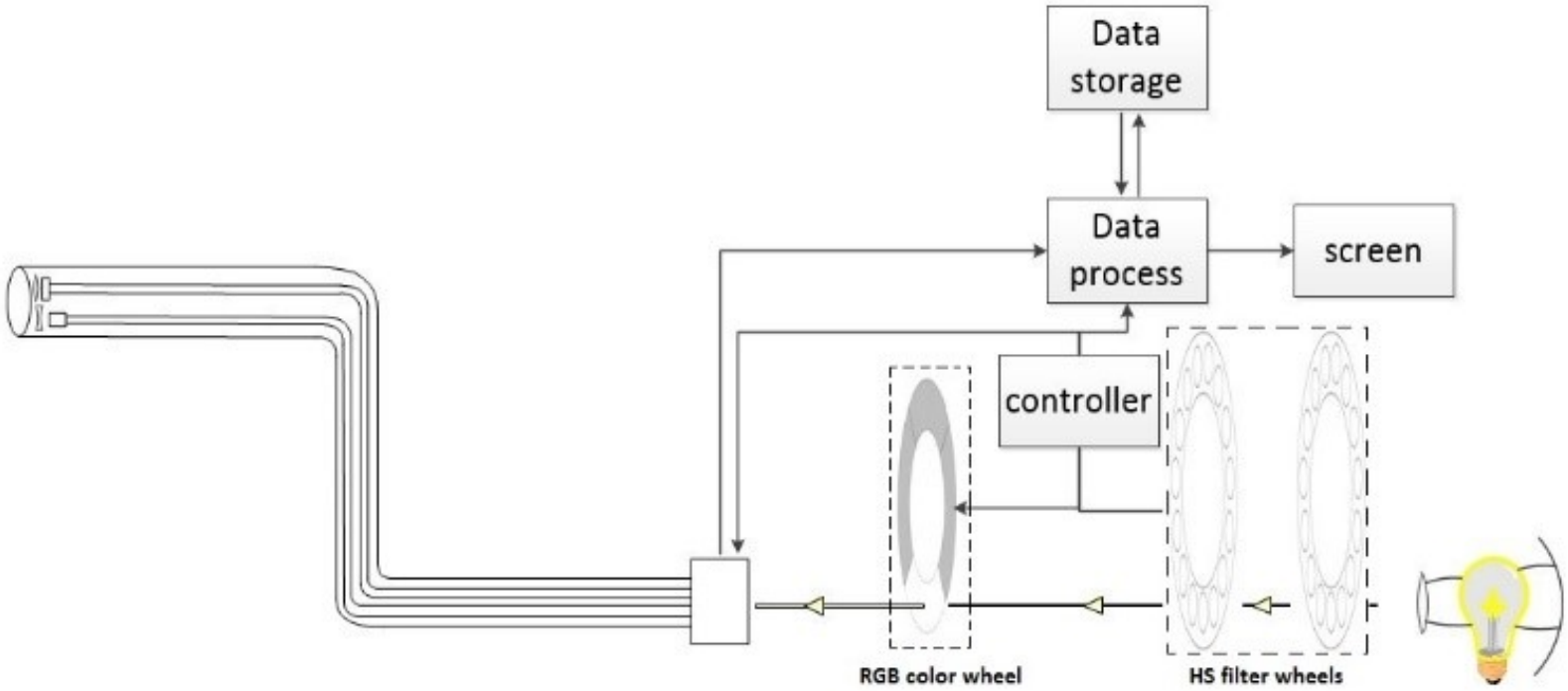

Figure 15: The diagram of the HS system contains two filter wheels

3.3 Geneva Mechanism to Drive Filter Wheels

As step motor has so slow moving speed that it needs more time to obtain the HS images and there will be more object shift and deformation during the acquisition, we drive the filter wheel and switch the filters using brush-less DC motor to meet the requirements of rapid data acquisition. Geneva mechanism is applied to connect the brush-less DC motor and the filter wheel. Figure 17 shows the working principle of Geneva mechanism.

There are two parts for the Geneva mechanism. Part 1 is master reel driven by the DC motor. Part 2 is slave wheel. When the master reel runs among the range of $2\varphi_1$ during a circle under the driving of DC motor, the slave wheel runs $2\varphi_2$ following the master reel. Beyond the range of $2\varphi_1$ for master reel, the slave wheel halts for CCD exposure. Thus the master runs continuously, the slave wheel runs step by step. As there are 17 holes on a wheel, the master reel run 17 circles and the filter wheel will run a circle which consists of 17 steps. Then we have $\varphi_2 = \frac{2\pi}{2\times 17}$, and $\varphi_1 = \frac{\pi}{2} - \varphi_2$. Figure 18 shows the prototype of the Geneva mechanism in our system. The physical device will be showed in later sections together with other parts.

Under driving by Geneva mechanism, all 34 HS images could be acquired in 4.2 seconds.

3.4 Other Modifications on the Platform

Although this part is the most time-consuming work for this thesis, it is mostly about engineering. Thus only brief introductions are given in this section. Generally, it has two aspects: optical modification, and electronics modification.

3.4.1 Optical Modification

To improve the light intensity, we modify the light source part. First, after verifying the fact that the applied filters are within the thermal safety threshold in short

Figure 16: The wheels that contain narrow-band filters and all-pass holes

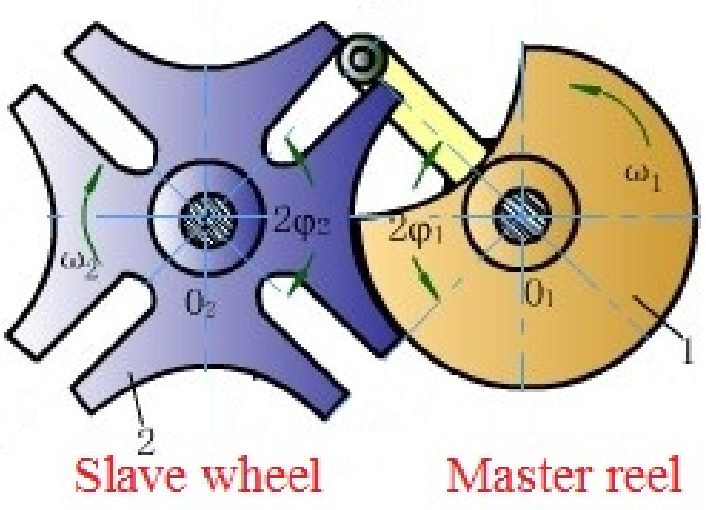

Figure 17: The working principle of Geneva mechanism

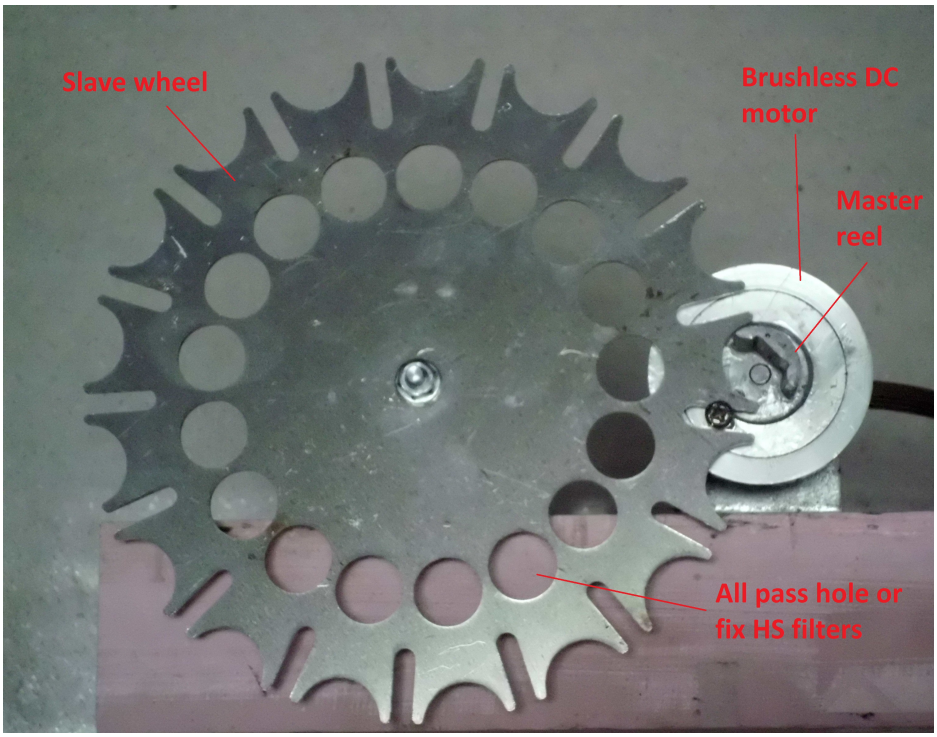

Figure 18: The prototype device of Geneva mechanism applied in our system

illumination period, we replaced the 150 Watts Xenon lamp of a 300 Watts one. Due to the different sizes of the lamp, we re-design the light source location and posture. Figure 19 shows the re-designed lamp unit.

Then we modify the optical path to improve the light efficiency. Distances between lens are changed following the simulation of Zemax. Figure 20 shows these changing. Figure 21 and 22 shows the optical path design before and after the modification. Table 9 shows the illuminance intensity improvement after the modification compared to that before the modification without filters.

Moreover, we modified the conventional RGB color filter. We add an all-pass hole on the filter together with locating sensor and driver Printed Circuit Board (PCB). Figure 23 shows the modified unit.

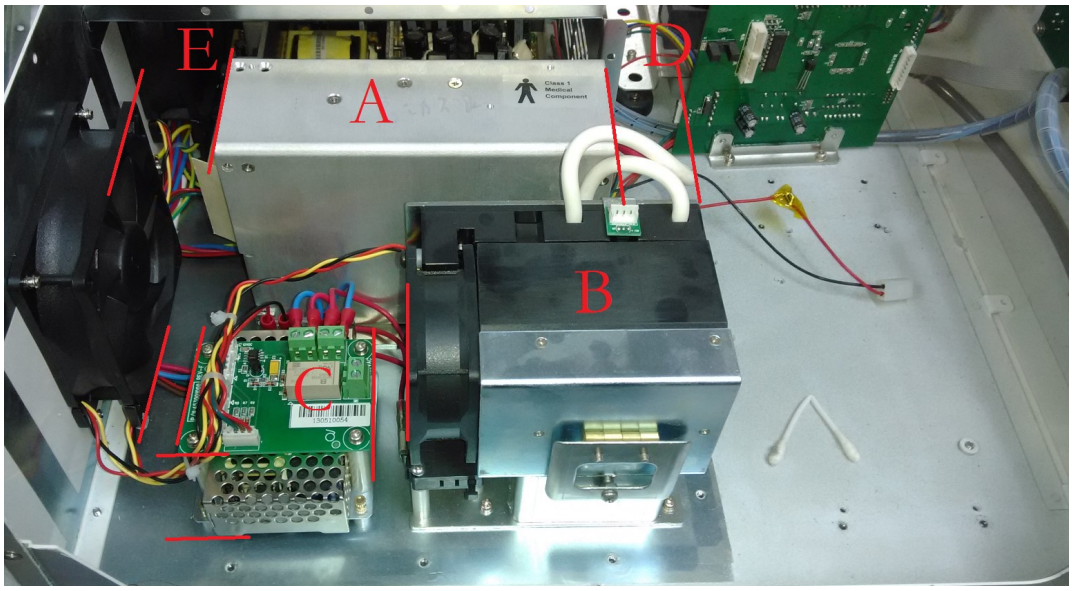

Figure 19: The re-designed light source with higher power. A is power unit, B is Xenon lamp, C is driver unit, D and E indicate other modified part, such as fan

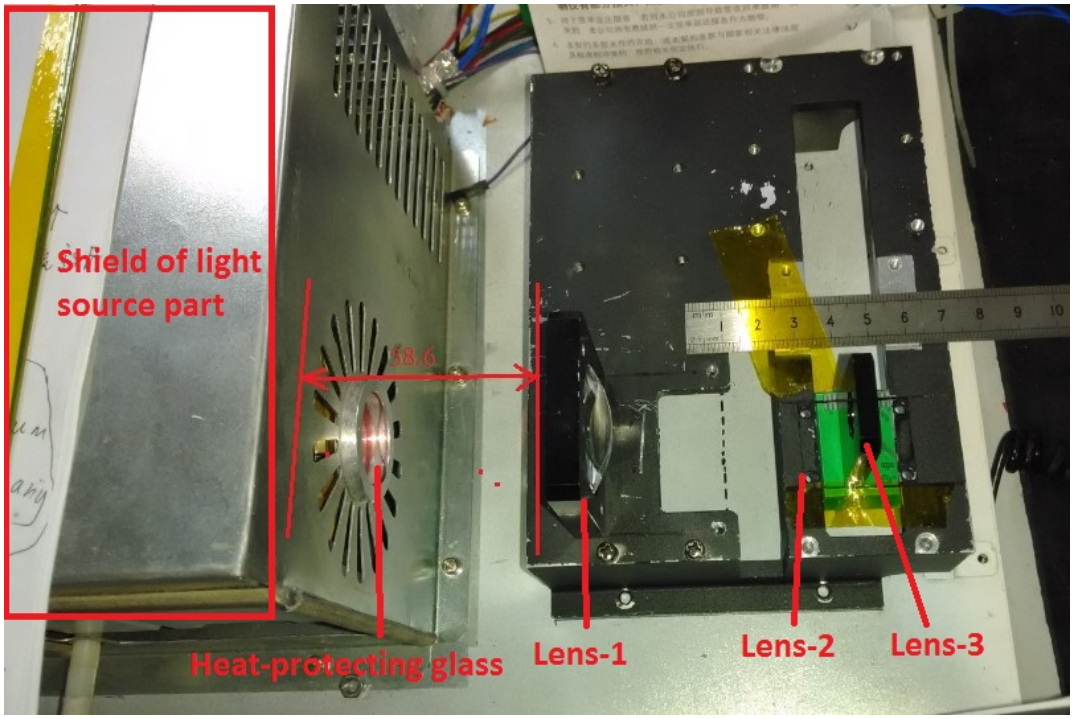

Figure 20: The lens in the system

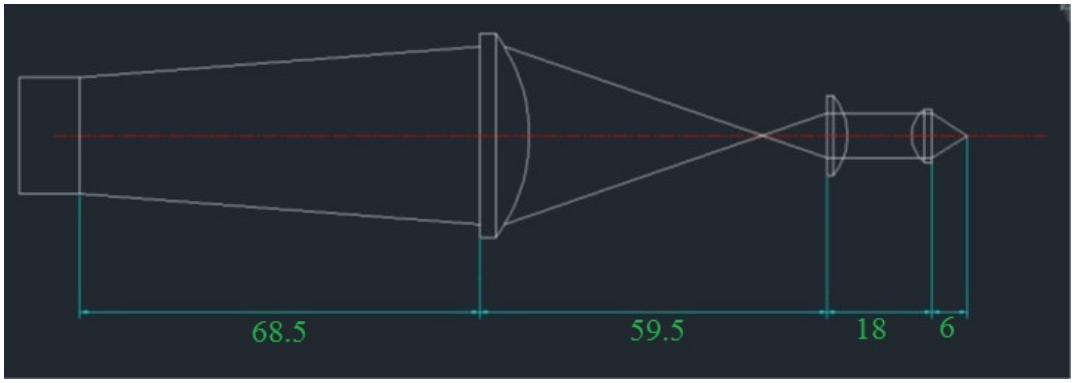

Figure 21: The optical path before the system modification

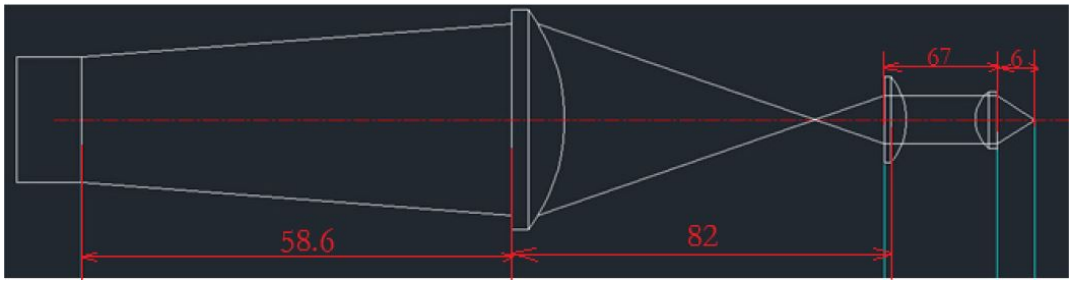

Figure 22: The optical path after the system modification

Table 9: Illuminance before and after the optical path modification without filters

Illuminance (Lux) & Locations	After heat-protecting glass	After Lens-1	After Lens-2	After Lens-3
Before modification	478200	451100	330000	48833
After modification	478200	471100	470000	94433

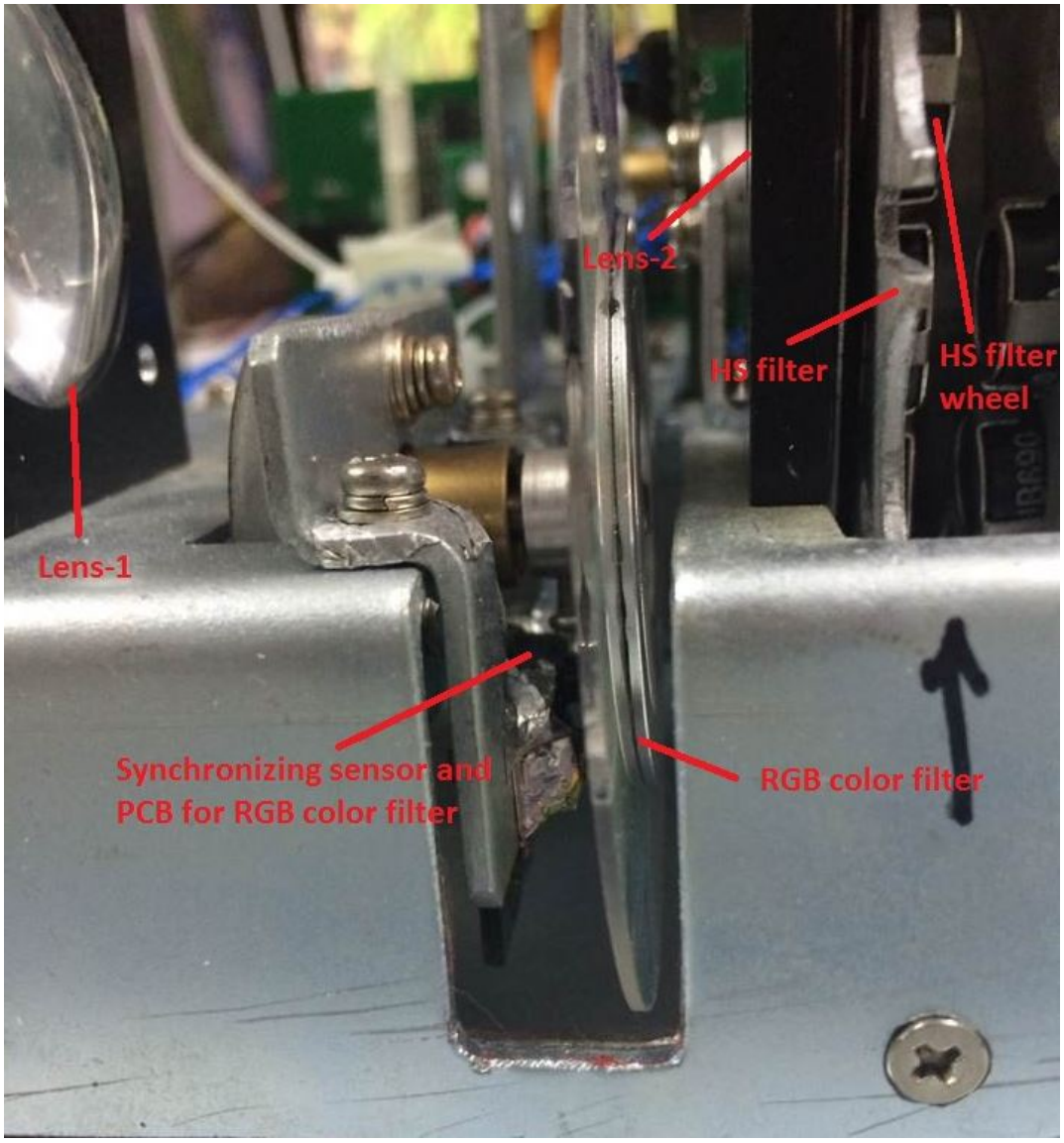

Figure 23: The modified RGB color filter unit. We add an all-pass hole on the filter, and corresponding locating sensor and driver PCB

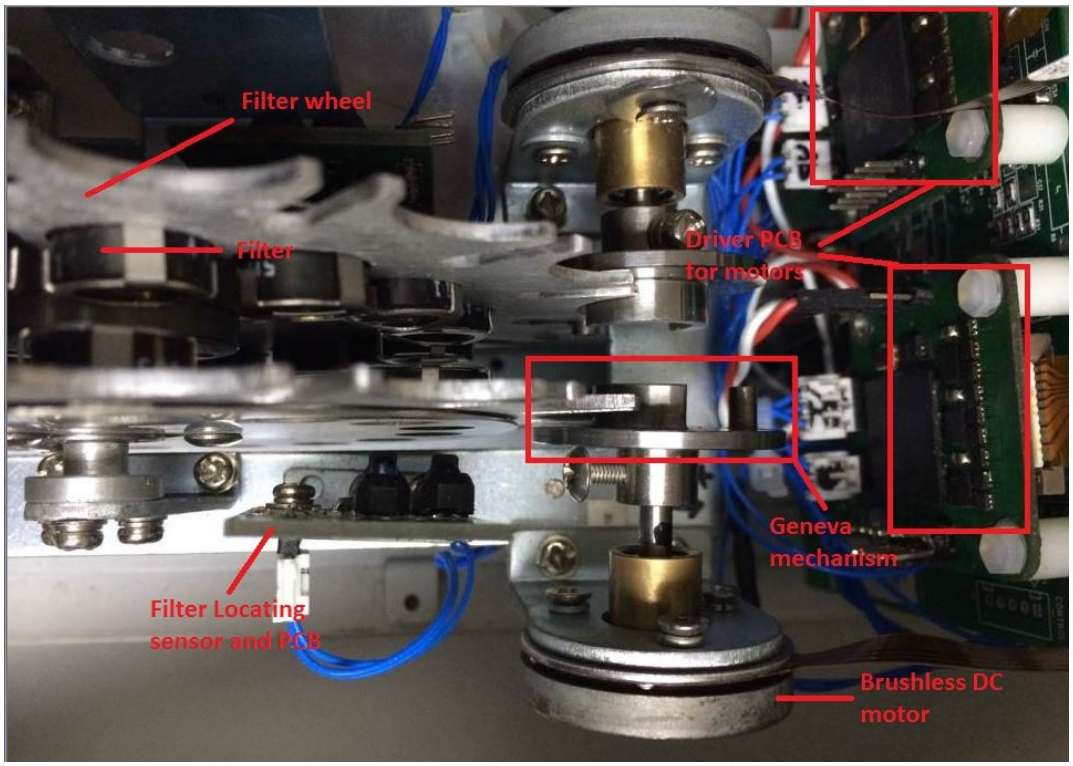

Figure 24: The location of PCBs which are used for driving motors and locating around physical filter wheel and Geneva mechanism

3.4.2 Electronics Modification

We designed and built another several new PCBs to run the system. First, around the physical units of filter wheel, as Figure 24 shows, we build two types of PCB: the motor driver PCB (Figure 25) and filter wheel locating sensor PCB (Figure 26).

Then, Figure 27 (Analog to Digital PCB) and Figure 28 (Digital processing PCB) show the major modified PCBs where image signals from CCD are processed and stored. Programs in Field-Programmable-Gate-Arrays (FPGA) were modified to synchronize the stored signal with Geneva part, and then transfer the images in Memory (Double Data Rate Synchronous Dynamic Random Access Memory(DDR SDRAM)) to workstation computer. A new PCB shown in Figure 29 is built to connect the Memory with computer, and transfer these images. All these hardware and software programs are the most time-consuming work for this thesis, but they will not be

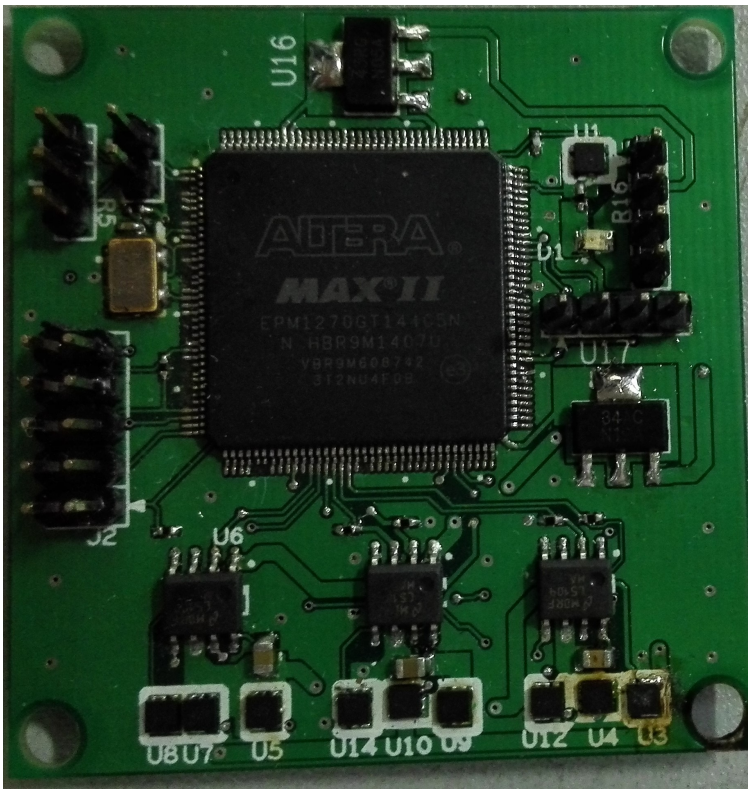

Figure 25: PCB used for driving the DC motor and filter wheel switching

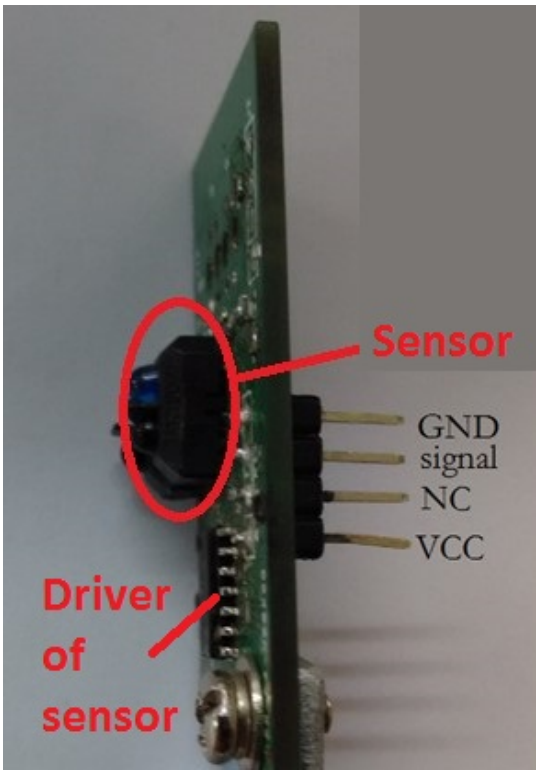

Figure 26: PCB containing locating sensor

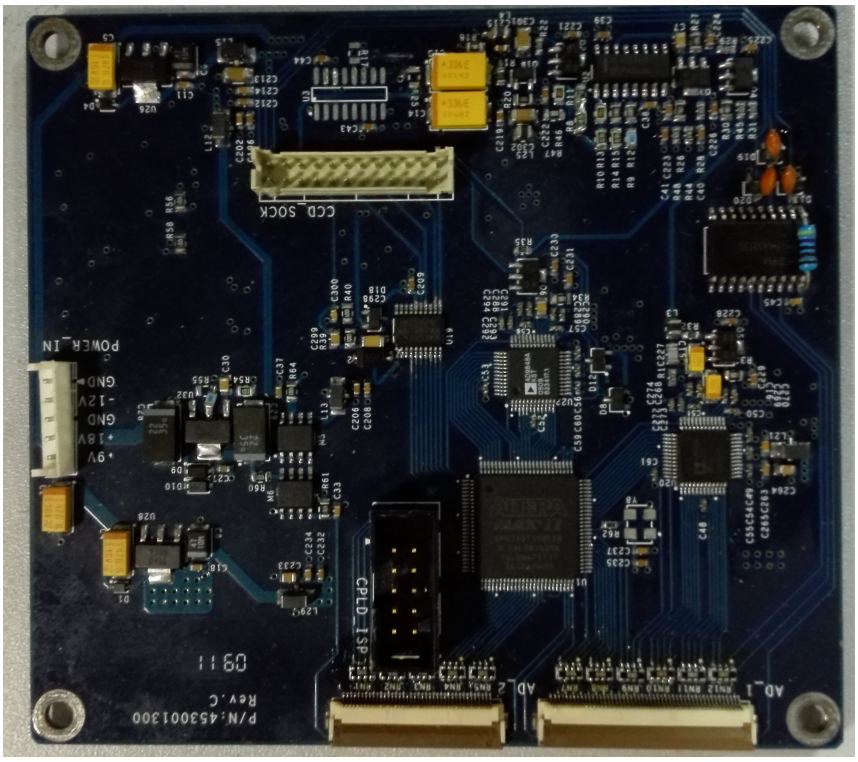

Figure 27: Analog to digital board modified for HS endoscope system

described in detail here.

Moreover, there are many other modifications and works during the system debugging. For example, the key function on the panel and the handshaking communication between different units. As the image signal stored in Memory and transferred to computer is binary data, a Matlab program is written to reconstruct images from these binary signals. All these time-consuming works will not be presented in detail here.

3.5 Prototype Machine

After all above mentioned modifications, the prototype machine of flexible HS endoscope system is developed, as Figure 30 shows. It is composed of four units: HS light source, endoscope imaging unit, image processing unit, and monitor unit (LMD-2451MD, Sony). The hyperspectral light source unit contains a xenon arc lamp (PE300AF, PerkinElmer Optoelectronics), which has an integrated parabolic

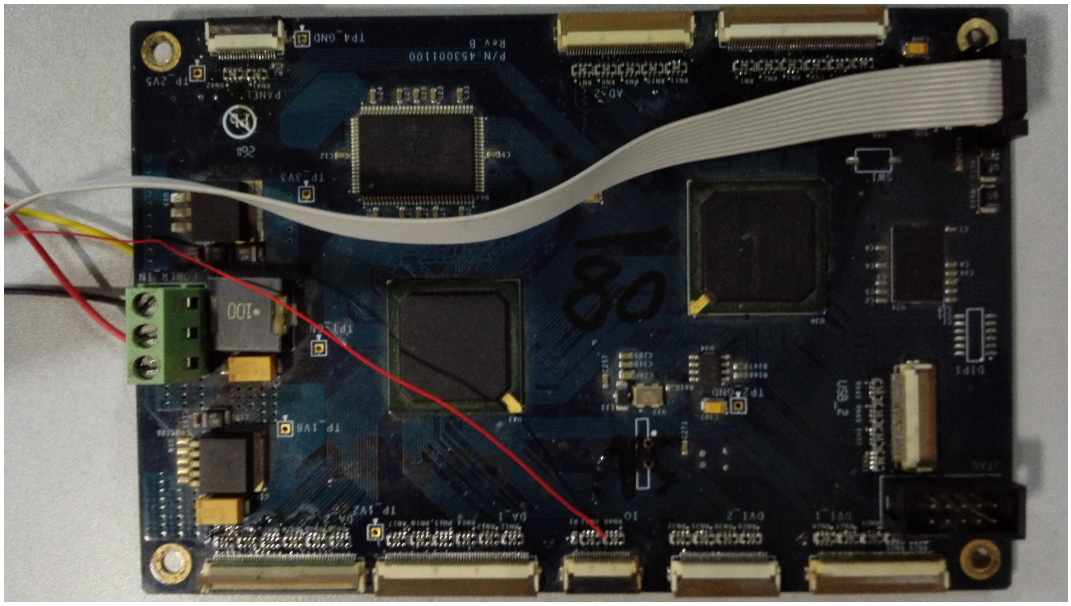

Figure 28: The PCB used for HS image processing. The Memory part and FPGA part are modified

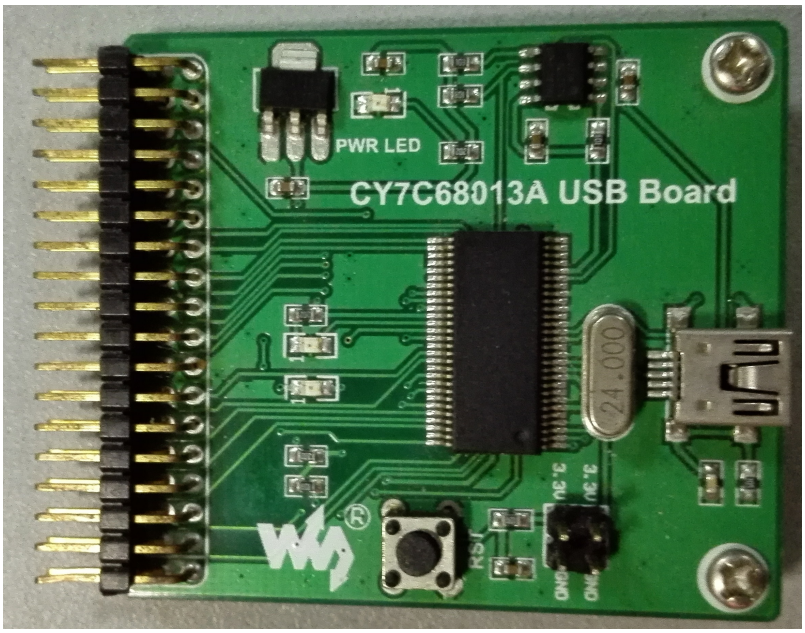

Figure 29: The PCB used for communication between Memory part of endoscope and workstation computer

reflector collecting light from the light bulb and producing a collimated output beam. Twenty-eighty sequential narrow-band band-pass interference filters together with two all-pass holes are mounted in two motorized filter wheels positioned in the path of the collimated beam. In conventional white light illumination mode, RGB color filters are switched and all-pass holes in HS wheels are in the illumination beam path. When suspect disease area is targeted and HSI mode is enabled on machine panel, the RGB color filters is stopped at the all-pass hole in 4 seconds, and then the 28 monochromatic spectral-channel light beams are produced sequentially in 4.2 seconds as the filter wheel rotates. An optical fiber bundle directs the beams to the mucosa after the optical taper focuses the light onto the bundle. A combination of lenses is attached to the distal end of the fiber bundle. Then lens combination generates a 5.0 cm diameter illumination spot at a working distance of 2.0 cm. A 582 $\times$ 752 pixel monochromatic CCD (ICX279AL, Sony) positioned at the distal end of the optical fiber bundle is used to spectrally resolve the reflectance images from the mucosa. Analog signals read from the CCD are sequentially transformed into digital signals in the image processing unit. A cable is used to connect the image processing unit to the medical monitor, which is used to display the reflectance images from the mucosa.

3.6 System Stability and Problems

Before the clinical trials, we test the system stability and potential problems in our lab. Table 10 shows the test results. The success rate of HS image acquiring function is 97% after 700 tests. And the solution of these potential problems is to restart the system power which cost only 5 seconds. As there is no serious problem or risk to cause patients any additional damage, this system is considered to be reliable enough for clinical evaluation.

Figure 30: The prototype machine of flexible HSI endoscope system

Table 10: Test results of system stability and potential problems before clinic trials

Test	Number
Success	679 (97%)
HS function cannot start	3
HS just enables one filter wheel	1
HS function is enabled, while there is no data received by computer	8
Conventional RGB imaging cannot recover after HS image acquisition	4
Color changes after HS image acquisition for conventional imaging	5
Total	700

3.7 Summary of The System

Compared to other HS endoscope systems mentioned in "State of Art" part, this new system has several advantages and innovations. First, two filter wheels driven by Geneva mechanism is used to switch the filters. It costs much lower ($ 3k v.s. $ 20k for AOTF), and provides higher light throughout under the same FWHM (maximum transmission rate ∼60% v.s. 45% for LCTF). Two patents has been authorized in China to this part. Second, this new system supports flexible endoscope, and is capable to make GI tract examination in vivo. Most other systems are rigid, and cannot be applied in GI tract. Compared to the few flexible systems, this system has the narrowest FWHM, which means the largest number of spectral channels, and most accurate measurement of spectral information. Third, this system does not trade off the spatial resolution for imaging speed. Compared to the system in literature[63], our system has higher spatial resolution (582×752 v.s. 350×350).

On the other hand, this system has its own limitations. First, compared to AOTF and LCTF, this system costs more time to finish the image scanning along spectral axis. Hence, the object deformation and moving during this imaging period must be compensated in following image processing part. Second, the dispersive device has

mechanical moving parts, and the stability during clinical trials is lower than AOTF and LCTF. The noise caused by the moving mechanical part is also needed to be resolved. Third, the applied CCD must be with small size to meet the requirement of clinical in-vivo application, so that cooled CCD with bigger size cannot be applied in our system now. Thus the wavelength range of this system is limited in VIS region, and cannot be extended to NIR and MIR regions. All these challenges are needed to be overcome in future.

CHAPTER IV

CLINICAL EVALUATION

In this chapter, we introduce how we evaluate this new developed HS endoscope system in clinic. First, we got ethics approval for clinical trials. Then, after designing the protocol on how to make the trials, we obtained HS images on GI diseases inside patients' bodies using this system. The summary of clinical trial results are presented in the following part. Next, we analyzed some typical HS images tentatively. After making first-glance studies, the method of Contrast Calculation, Dependence of Information, and Recursive Divergence are implemented to extract valuable and diagnostic information from HS images. All these results prove the effect and applicability of this new HS endoscope system.

4.1 Ethical Approval

We got ethical approval for clinic data acquisition at Zhongshan Hospital (Shanghai) on November, 2012. The clinical trial should be started in one year since the approval. Appendix A shows the ethical approval files.

4.2 Protocol For Clinical Data Acquisition

Before we made clinical trials, a protocol was designed. Appendix B shows the protocol file. It consists of six components: Background, Aims and Contents for Clinic Trial, Overall Design, Manipulation of the System, Targeted Capacity of Trials, and Record Table. The "Background", "Aim and Contents", and "Manipulation of the system" parts are brief edition of "introduction" and "system development" parts of this thesis. The planned capacity of this clinic trial is ∼100 patients with 2-3 HS image cubes for each patient. Both normal mucosa and disease tissues would

Table 11: System stability in clinic trials

Clinical Trial Date	Success Rate
2013	0/3
2015	63/66 (95.4%)

be observed. The "Overall Design" part contains four units: 1) Patients' condition and test range. We just acquire data on patients who have the ability to undertake examination using GI endoscope. 2) Equipment preparation. We will prepare in advance all kits and materials that patients need in the examination. 3) Procedure of clinical trials. Figure 31 shows the diagram of the procedure. First, we need to inform the patient of the clinic trial in detail, and get consent. Second, endoscope doctors manipulate the system and make conventional endoscopy examination under white light illumination. If disease or normal mucosa area is targeted, we enable HS data acquisition, and obtain and transfer HS images into workstation computer. After this, doctors may take biopsy on the disease area. Next, doctors will continue the conventional examination, until the next HS data acquisition or the end of examination. After finishing the examination, we will record the report according to the table in Appendix B. And the endoscope will be sterilized to get ready for the next patient. HS images will be analyzed finally after all clinical trials. 4) Future work. This part includes the plan for HS image analysis and possible achievement for this clinical trial, such as published articles or patents.

4.3 Clinical Trials

We made clinical trials for two times. The first time last from November 8^{th}, 2013 to November 10^{th}, 2013. The second time last from September 1^{st} to 18^{th}, 2015. Table 11 shows the system stability in clinic.

Until now (September 22nd, 2015), we have obtained 58 HS image cubes from 23 patients in clinic trials. Table 12 shows the results summary. Table 13 shows the

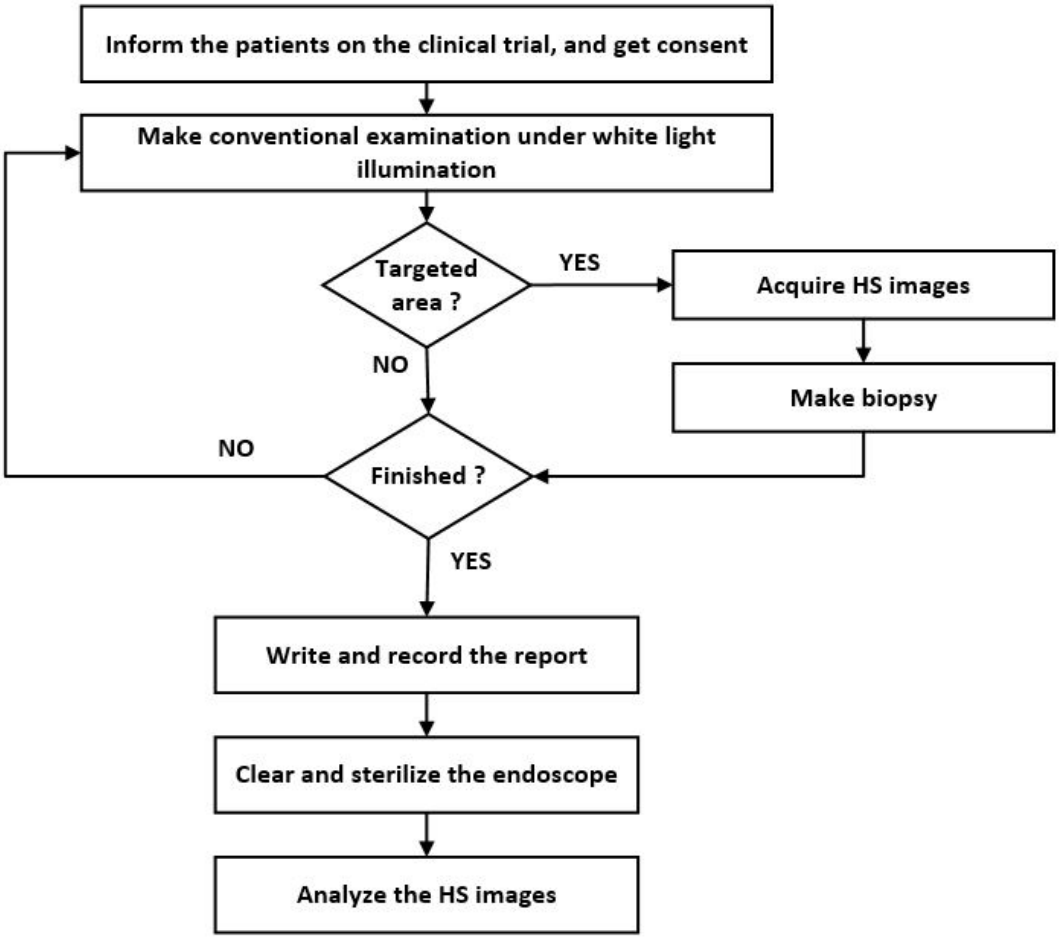

Figure 31: The block diagram of procedure to make clinic trials

Table 12: Summary of results of clinic trials

Patients	HS image cubes	Organs		Diseases	
23	58	Esophagus	3	Normal	2
				Malignant Tumor	1
		Stomach	29	Normal	1
				Gastritis	3
				Polyps	2
				Erosion	5
				Ulcer	2
				Hyperemia	9
				Submucosa masses	7
		Duodenum	5	Frost-spot ulcer	2
				Bulbar ulcer	3
		Colon	21	Normal	3
				Polyps	14
				Malignant Tumor	4

Table 13: Summary of HS image cubes before clinic trials

Volunteer	HS image cubes	Organs		
15	48	Under tongue		23
		Upper jaw		8
		Inside gill		3
		Lip	Normal	2
			Ulcer	8
		Wrist skin		4

summary of obtained HS image cubes from volunteers before the clinic trials. These HS cubes are mostly on oral mucosa and skin.

4.4 First Glance Findings

Figure 32 shows some images from a clinical HS image cube on colon polyps. And we can see from these images that vessel patterns and spectral information are different.

Figure 33 shows images from another HS cube. The boxes shows the area of residual. Figure 34 shows the enlargement images of the box.

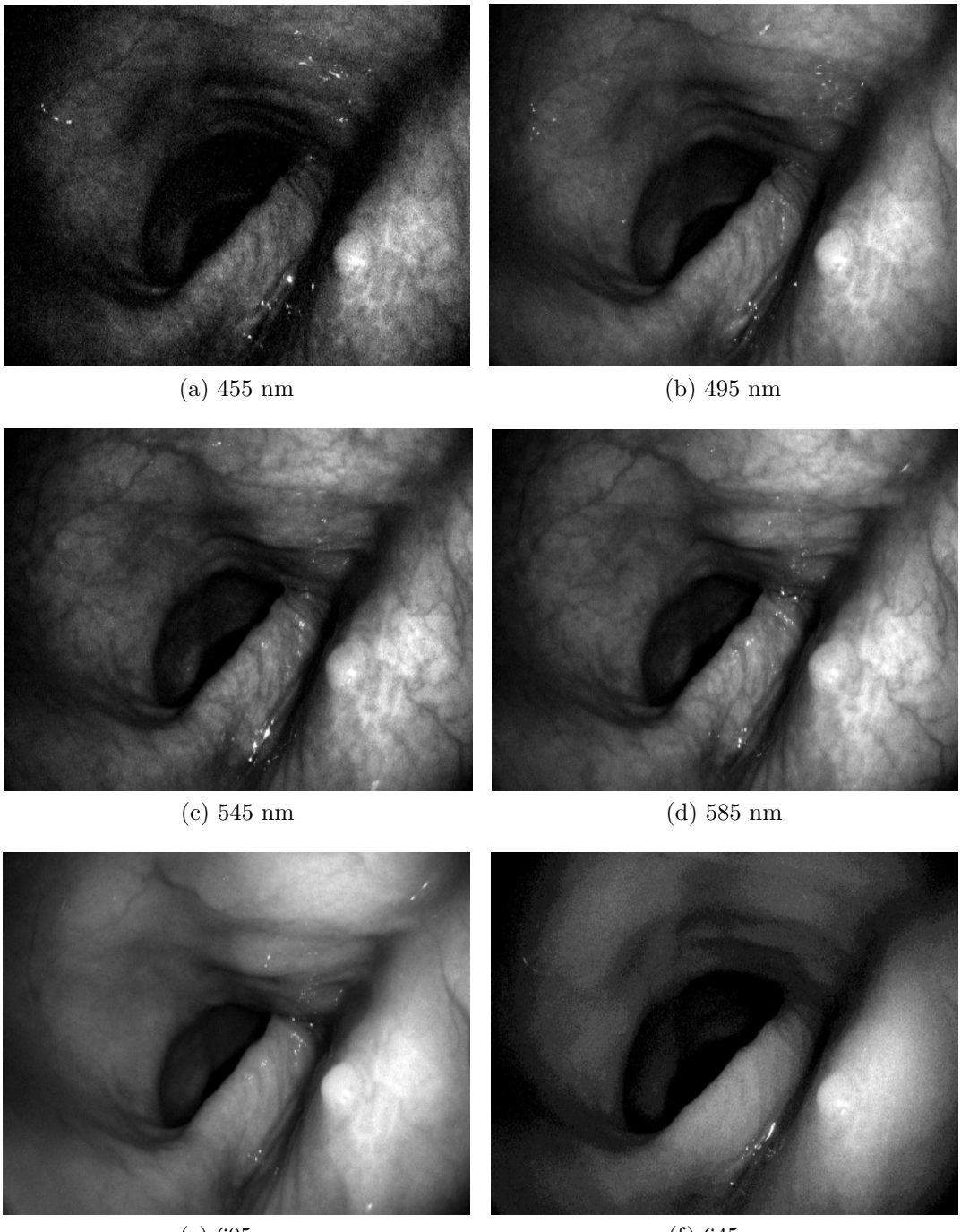

(a) 455 nm (b) 495 nm

(c) 545 nm (d) 585 nm

(e) 605 nm (f) 645 nm

Figure 32: Some images from a clinical HS image cube on colon polyps. The wavelength of these images are centered at 425 nm, 455 nm, 495 nm, 545 nm, 585 nm, 605 nm, 645 nm, 680 nm (25nm)

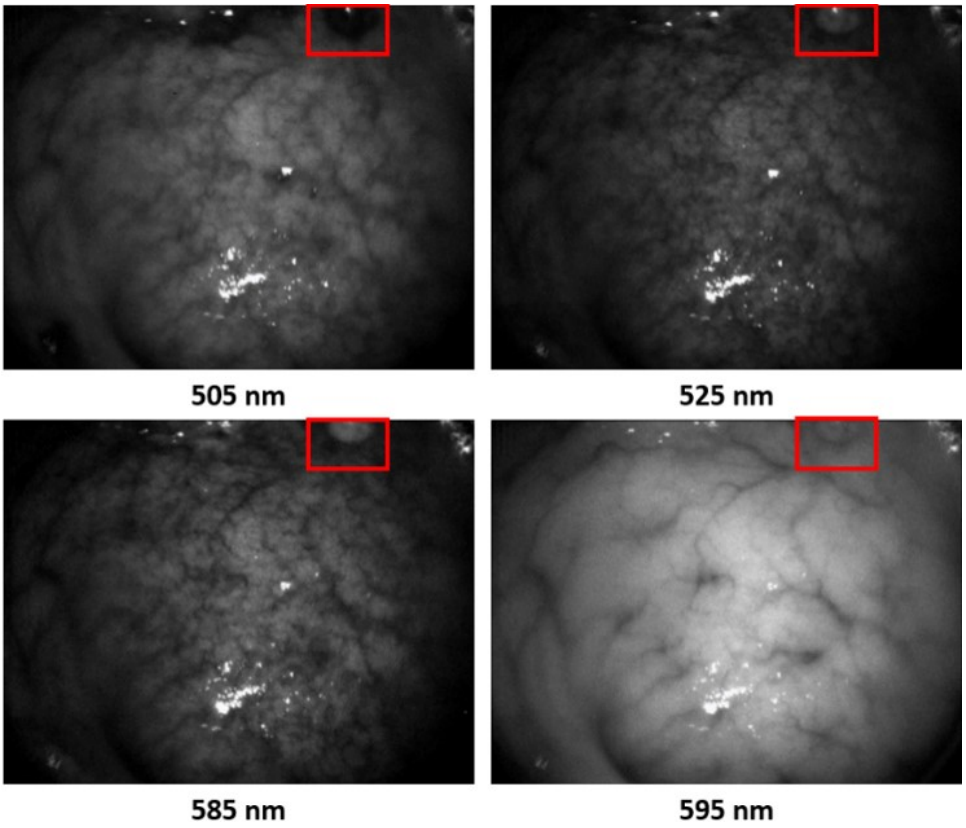

Figure 33: Some images from an HS cube on normal tissue and residual

We can find something interesting from this HS image cube from the first glance. First, there is significant difference between image centered at 505 nm and that at 525 nm. Second, there is significant difference between image centered at 585 nm and 595 nm. These differences displays distribution information on residual and vessels. Third, the difference between image centered at 505 nm and that at 585 nm contains vessel depth information. These first-glance findings prove that the HS images on GI mucosa in vivo could indeed provide useful spectral information to help diagnosis.

4.5 HS Image Analysis

Image analysis extracts diagnostically useful information from spectral images on tissue, cellular and even molecular levels. Therefore, it is critical for digestive tract disease detection, diagnosis and treatment. Generally, as Figure 13 shows, the basic

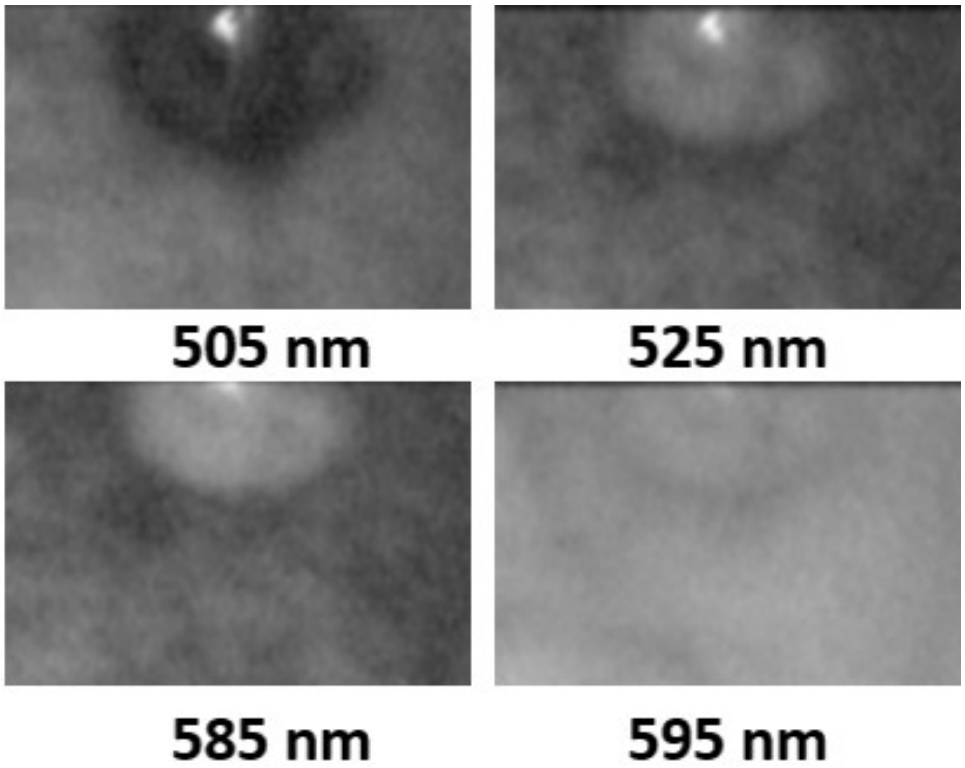

Figure 34: Enlargement of images marked by boxes of Figure 33

procedure for spectral image analysis involves preprocessing, feature extraction and selection, image classification, and image enhancement. As there are many review papers on spectral image analysis in medical area, we introduce this part in brief, focusing on some particular cases in digestive tract examination field. Detailed description of these algorithms is beyond this paper and interested readers may check references to identify them. In this chapter, we do not propose new methods to make HS image analysis. We just applied methods in previous literatures on the data we obtained and got different results.

4.5.1 Pre – processing

We make pre-processing from four respects: CCD calibration, illumination normalization, image registration, and contrast tuning. All these four methods are from previous literatures. We just introduce the algorithms briefly.

CCD Calibration

In above chapters, we introduce a model for endoscope imaging, as Equation 1 shows. In the Equation, $t_i(\lambda)$, $E(\lambda)$, $S(\lambda)$, and $\gamma(x, y, \lambda)$ are the spectral transmittance of the i^{th} spectral filter, the spectral radiance of the illuminance, the spectral sensitivity of the camera, and the spectral reflectance of an object, respectively. Given $E(\lambda)$, $S(\lambda)$, and $t_i(\lambda)$, $\gamma(x, y, \lambda)$ of the object can be evaluated. We can measure transmission curve of filters, and obtain the Xenon lamp spectrum and CCD sensitivity curve that can be used for CCD calibration on device Datasheets.

Illumination Normalization

Foracchia et al.[36] proposed a method to make background estimation and contrast enhancement for retinal vessels at the same time. They first calculated average value and deviation of a pixel's neighborhood. If the value of the pixel is beyond the variance of its neighborhood, they considered the pixel as one of the vessels. If not, the pixel is considered as background. We apply this method on HS images to normalize the illumination.

Image Registration

There have been a lot of image registration algorithms to compensate the shift and deformation among HS images, such as SURF, SIFT, ORB, and BRIEF, described in above chapters. We just apply ORB methods on our HS images, and Figure 35 shows the registration results. The highlight pixels on the images are manually invalidated, and will not be calculated.

Figure 35 shows the registration results for HS images.

Contrast Tuning

Before making information extraction, we also make contrast tuning using method in literature[49]. For pixels inside targeted area, we calculate the average value among

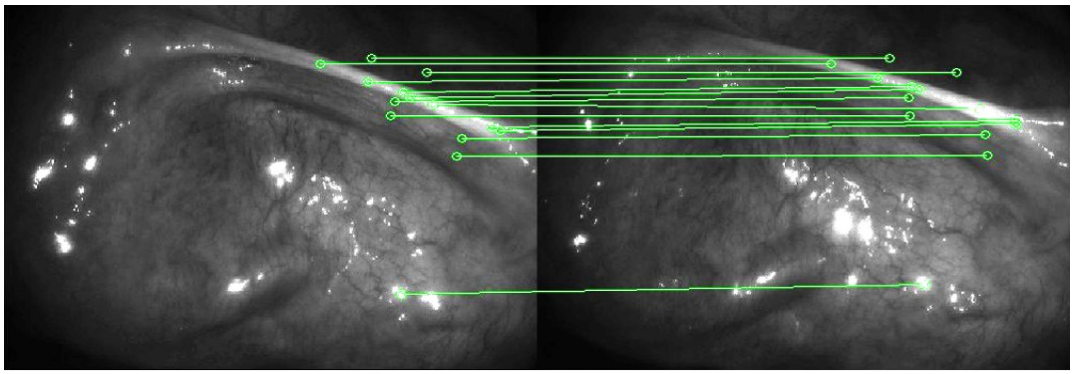

Figure 35: The registration results of HS images

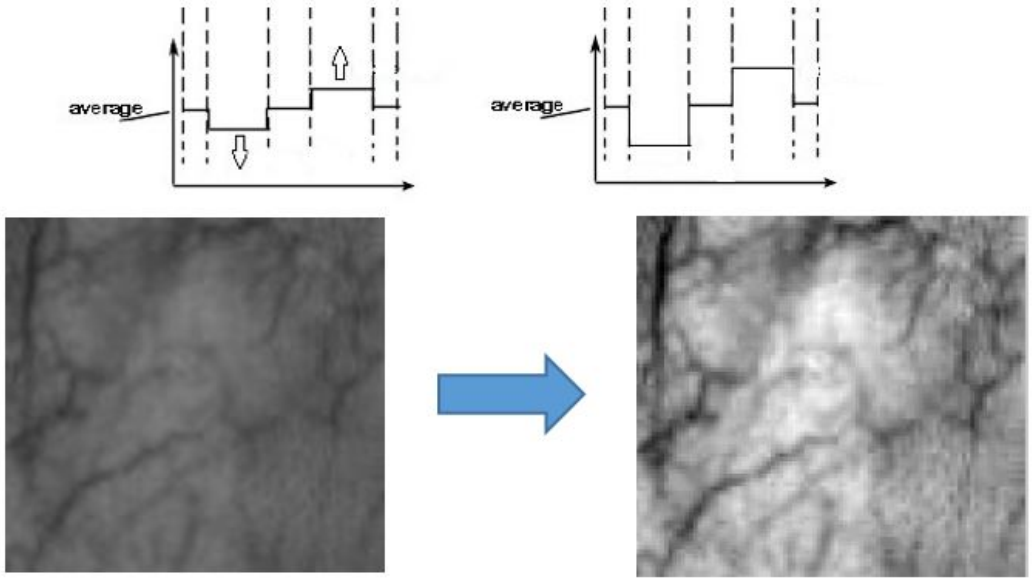

Figure 36: The principle diagram and simulation results of contrast tuning method

the area at first. For the pixels with value larger than the average value, they will get larger. While for the pixels lower than the average value, they will get lower. Figure 36 shows the working principle and simulation results of this method.

4.5.2 Information Extraction

In this section, we apply three methods from previous literatures on the HS images we obtain: Contrast Calculation, Dependence of Information, and Recursive Divergence. Again, methods will be introduced briefly, and simulation results applying these methods on our acquired HS images will be presented.

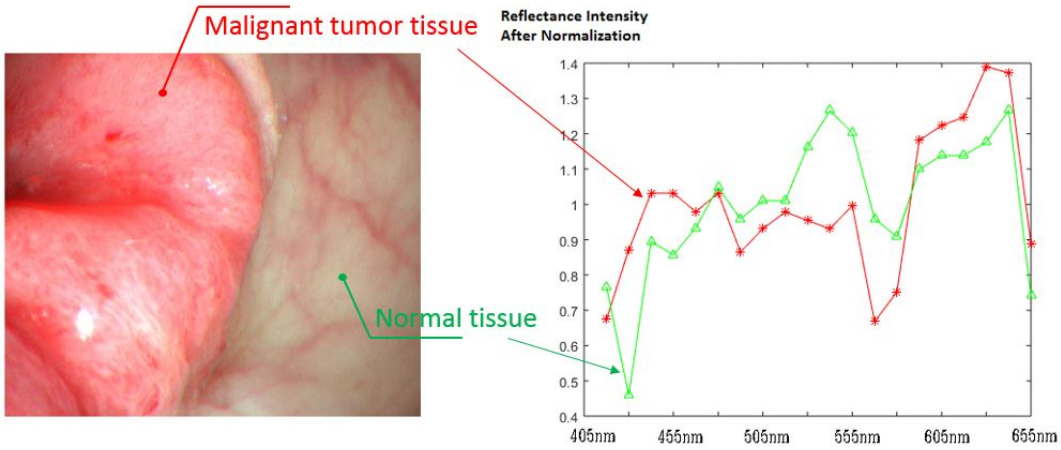

Figure 37: Color image of a colorectal malignant tumor and a graph showing spectral reflectance of the tumor and normal mucosa in the wavelength range of 405 to 655 nm

Pixel – based Analysis

Figure 37 shows a color image of a colorectal malignant tumor and its surrounding normal tissue, together with a graph showing spectral reflectance (SR) of the tumor and normal mucosa in the wavelength range of 405 to 655 nm. We can see that the spectral curve of tumor tissue is different with that of normal tissue.

Figure 38 shows some images from an HS image cube for the colorectal tumor. These images are centered at 405 nm, 455 nm, 545 nm, 585nm, 595nm, and 655 nm respectively. The spectral characteristics in the tumor and normal tissue regions are significantly different corresponding to wavelengths. Except for the image centered at 405 nm which is with low light intensity, the microvascular patterns are clearer on the images centered at 455 nm, 545 nm, and 585 nm than those centered at 595 nm and 655 nm.

Figure 39 shows SR for all pixels in the tumor region and in the normal mucosa. The SRs in the tumor regions tend to be high in wavelength bands above 585 nm and low in the region of 475 to 585nm.

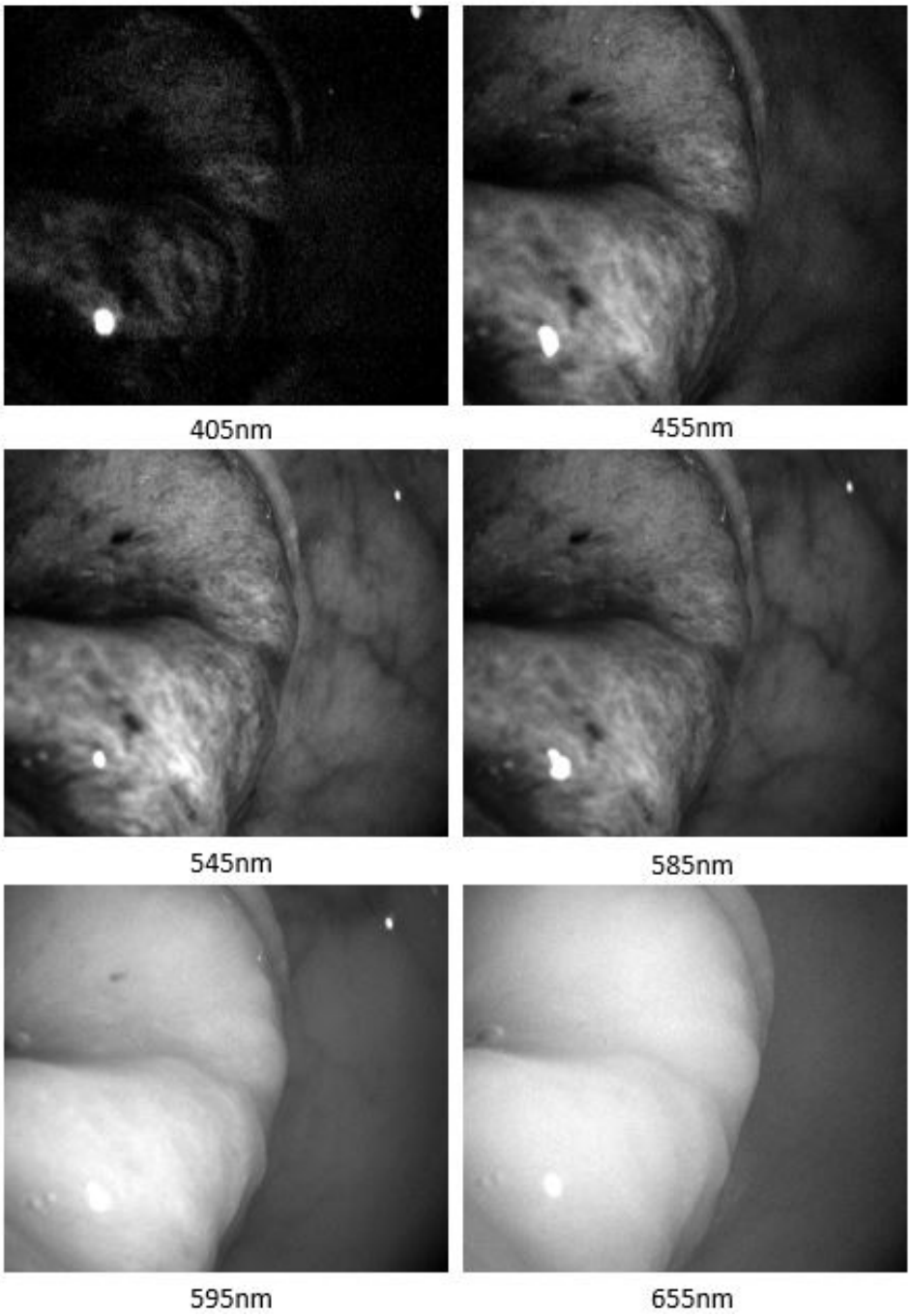

Figure 38: Images from an HS image cube for colorectal malignant tumor. Images are centered at 405 nm, 455 nm, 545 nm, 585nm, 595nm, and 655 nm respectively. The spectral characteristics in the tumor and normal tissue regions are significantly different corresponding to wavelengths

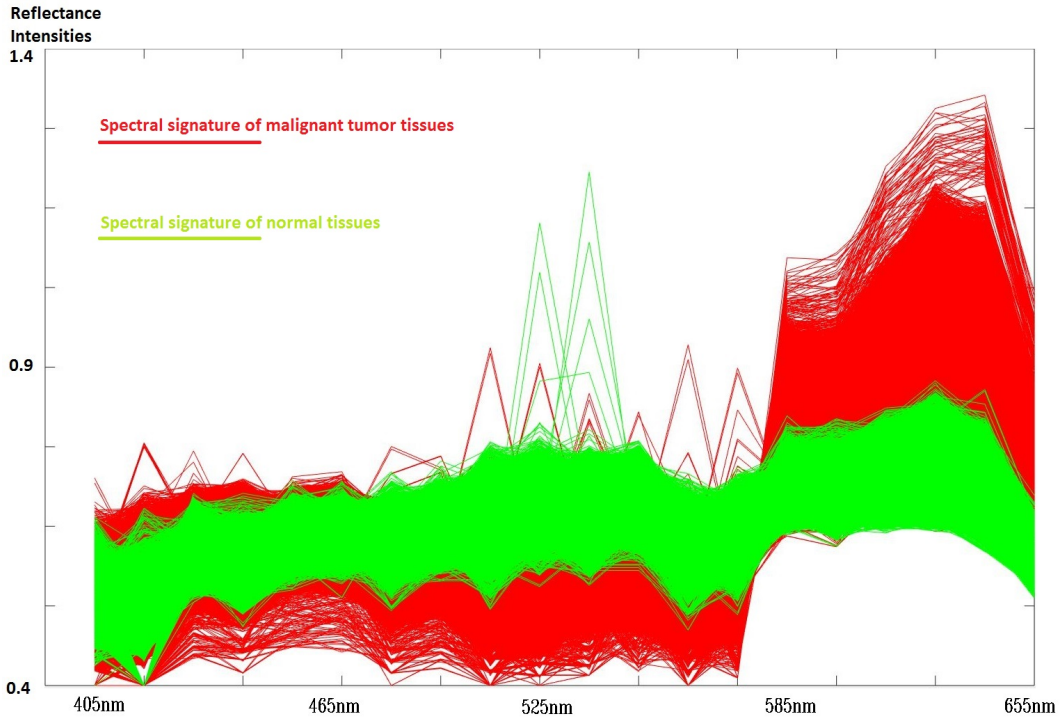

Figure 39: All SR for pixels in the tumor region and in the normal mucosa. The SRs in the tumor regions tend to be high in wavelength bands above 585 nm and low in the region of 475 to 585nm

Hemoglobin Distribution In theory, Index of Hemoglobin (IHb) has been come up with to indicate the hemoglobin distribution and oxygen content which are signals that can be used to make slight color tone change clear[101]. IHb is defined as Equation 8[134] shows. R and G are red and green components of conventional color image, respectively.

$$IHb = 32 \times \log \frac{R}{G} \tag{8}$$

As Figure 40 shows, hemoglobin absorbs light largely around 540nm[128], thus G component contains much spectral information on concentration of hemoglobin, penetrating deeper than B component. However, the R and G components dilute the spectral information. We calculated the IHb using the spectral images around 540 nm and 620 nm (replacing G and R components). This new type of IHb is expected to be more accurate than that based on R and G components. Figure 41 shows the calculation results of new IHb after assigning pseudo colors. We can find that

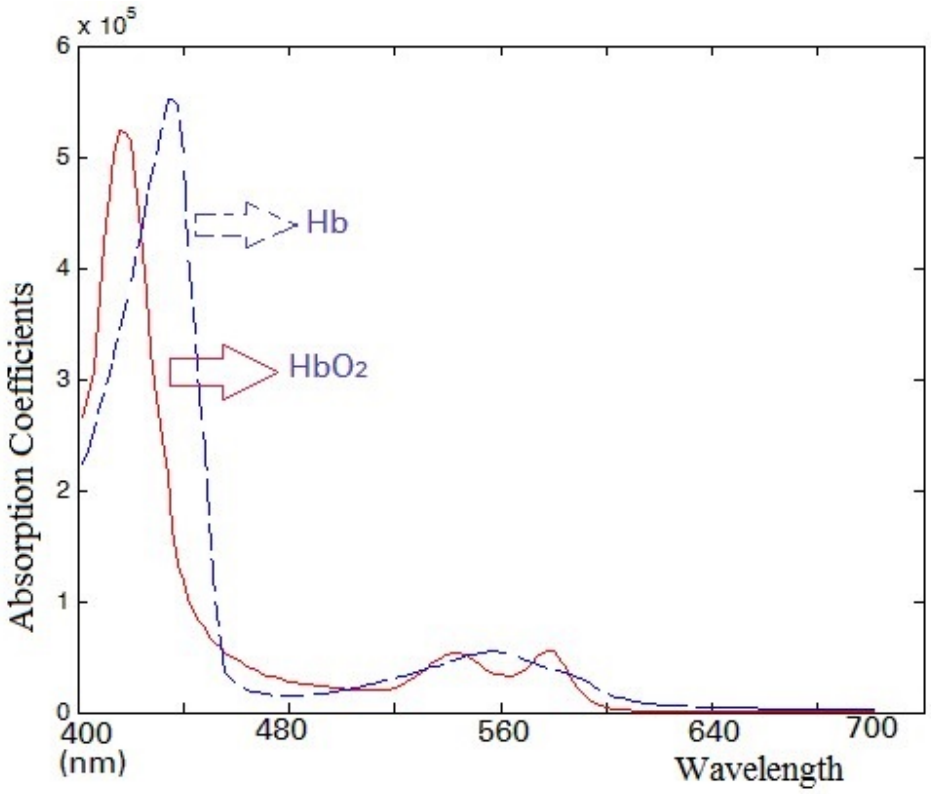

Figure 40: Absorption coefficients of oxy-hemoglobin and deoxy-hemoglobin

there are significant differences among hemoglobin distribution and oxygen contents between tumor tissue and normal tissues, and that new IHb definition could be used to classify the tumor region from normal tissues.

Contrast Calculation

Method Introduction This method is applied on the HS images of vessels. As we know, there is no step edge for intensity of vessel pixels along the direction that is perpendicular to vessel direction[17]. It is Gaussian distribution. Thus the contrast for vessels is defined as $C = \frac{B-A}{B}$, where A is minimum value of the Gaussian curve, and B is the ground value of the curve. B can be estimated by average value of a pixel's neighborhood in a window centered at this manually selected pixel. We can calculate the contrast of a spectral image by getting average contrast value of 30 manually selected pixels on this image. Through this method, we can find the

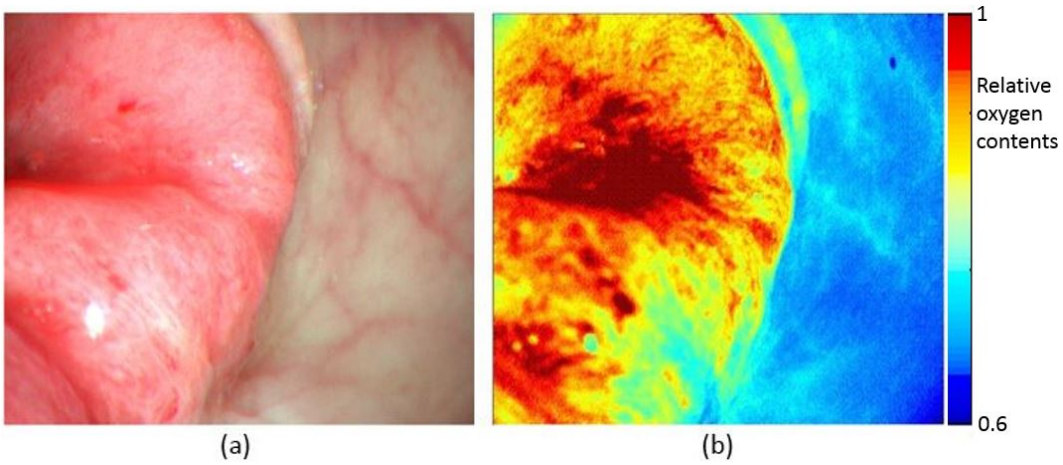

Figure 41: The hemoglobin distribution and oxygen contents calculated by the new IHb definition. Pseudo colors are assigned according to the new IHb values. There are significant differences among hemoglobin distribution and oxygen contents between tumor tissue and normal tissues, and the new IHb definition could be used to classify the tumor region from normal tissues

wavelength at which image has the highest contrast and shows the most clear vessels.

Simulation results applying this method on clinical images We apply this method on sub-tongue mucosa HS images. The object of evaluation is vessels. Figure 42 shows an HS image cube which is simulated using the contrast calculation method. Figure 43 shows the contrast calculation results for eight HS image cubes like Figure 42. As the light intensity is low among 400-440 nm and 660-700 nm and signal-noise-ratio (SNR) is also low, the contrast calculation results among these regions are inaccurate. Thus we just measure the simulation results between the two red line in sub-figure (a) of Figure 43. The same for the other sub-figures. At the same time, Figure 44 shows the absorption curve of hemoglobins.

We can see from these results that the contrast calculation result curve is similar to the hemoglobin absorption curve. Thus the vessel contrast is related to hemoglobin absorption. And this is consistent with the common sense which indicates that the HS imaging could provide useful and accurate diagnostic information.

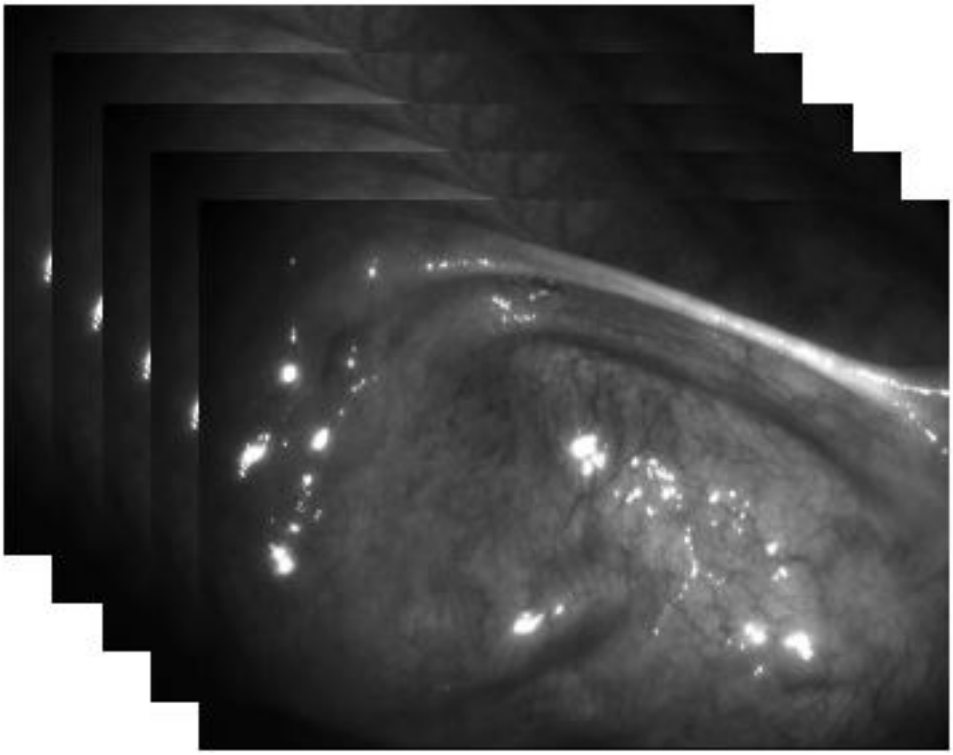

Figure 42: An HS image cube on sub-tongue mucosa which is simulated using the contrast calculation method

Dependence of Information

Method Introduction The entropy of an image is defined as Equation 9[47, 127]:

$$H(A) = -\sum_{A \in A} p(A) \log p(A) \tag{9}$$

where H is entropy, A is pixel variable of the image, and p is the possibility distribution function of A. And joint entropy is defined as Equation 10[47, 127]:

$$I(A, B) = \sum_{A \in A, B \in B} p(A, B) \log \frac{p(A, B)}{p(A)p(B)} \tag{10}$$

where I indicates the joint entropy, A and B represent pixel variable on two different spectral images, and $p(A, B)$ indicates the joint possibility distribution function of A and B. It can be represented as Equation 11:

$$I(A, B) = H(A) + H(B) - H(A, B) \tag{11}$$

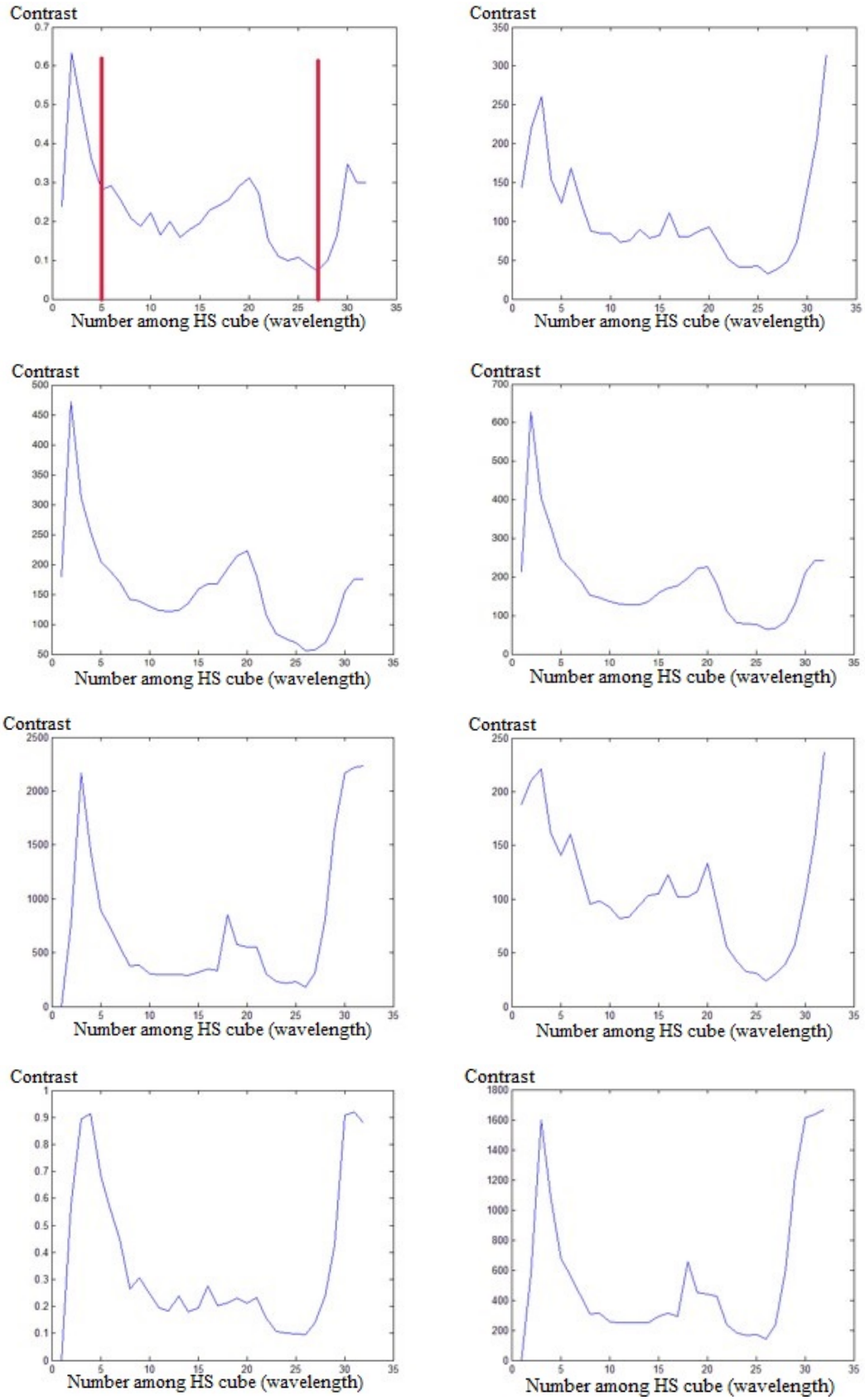

Figure 43: The contrast calculation results for eight HS image cubes on sub-tongue mucosa

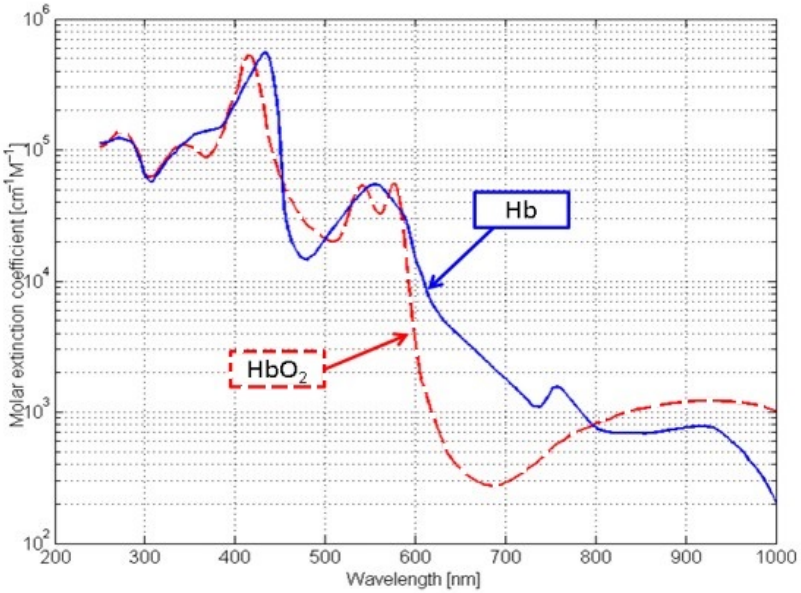

Figure 44: The absorption curve of oxy- and deoxy-hemoglobin

Then Dependence of information (DI) is defined by Equation 12[47, 127]:

$$\Theta_{DI} = H(A_1, ..., A_n) - \sum_{i_1=1}^{n} H(A_{i_1}|A_{i_2}, ..., A_{i_n}) \tag{12}$$

where Θ_{DI} is dependence of information and

$$H(A_1, ..., A_n) = -\sum p(a_1, ..., a_n) \log_2 p(a_1, ..., a_n) \tag{13}$$

$$H(A|B) = H(A, B) - H(B) \tag{14}$$

The index of dependence of information (DI) also can be used to make band selection among the HS image cube. The procedure is as following[127]: 1) Calculate entropy for each image in an image cube, make the image with highest entropy as first main component W_1. 2) Calculate mutual information (MI) between W_1 and other images in image cube, make the image with lowest MI as second main component W_2. 3) Calculate DI among W_1, W_2, and other images in image cube, make the image that minimizes DI as third main component W_3. 4) Continue Step 3) until enough components are found.

Table 14: Band selection result based on DI index

Data acquisition date	Object	1^{st} band	2^{nd} band	3^{rd} band	4^{th} band
9.27.2013	sub-tongue mucosa vessels	580 nm	450 nm	670 nm	520 nm
9.27.2013	sub-tongue mucosa vessels	580 nm	450 nm	620 nm	540 nm
12.7.2013	sub-tongue mucosa vessels	530 nm	450 nm	670 nm	560 nm
12.7.2013	sub-tongue mucosa vessels	550 nm	510 nm	640 nm	620 nm

Simulation results applying this method on clinical images We also apply this method on HS image cubes of sub-tongue mucosa like Figure 42 shows. Four HS image cubes are simulated and four bands are selected for each cube. Table 14 shows the simulation results.

We can find from the simulation results that even for the same object, different HS image cubes may show different band selection results. This may due to the information redundancy among spectral images and the influence of noise and highlight spots. Different environments of acquiring the images may also lead to the different band selection results. However, in statistical research based on large mount of data, the major bands representing the spectral information can be selected: 580 nm and 450 nm. The first band is around the absorption peak of oxy-hemoglobin at 576 nm, and taking the low intensity region (400-440 nm) into consideration, the latter band covers information around absorption peak of hemoglobin at 415 nm. Thus we can find that the band selection method extracts information of vessels relating to absorption curve of hemoglobin. This follows the common sense, similar with results of contrast calculation.

Recursive Divergence

Method Introduction For the training samples of the obtained in vivo HS images, we manually classify them into two classes: disease pixels ω_i, and normal tissue pixels ω_j. Each pixel is a vector along spectral axis. The divergence is defined[30] as the total average information for discriminating class ω_i from ω_j, and given by Equation 15:

$$J_{ij}(\boldsymbol{x}) = \int [p_i(\boldsymbol{x}) - p_j(\boldsymbol{x})] \ln \frac{p_i(\boldsymbol{x})}{p_j(\boldsymbol{x})} \mathrm{d}\boldsymbol{x} \tag{15}$$

where $p_i(\boldsymbol{x})$ is the probability density function of $\boldsymbol{x}$ in class ω_i. The divergence is the symmetric version of Kullback-Leibler distance, and it is non-negative, monotonic, and additive for independent variables. Suppose that signal classes are characterized by p-dimensional multivariate normal distributions: $N(\theta_i, \Sigma_i)$, where θ_i and Σ_i are the mean vector and covariance matrix of class ω_i, respectively. Then the divergence between these two classes is given by

$$J_{ij}(\boldsymbol{x}) = \frac{1}{2} tr\left[(\boldsymbol{\Sigma}_i^{-1} + \boldsymbol{\Sigma}_j^{-1})(\boldsymbol{\theta}_i - \boldsymbol{\theta}_j)(\boldsymbol{\theta}_i - \boldsymbol{\theta}_j)^t\right] + \frac{1}{2} tr\left[(\boldsymbol{\Sigma}_i - \boldsymbol{\Sigma}_j)(\boldsymbol{\Sigma}_j^{-1} - \boldsymbol{\Sigma}_i^{-1})\right] \tag{16}$$

where tr is the notation for the trace of a matrix. For the training samples of the obtained in vivo HS images, the covariance matrix of class ω_i can be calculated as follows:

$$\hat{\boldsymbol{\Sigma}}_i = \frac{1}{n_i} \sum_{j=1}^{n} z_{ij} (\boldsymbol{x}_j - \hat{\boldsymbol{\theta}}_i)(\boldsymbol{x}_j - \hat{\boldsymbol{\theta}}_i)^t \tag{17}$$

where

$$z_{ij} = \begin{cases} 1, & \text{if } \boldsymbol{x}_j \in \omega_i \quad (18) \\ 0, & otherwise \quad (19) \end{cases}$$

, and $n_i = \sum_{j=1}^{n} z_{ij}$, n is total number of samples, and $\hat{\boldsymbol{\theta}}_i$ is the sample mean vector of class ω_i given by $\hat{\boldsymbol{\theta}}_i = \frac{1}{n_i} \sum_{j=1}^{n} z_{ij} \boldsymbol{x}_j$.

Let $J_{ij}(\boldsymbol{x}_p^*)$ be the divergence with p selected bands and $J_{ij}(\boldsymbol{x}_p^*, x_{p+1}^*)$ the divergence with the additional band x_{p+1}^*. Suppose the additional band x_{p+1}^* has mean θ_k^*, variance σ_k^2, and the covariance vector between x_{p+1}^* and the elements of $\boldsymbol{x}_p$, $\boldsymbol{z}_k$ for class k ($k = i$ or j). Then the new mean vectors and new covariance matrix are $\boldsymbol{\theta}_{\boldsymbol{k}}^{\nu} = (\boldsymbol{\theta}_{\boldsymbol{k,p}}^*; \theta_k^*)^t$, $k = i$ or j and

$$\sum_{\boldsymbol{k,p+1}} = \begin{pmatrix} \sum_{\boldsymbol{k,p}} & \boldsymbol{z_k} \\ \boldsymbol{z_k^t} & \sigma_k^2 \end{pmatrix}$$

The divergence with an additional band x_{p+1}^* can be recursively calculated in an efficient way as follows:

$$J_{ij}(\boldsymbol{x}_p^*, x_{p+1}^*) = J_{ij}(\boldsymbol{x}_p^*) + \Delta_{ij}(x_{p+1}^*) \tag{20}$$

where $\Delta_{ij}(x_{p+1}^*)$ is the incremental divergence due to the addition of a band x_{p+1}^*, and can be calculated by the following formulae:

$$\begin{aligned}
\Delta_{ij}(x_{p+1}^*) =& \frac{1}{2\delta_i}(\theta_i^* - \theta_j^*)\left[(\theta_i^* - \theta_j^*) - (\boldsymbol{\theta}_{\boldsymbol{i,p}}^* - \boldsymbol{\theta}_{\boldsymbol{j,p}}^*)^t\gamma_i\right] \\
&+\frac{1}{2\delta_j}(\theta_i^* - \theta_j^*)\left[(\theta_i^* - \theta_j^*) - (\boldsymbol{\theta}_{\boldsymbol{i,p}}^* - \boldsymbol{\theta}_{\boldsymbol{j,p}}^*)^t\gamma_j\right] \\
&+\frac{1}{2}(\boldsymbol{z_i^t} - \boldsymbol{z_j^t})(\delta_i^{-1}\gamma_i - \delta_j^{-1}\gamma_j) \\
&+\frac{1}{2}(\sigma_i^2 - \sigma_j^2)(\delta_j^{-1} - \delta_i^{-1}) \\
&+\frac{1}{2}tr\{\sum_{\boldsymbol{i,p}}(\gamma_j - \gamma_i)\delta_j^{-1}\gamma_j^t - \sum_{\boldsymbol{j,p}}(\gamma_j - \gamma_i)\delta_i^{-1}\gamma_i^t \\
&+[(\gamma_i\delta_i^{-1}\gamma_i^t + \gamma_j\delta_j^{-1}\gamma_j^t)(\boldsymbol{\theta}_{\boldsymbol{i,p}}^* - \boldsymbol{\theta}_{\boldsymbol{j,p}}^*) \\
&-(\gamma_i\delta_i^{-1} + \gamma_j\delta_j^{-1})(\theta_i^* - \theta_j^*)](\boldsymbol{\theta}_{\boldsymbol{i,p}}^* - \boldsymbol{\theta}_{\boldsymbol{j,p}}^*)^t\}
\end{aligned}$$

where $\gamma_k = \sum_{\boldsymbol{k,p}}^{-1}\boldsymbol{z_k}$, and $\delta_k = \sigma_k^2 - \boldsymbol{z_k^t}\sum_{\boldsymbol{k,p}}^{\boldsymbol{-1}}\boldsymbol{z_k}$. See literature[30] for detailed derivation of the incremental divergence. Equation 21 gives an efficient way to calculate the divergence with the additional band. And the procedure for an efficient band selection based on the recursive equation of divergence can be described as follows. The block diagram is shown in Fig. 45.

Table 15: Band selection result through RD method

Method	Selected band (nm)							
	1st	2nd	3rd	4th	5th	6th	7th	8th
RD	465	625	495	525	505	645	595	605

Step 1) Set $\boldsymbol{D}$ to the initial band set, $\boldsymbol{S}$ to the empty set. Select a starting band (λ_i) by exhaustively calculate all bands and find the one with the maximum divergence. Step 2) Calculate $\Delta_{ij}(x^*_{p+1})$ according to equation 21 for all the remaining bands. Step 3) Select the band having the largest incremental effectiveness (λ_k), and add it to the selected band set. The algorithm will stop when certain criterion is met. Otherwise, go to Step 2).

Simulation results applying this method on clinical images We apply this method on HS image cube which is shown in Figure 33, and classify the images into two classes: residual (inside red box), and normal tissue. Table 15 shows the band selection results. And we can see that the wavelengths in our first-glance findings (525 nm, 525nm, 595 nm) are selected by this method, which indicates that the method gives the first-glance information correctly to a certain degree and that useful diagnostic information is successfully extracted.

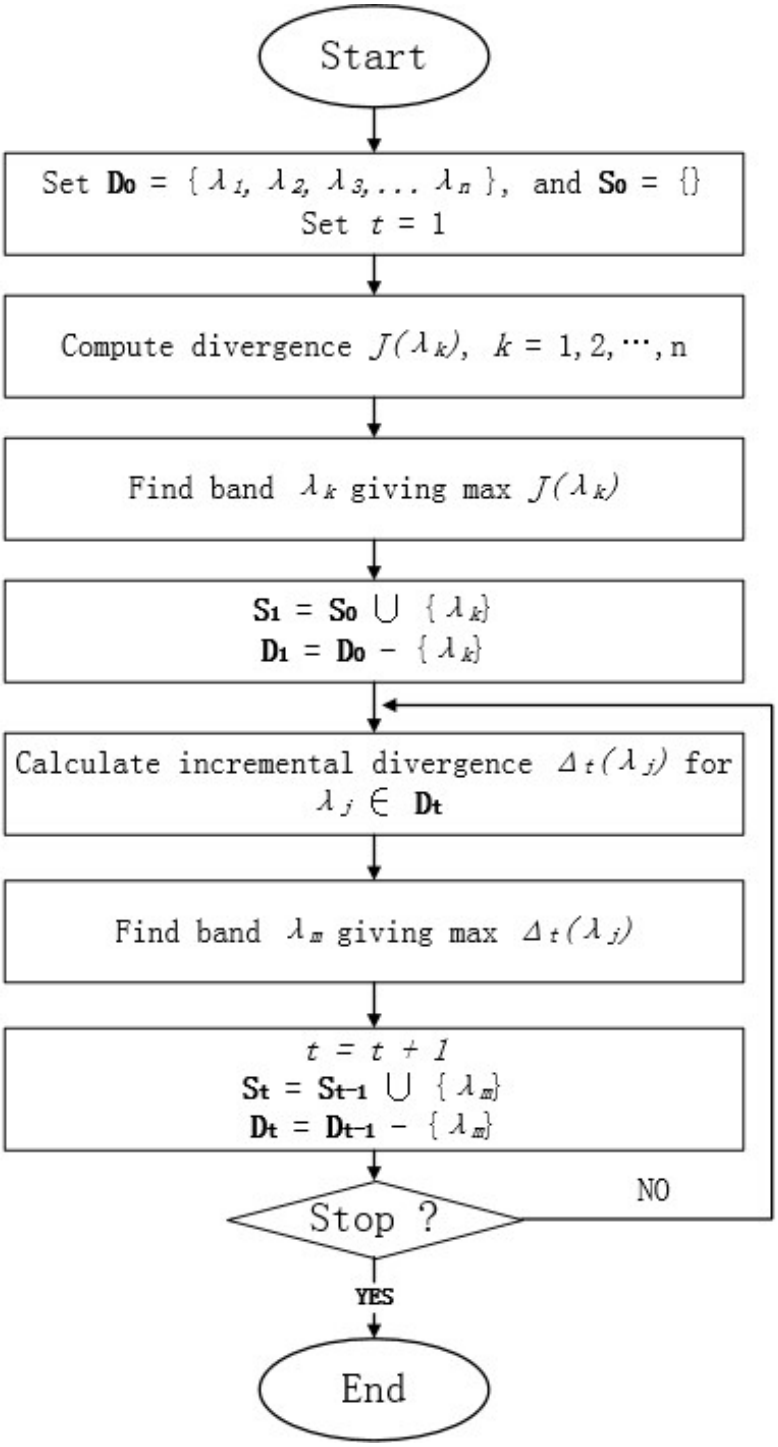

Figure 45: The block diagram of band selection method based on recursive divergence

CHAPTER V

FURTHER APPLICATION BASED ON HS ANALYSIS

As above mentioned, conventional NBI employs only two defined wavelengths – 420 nm and 540 nm (some early-stage NBI systems also implement 600 nm as a third wavelength)[44, 116], and identifies Hemoglobin as intrinsic bio-marker for detection of disease or targeting object region. Actually, many bio-markers – such as nuclear crowding, degradation of collagen in the extracellular matrix, and increased nuclear/cytoplasmic ratio – facilitate distinguished spectral information of disease progression[87]. NBI applying different and more wavelengths is potential to provide more spectral information and aid in increasing the disease detection rate. Thus in this chapter, we propose an adaptive narrow-band imaging (ANBI) method, which employ different subsets of wavelengths for different diseases specifically. The method is based on band selection of in vivo HS endoscopic images. It is further application of HS endoscopy imaging.

5.1 Principle of ANBI

At first we use the flexible endoscopy system that we introduce in previous part to obtain HS images on colorectal diseases or other objects in vivo. Then corresponding to a specific region, band selection algorithm on the foundation of RD finds a subset of significant spectral bands in terms of spatial information among HS image-cubes. Finally these bands are implemented in ANBI specific to this disease region in vivo.

5.2 Discussion

For those endoscopy system with slow speed CCD, five or more bands may be too many to meet the real time requirement. Then four, three, even two bands may be

employed to help diagnosis, as all the bands are specifically selected corresponding to individual diseases and narrower in FWHM compared to conventional NBI. Actually, it is easy to employ ANBI in endoscopy systems. For endoscopy systems applying color CCD, it just needs to change conventional NBI filters in a filter wheel. But for those applying monochromatic CCD, fast wavelength switching device such as AOTF may be required.

We need to employ these bands selected in previous band-selection part in clinic and verify them in application in future. Moreover, as the reflected spectral images may differ correlating with many factors, such as organs, locations, disease stages, and even environment changes, we do not expect that this conclusion would apply to all individuals. In this dissertation, we just hope that ANBI is helpful and with great potential to be implemented in clinic, with the ability to improve accuracy, sensitivity, and specificity of disease diagnosis.

In the future, after summarizing large amount of ANBI application cases and the concluded bands selected for each disease and individual, we can offer an optimal spectral band subset that is effective for most patients with a specific disease. Even more, ANBI can be extended to be individual-specific and disease-stage-specific.

CHAPTER VI

DISCUSSIONS AND FUTURE WORK

This chapter discusses future directions for the new HS endoscope system. There is a lot of work needed to be done before the system could help more in GI disease diagnosis. First, clinical evaluation is needed for the new application ANBI regarding different diseases and band selections. Second, the system needs further improvement. To improve light intensity and SNR, we also propose a new HS imaging method using broad- and overlapped-band filters. Third, more accurate pre-processing methods are needed to calibrate the HS images. Fourth, further theoretical analysis is required to be made on relationship between optimal filter bandwidth and accuracy of spectral curve reconstruction.

6.1 Clinical Evaluation

As the new application ANBI is based on analysis of only a few HS image cubes on this specific object, there may be large variance for the band selection results. Thus we cannot evaluate this technique in clinic now. Only after acquiring and analyzing large mount of HS image cubes on one specific object, the band selection results are meaningful and ANBI can be evaluated in clinic. For other objects and diseases, the same applies.

6.2 Further System Improvement

Although the flexible HS endoscope system is now applied in clinic, there are actually still several problems needed to be improved: first, there is big noise when acquiring HS images now due to the moving mechanical parts; second, the stability of system needs to be improved further as there are still potential electronics problems affecting

conventional imaging and data acquisition; third, the optical design of endoscope distal end needs to be improved further; fourth, the imaging speed needs to be improved to resolve the image color drift problem which will affect the taste and comfort of endoscope manipulator. Especially, in order to improve light intensity and SNR for spectral images, we propose a new HS imaging method on the foundation of broad- and overlapped-band filter sets.

6.2.1 Broad – and Overlapped – Band Imaging

Due to the narrow FWHM of filters, light intensity among some special spectral regions is low. To improve light intensity and SNR for HS images, we propose a new method to make HS imaging. This method applies broadband filters. The transmission band of these filters are overlapped. The final spectral curve at each pixel is reconstructed through the broadband and overlapped HS image cube. Simulation shows exciting results for this method. But due to some reasons, we do not apply it in our system now.

Background

Sensors of HSI systems, such as charged-couple-device (CCD), work by converting photons into electrons which are then stored in each pixel. The number of electrons stored in each pixel well is proportional to the number of photons that struck that pixel[95]. However, in actual pixel well, electrons are not only generated when receiving photons, but also due to physical processes within CCD itself, such as thermal noise which generates additional electrons dependent to temperature[129].

At the same time, dispersive device is key component for HSI systems. Monochromators (such as prism and grating), and optical filters (including interference filters and tunable filters, such as acoustic-optical tunable filters and liquid-crystal tunable filters) are commonly used. In these traditional approaches for spectral illumination filtering, only a relatively low fraction of photons are transmitted to the sensor. This

is of no importance if the light has sufficient exposure time as it is the case in remote earth sensing. However, for in-vivo and real-time application in medical domain, illumination cannot be performed with a high intensity due to the requirement of keeping the integration and exposure time per image as short as possible.

Thus under identical noise level and low intensity illumination, SNR is low[112]. Of course there are many methods to improve SNR for HSI, such as better hardware design, application of cooler CCD and larger irradiate spot. However, these methods may be not applicable for in-vivo medical devices such as endoscope. Thus broadband and overlapped sampling along spectrum is needed for medical HSI.

CCD works by converting photons into electrons which are then stored in each pixel (sensor cell or well). Each pixel can hold a fixed maximum number of electrons, typically from 35,000 to 500,000[112], depending on the specific model of CCD. While exposing an image, photons strike individual pixels and are converted to electrons and stored in each pixel well. The number of electrons stored in each pixel well is proportional to the number of photons that struck that pixel. After an exposure has been completed, the electrons for each pixel are shifted out of CCD one by one, and converted to a digital variable. However, in actual pixel well, electrons are not only generated when receiving photons, but also due to physical processes within CCD itself. As shown in Figure 46, the additional photons are dependent to temperature[95], which is also known as thermal noise or dark current noise. Thermal noise is an important source among many noise sources[133].

Method

HSI and its Linearly – Shift – Invariance (LSI) property According to operating principles of CCD sensor[112, 133], CCD has fixed sensitive curve corresponding to light wavelength, thus the sensitivity can be corrected to be identical along the spectral axis. Thus when the signal shifts along wavelength axis, CCD output along

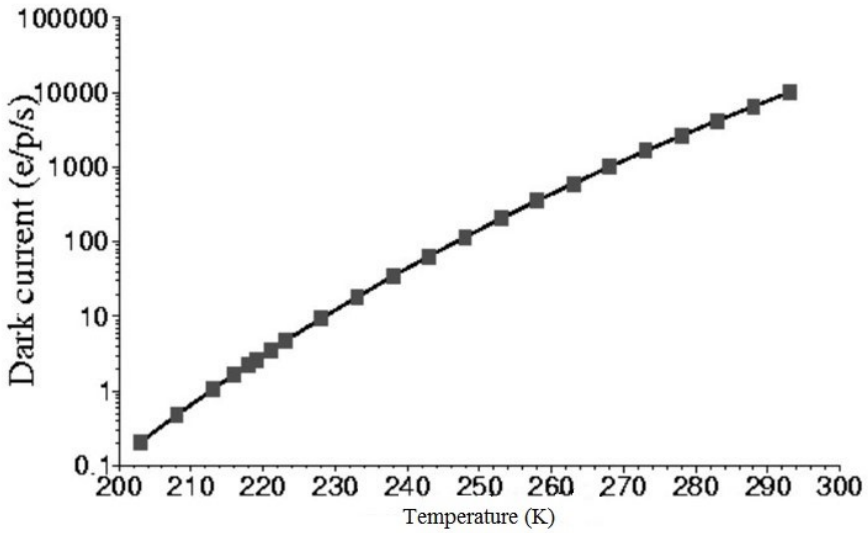

Figure 46: The number of thermal photons in a pixel well is dependent to temperature. This picture is cited from CCD Datasheet[95]

observed-sample axis (also is a type of wavelength axis) shifts the same distance, as Figure 47 shows. Then the sensor system is linear shift invariant (LSI), and the HSI sampling process along λ axis can be represented by a matrix model, which can be represented by Figure 48 and equation 21[114].

$$\boldsymbol{y} = \boldsymbol{C}\boldsymbol{x} \tag{21}$$

Vector $\boldsymbol{x}$ indicates discrete spectral signature in small enough discretization step. $\boldsymbol{M}$ represents the length of vector $\boldsymbol{x}$. Vector $\boldsymbol{y}$ is observed samples vector, with length of N. $\boldsymbol{C}$ is sampling matrix. Every row of $\boldsymbol{C}$ is transmission curve of a filter along spectral dimension representing a sampling window along spectral axis, corresponding to an observed image in the HSI cube.

Big – size and overlapped window sampling The main idea of overlapped and big-size sampling is described in Figure 48. In the new HSI method, the transmission window size (bandwidth on wavelength axis) of filters is bigger than those of narrow-band filters, and the windows are overlapping with those of adjacent rows. Figure

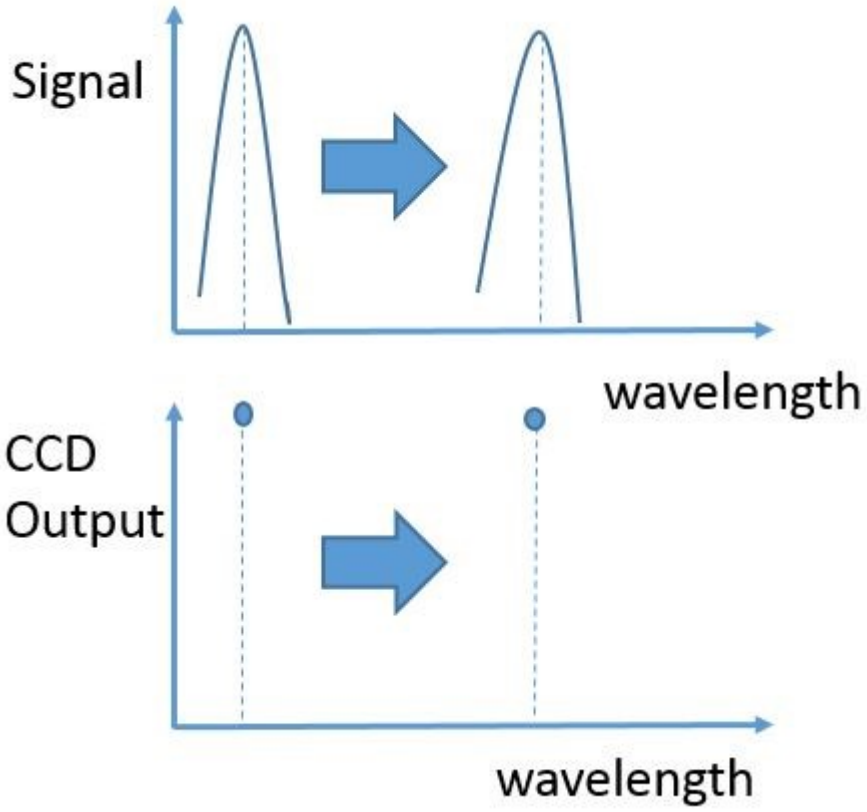

Figure 47: The Linearly-Shift-Invariance (LSI) of the HSI sensor model. When signal shifts along the wavelength axis, the CCD output (observed vector, also along the wavelength axis) shifts the same distance along the wavelength axis.

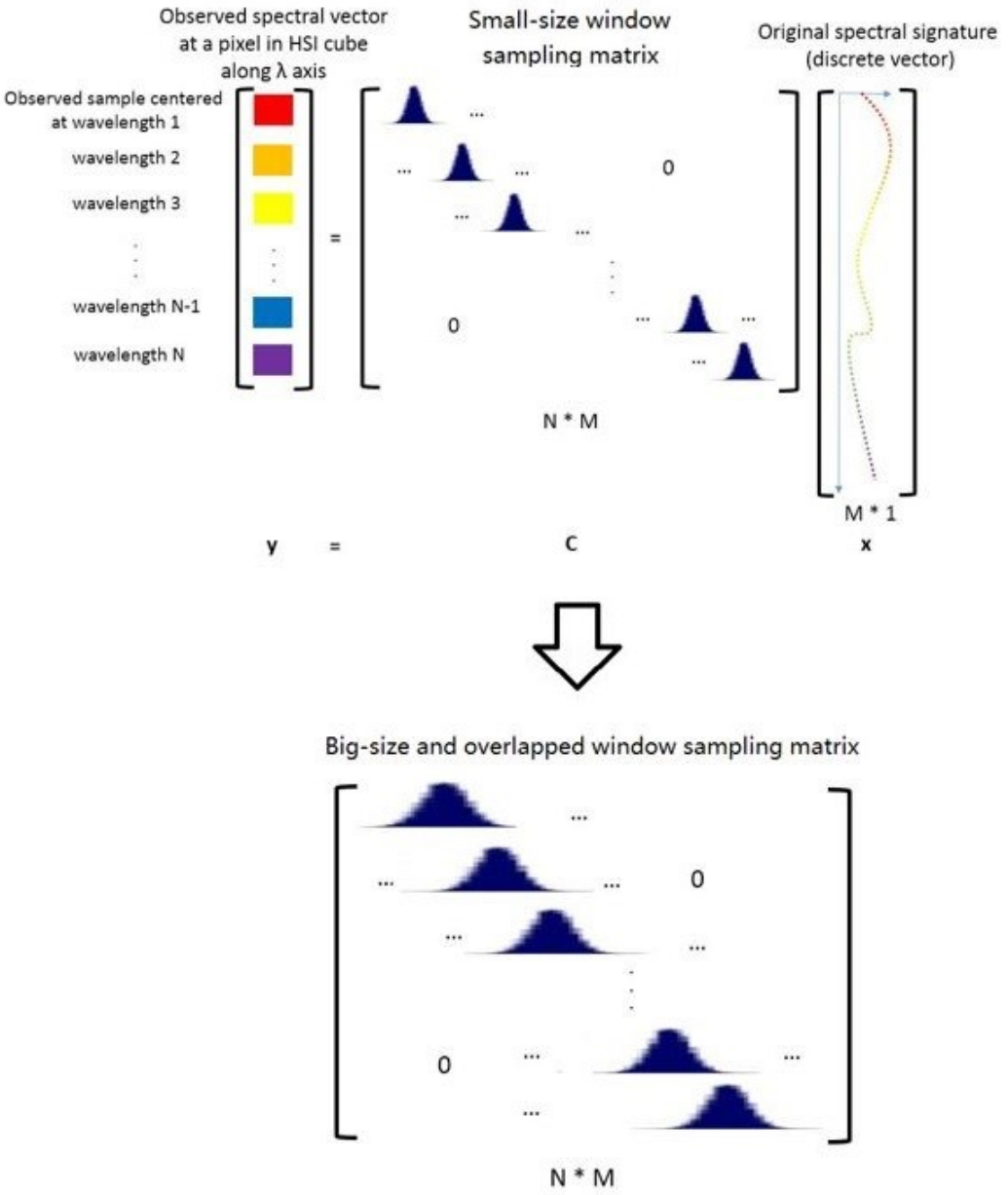

Figure 48: The matrix model of HSI in the spectral dimension. Vector x indicates discrete spectral signature in small enough discretization step. M represents the length of vector x. Vector y is observed samples vector, with length of N. C is sampling matrix. Every row of C is transmission curve of a filter along spectral dimension representing a sampling window along spectral axis, corresponding to an observed image in the HSI cube. In the overlapping and big-size window sampling method, the transmission window size of filters is bigger than those of narrow-band filters, and the windows are overlapping with those of adjacent rows.

49 shows the conventional FT analysis of this overlapping and big-size window sampling. Actually, it is a convolution process between spectral signal $f(t)$ and sampling window $g(t)$, followed by down-sampling to get the observed vector $\boldsymbol{y}$. In FT domain, it is multiplication of $F(s)$ and $G(s)$, which are FT representation of signal $f(t)$ and sampling window function $g(t)$. Due to the down-sampling, the size of sampling window and step of down-sampling are limited by Nyquist theorem. When reconstructing signal, we just need to get FT representation of $\boldsymbol{y}$, and divide it by $G(s)$ which can be designed and measured, then make inverse FT. This is the conventional de-convolution reconstruction method.

Discussion on This Method

In this thesis, we build a model for HSI sampling, and come up with a new HSI method, on the basis of overlapping and big-size window sampling combining with conventional FT reconstruction.

The new method aims to improve SNR for HSI in medical application under low light intensity illumination, such as HSI endoscopy in vivo. Most of the sampling windows are designed with fixed or tunable filters. However, there are always some differences among shapes of filters' transmission curve. Thus the convolution part in simulation is actually an approximation in application. In the future, more work is needed on applying this method integrating with an endoscope system and verifying its effectiveness in clinic.

However, we did not apply this method in clinical machine. There are several challenges before it could be used in practice. First, this method works greatly on static HS images. For moving-object HS images, it needs accurate sub-pixel image registration. As there is no such registration method now that could meet medical requirements, there is long way before this method could be applied in our clinical system. Second, the convolution window is ideal assumption while sampling windows

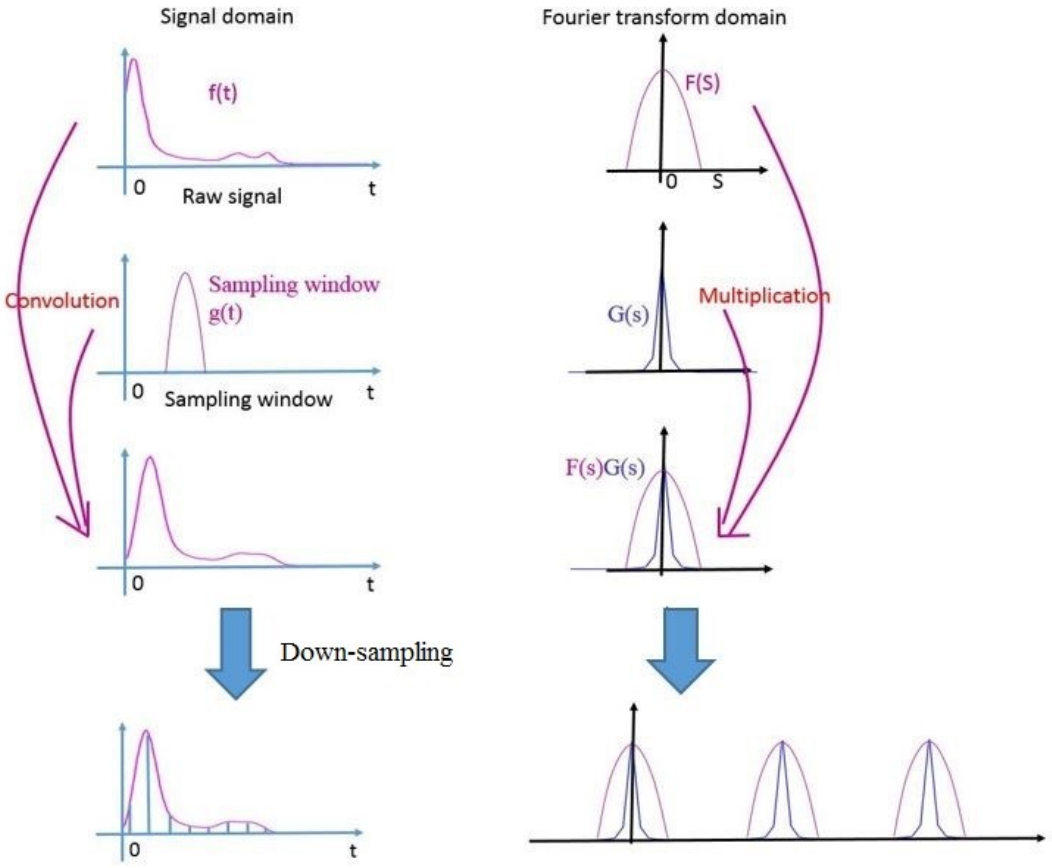

Figure 49: The conventional Fourier Transform (FT) analysis of overlapping and big-size window sampling. It is a convolution process between spectral signal $f(t)$ and sampling window $g(t)$, followed by down-sampling to get the observed vector y. In FT domain, it is multiplication of $F(s)$ and $G(s)$, which are FT representation of signal $f(t)$ and sampling window function $g(t)$. Due to the down-sampling, the size of sampling window and step of down-sampling are limited by Nyquist theorem.

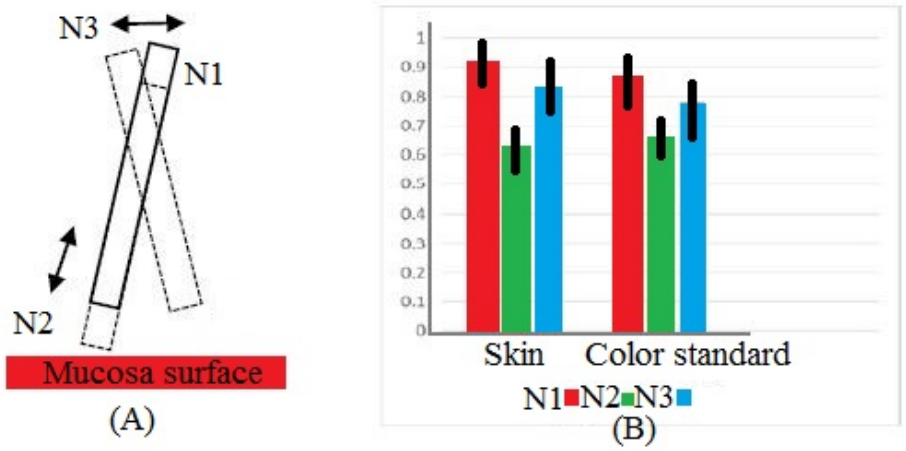

Figure 50: Spectral calibration parameter is different due to different orientations and distance of the object. This picture is modified based on those on liturature[152]

actually are not exactly identical in application. There is errors of reconstruction in clinical application. Third, FWHMs of sampling window is still limited by Nyquist theory. Despite of all these challenges, we hope to apply it in our system in the future.

6.2.2 More Accurate Pre – Processing

According to previous studies, spectral calibration parameter is different due to different orientations and distance of the object[152]. Figure 50 shows the variance of measured spectrum at different orientations and distances. Thus our obtained HS images need more accurate pre-processing to compensate this variance. Luckily, the variance only influence the HS analysis among different cubes. For analysis inside one cube just as we present above, this variance could be ignored.

6.3 Further Analysis

As we introduced in previous part, the narrower filter bandwidth will lead to more accurate spectral measurement, together with lower light intensity and larger number of channels, which would cost more time to finish the data acquisition and cause lower ability for real-time application. In the future, we will discuss this trade-off further

and find the optimal filter bandwidth which could show the best clinical effect.

CHAPTER VII

SUMMARY AND CONCLUSION

HSI originated from remote sensing field combines spectral measurement of a pixel with 2-D imaging technology. It is capable to provide a series of images containing both spectral and spatial information, and has been widely used in medical domain for diagnosis and surgery guidance. However, most researches on medical HS imaging are focused on ex-vivo biopsy or skin and oral mucosa. The study on HS imaging regarding in-vivo disease lags far behind. Especially, cancers on esophagus, stomach, and colon lead to many deaths. In-vivo HS imaging applied on digestive diseases provides opportunities for early-detection and early-therapy, which could increase survival rate significantly. In this thesis, we did some research on in-vivo HS imaging regarding GI tract diseases.

In this thesis, we developed a novel flexible HS endoscope system. It is capable to acquire a series of HS images in vivo in a non-contact way among the wavelength range of 405 - 665 nm. Twenty-eight sequential narrow-band interference filters are mounted in two motorized filter wheels positioned in the optical path of light source, and generates narrow-band illumination. The filter wheels are driven by Geneva Mechanism, and this dispersive device is the major innovative part for this system, with two authorized patents. At the same time, many printed circuit boards, hardware programs, and software programs were designed to drive the motors and process the acquired HS images. After a lot of time-consuming modifying and debugging work, this new system has high stability and convenience to be applied in clinic now.

We evaluated this system in clinic. First, we got ethics approval for clinical trials. Then, we obtained HS images regarding GI diseases inside patients using this system.

As far as we know, there is no such in-vivo image data reported in previous literatures. Thus based on these HS images, we built a database for GI mucosa, including both normal tissues and disease tissues on different organs. Next, we analyzed some typical HS images tentatively. The method of Contrast Calculation, Dependence of Information, and Recursive Divergence are implemented to extract valuable and diagnostic information from HS images. All these results prove the effect and applicability of this new HS endoscope system, and show its great potential to be used as a platform and guidance for further medical studies.

To further apply these analysis results, we proposed a novel endoscopy imaging technique that could enhance the display of valuable information on images. This technique is named as Adaptive Narrow-Band Imaging (ANBI) based on band selection of HS images of a specific type of disease. It is expected that it has higher accuracy, sensitivity, and specificity compared to conventional Narrow-Band Imaging (NBI).

In this thesis, we also discussed the future directions of the new system. There is still a lot of work to be done so that HS endoscopy could help more in clinical disease diagnosis, or even endoscopy therapy. Especially, to improve light intensity and signal-noise-ratio of HS images in wide-field view, we proposed a new imaging method using broad- and overlapped-band filters. Although this method only performs greatly on the foundation of accurate image registration, we hope to apply it in our system in the future.

In conclusion, we succeeded in combining HS imaging technique with flexible endoscope, and did some researches on in-vivo HS imaging regarding digestive tract diseases. These researches enlarge the application of HS imaging in medical domain, and provide a platform for further clinical studies.

APPENDIX A

ETHICAL APPROVAL DOCUMENTS

复旦大学附属中山医院伦理委员会

伦理委员会批准函

Approval Letter of Ethics Committee

审查编号 Approval No.: 2012-06(2)　　审查日期 Date of Review: 2012 年 11 月 01 日

项目名称 Study Title	AQ-100 型医用内窥镜图像处理器及 AQL-100 型氙灯冷光源临床验证				
试验产品名称 Study Product Name	医用内窥镜图像处理器/氙灯冷光源	产品类别/型号 Product Category	AQ-100/ AQL-100	研究分期 Phase of Study	NA
批准文号及发文单位（Approval No. and Issued By）： NA			药检报告及批号（Certificate of Analysis and Batch No.）： NA		
主要研究者（Principal Investigator）： 姚礼庆 教授			申办者（Sponsor）： 上海澳华光电内窥镜有限公司		
审查方式 (Type of Review)	■会议审查 (Meeting Review)　□快速审查(Expedited Review)				
会议地点(Meeting Location)	复旦大学附属中山医院 5 号楼 507 会议室				
会议出席情况 (Meeting Attendance)	出席(Attendance)10 人，投票(Vote)10 人，回避(Avoidance)0 人（　）				

下面划[√]的研究相关文件已经审阅

The following items[√] have been reviewed in connection with the above study to be conducted by the above investigator

[√] 研究方案及日期 Protocol No.,dated and version: v3.1,2012.11.14

[√] 受试者知情同意书及日期 Consent Form(s) dated and version: v3.0,2012.10.9

[ ] 受试者招募广告及日期 Advertisements for Recruitment dated:

[√] 其他(请具体列出) Other(specify):CRF: v3.1,2012.11.14

审查决定 **Decision for this proposal** and have been [√]:

[√] 同意 Approval

持续审查频率：□3 个月/3 months　□6 个月/6 months　□1 年/1year　□√不适用/NA

主任委员/副主任委员签名：

批准日期：2012.11.30

复旦大学附属中山医院伦理委员会（盖章）

注：本批件有效期为一年，逾期未实施的，则自行废止。

联系方式：上海市枫林路 180 号，黄锦培/杨梦婕，电话/传真：　64041990-3257

Figure 51: Ethical approval document for clinical data acquisition - 1

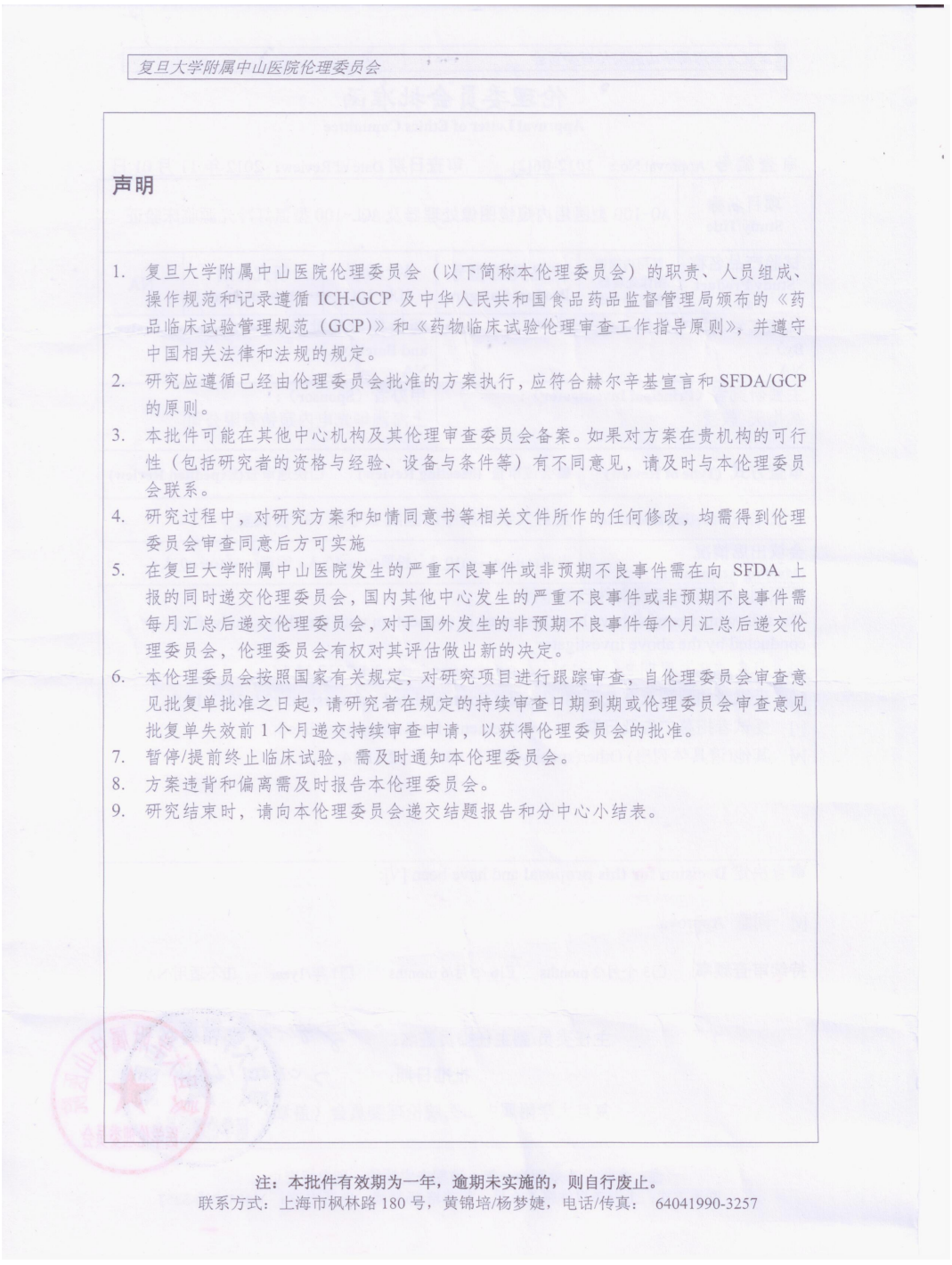

复旦大学附属中山医院伦理委员会

声明

1. 复旦大学附属中山医院伦理委员会（以下简称本伦理委员会）的职责、人员组成、操作规范和记录遵循 ICH-GCP 及中华人民共和国食品药品监督管理局颁布的《药品临床试验管理规范（GCP）》和《药物临床试验伦理审查工作指导原则》，并遵守中国相关法律和法规的规定。
2. 研究应遵循已经由伦理委员会批准的方案执行，应符合赫尔辛基宣言和 SFDA/GCP 的原则。
3. 本批件可能在其他中心机构及其伦理审查委员会备案。如果对方案在贵机构的可行性（包括研究者的资格与经验、设备与条件等）有不同意见，请及时与本伦理委员会联系。
4. 研究过程中，对研究方案和知情同意书等相关文件所作的任何修改，均需得到伦理委员会审查同意后方可实施
5. 在复旦大学附属中山医院发生的严重不良事件或非预期不良事件需在向 SFDA 上报的同时递交伦理委员会，国内其他中心发生的严重不良事件或非预期不良事件需每月汇总后递交伦理委员会，对于国外发生的非预期不良事件每个月汇总后递交伦理委员会，伦理委员会有权对其评估做出新的决定。
6. 本伦理委员会按照国家有关规定，对研究项目进行跟踪审查，自伦理委员会审查意见批复单批准之日起，请研究者在规定的持续审查日期到期或伦理委员会审查意见批复单失效前 1 个月递交持续审查申请，以获得伦理委员会的批准。
7. 暂停/提前终止临床试验，需及时通知本伦理委员会。
8. 方案违背和偏离需及时报告本伦理委员会。
9. 研究结束时，请向本伦理委员会递交结题报告和分中心小结表。

注：本批件有效期为一年，逾期未实施的，则自行废止。

联系方式：上海市枫林路 180 号，黄锦培/杨梦婕，电话/传真： 64041990-3257

Figure 52: Ethical approval document for clinical data acquisition - 2

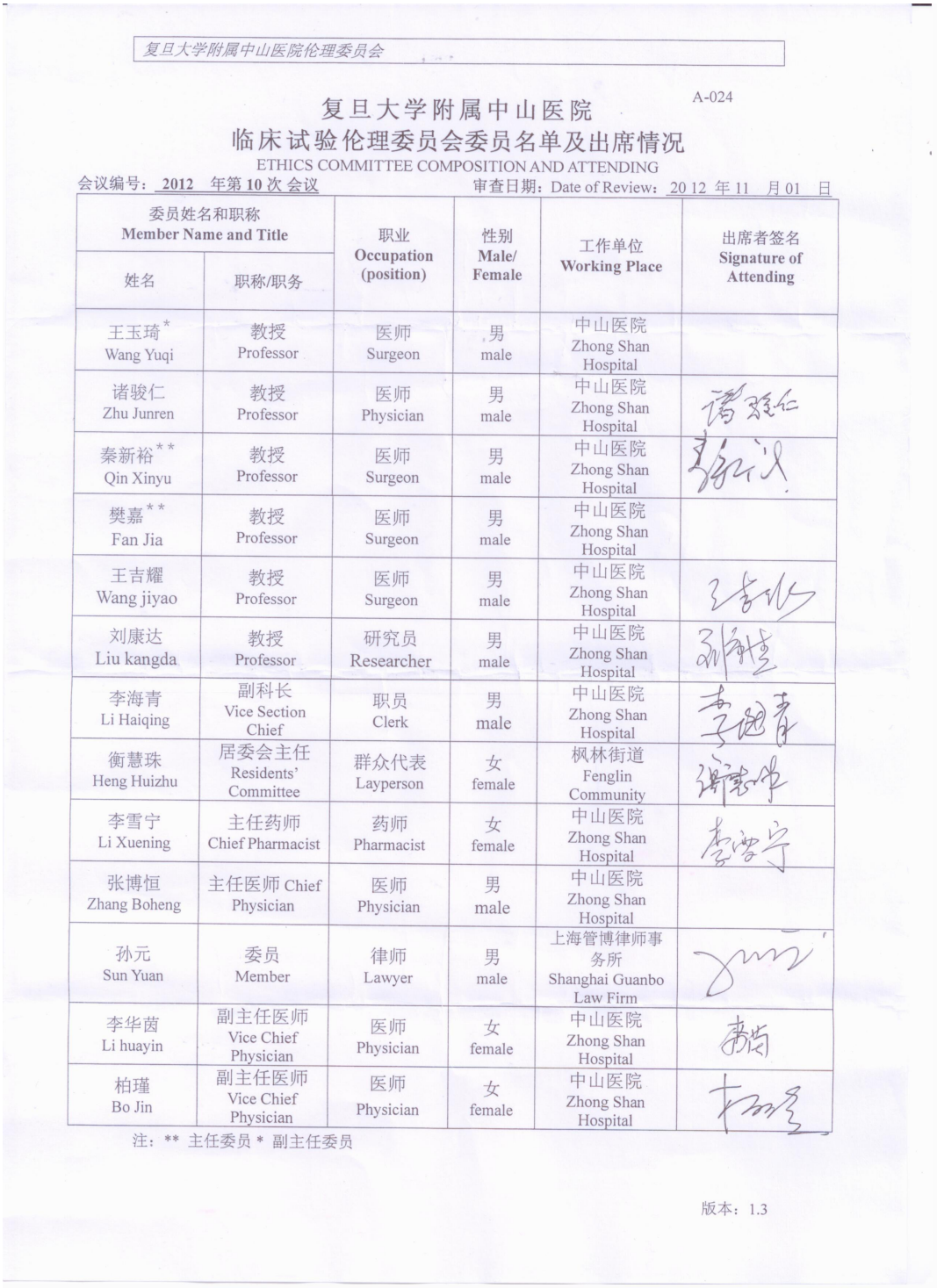

复旦大学附属中山医院伦理委员会

A-024

复旦大学附属中山医院
临床试验伦理委员会委员名单及出席情况

ETHICS COMMITTEE COMPOSITION AND ATTENDING

会议编号：2012 年第 10 次 会议　　审查日期：Date of Review：20 12 年 11 月 01 日

委员姓名和职称 Member Name and Title		职业 Occupation (position)	性别 Male/ Female	工作单位 Working Place	出席者签名 Signature of Attending
姓名	职称/职务				
王玉琦* Wang Yuqi	教授 Professor	医师 Surgeon	男 male	中山医院 Zhong Shan Hospital	
诸骏仁 Zhu Junren	教授 Professor	医师 Physician	男 male	中山医院 Zhong Shan Hospital	
秦新裕** Qin Xinyu	教授 Professor	医师 Surgeon	男 male	中山医院 Zhong Shan Hospital	
樊嘉** Fan Jia	教授 Professor	医师 Surgeon	男 male	中山医院 Zhong Shan Hospital	
王吉耀 Wang jiyao	教授 Professor	医师 Surgeon	男 male	中山医院 Zhong Shan Hospital	
刘康达 Liu kangda	教授 Professor	研究员 Researcher	男 male	中山医院 Zhong Shan Hospital	
李海青 Li Haiqing	副科长 Vice Section Chief	职员 Clerk	男 male	中山医院 Zhong Shan Hospital	
衡慧珠 Heng Huizhu	居委会主任 Residents' Committee	群众代表 Layperson	女 female	枫林街道 Fenglin Community	
李雪宁 Li Xuening	主任药师 Chief Pharmacist	药师 Pharmacist	女 female	中山医院 Zhong Shan Hospital	
张博恒 Zhang Boheng	主任医师 Chief Physician	医师 Physician	男 male	中山医院 Zhong Shan Hospital	
孙元 Sun Yuan	委员 Member	律师 Lawyer	男 male	上海管博律师事务所 Shanghai Guanbo Law Firm	
李华茵 Li huayin	副主任医师 Vice Chief Physician	医师 Physician	女 female	中山医院 Zhong Shan Hospital	
柏瑾 Bo Jin	副主任医师 Vice Chief Physician	医师 Physician	女 female	中山医院 Zhong Shan Hospital	

注：** 主任委员 * 副主任委员

版本：1.3

Figure 53: Ethical approval document for clinical data acquisition - 3

APPENDIX B

PROTOCOL FOR CLINICAL TRIALS

临 床 试 验 方 案

Protocol of Clinical Trials

产品名称：高光谱医用内窥镜光源及图像处理器

Product Name: Hyperspectral Medical Endoscopy Light Source and Image Processing Device

型号规格：AQ-100 型

Product Model: AQ-100

实施者：北京大学工学院生物医学工程系

Executor Entity: Biomedical Engineering Department of Peking University

承担临床评估的医疗机构：上海复旦大学附属中山医院

Medical Assessment institution: Zhongshan Hospital, Shanghai

临床试验的背景 (Background)

AQ-100 型高光谱医用内窥镜光源及图像处理器（以下简称光源及图像处理器）是由上海澳华光电内窥镜有限公司生产的，配套医用电子内窥镜可供临床使用。该产品作为采用光学纤维导光束的各类医用电子内窥镜产品的光源及图像处理部分，属于内窥镜配套产品，本身不与患者接触。

AQ-100 型高光谱医用内窥镜光源具有白光照明及高光谱照明两种照明模式，白色照明光用于常规内窥镜检查，高光谱照明光用于高光谱数据采集。这些高光谱照明光由不同时产生的多个窄带照明光组成，可覆盖全部看见光波段。图像处理器具有峰值测光，平均值测光两种测光模式，并具有白平衡，图像结构强化等图像处理方式。该光源及图像处理器在设计过程中力求产品的主要结构、性能指标等要素与已上市的同类产品相一致，在电气安全方面提高了相关要求。该光源及图像处理器配套医用电子内窥镜可有助于早期病变的发现。

临床试验的目的和项目内容 (Goal and Contents)

临床试验目的：基于 AQ-100 型高光谱医用内窥镜光源及图像处理器，获取人体正常粘膜组织及疾病组织的高光谱图像，用于后续医学研究。

临床试验评价项目内容见表 1。(Table 1 shows the Contents)

试验总体设计 (Overall Design)

本临床试验采用随机(Random)、开放的试验设计。对于需做电子内窥镜检查的病人，采用上海澳华光电内窥镜有限公司生产的 AQ-100 型高光谱医用内窥镜光源及图像处理器进行常规检查。在病人的病变部位及随机选取的正常组织部位进行高光谱照明，采集高光谱图像。

1、适用症检查患者的条件和试验范围 (Patients' condition and test range)：
早期内镜检查已发现有可疑病变，能够接受常规内镜检查的患者。（视镜子类型，如为结肠电子内窥镜，则为结肠疾病患者）

2、试验用设备及准备 (Equipment and Preparation)：

试验用设备名称：AQ-100 型高光谱医用内窥镜光源及图像处理器

试验所需配套设备：VME-1300S 型电子结肠镜及电子胃镜（也为澳华公司产品），医用图像显示器，内窥镜台车（用于推动内窥镜光源及图像处理器），医学工作站（电脑集成），彩色打印机，工作站桌子（用于放置工作站电脑及打印机），病人床，内窥镜消毒器具及测漏系统。其中，消毒器具，测漏系统，病人床，工作站桌子，由医院提供。

器械能保证试验项目按要求进行。出现失败可能性是在高光谱照明时，光源滤光片切换出现卡顿。该问题不影响与病人接触的医用电子内窥镜，但会影响图像处理器的显示。如果出现问题，重启系统即可。

3、试验流程 (Procedure)：

1）医生向患者说明实验目的。(Informed consent)

2）医生对就诊患者用配套 AQ-100 型高光谱医用内窥镜光源和图像处理器的 VME-1300S 型电子结肠镜及电子胃镜进行常规检查，并通过工作站采集白光照明下的图像。(Conventional white light examination)

3）根据需要，由韩志敏操作装置对病变组织及随机选取的正常组织进行高光谱照明，并获取高光谱图像。(Acquire HS images)

4）医生继续对患者的病变组织进行活检等处理。(Take biopsy)

5）重复步骤2,3,4，直到检查结束。

6）医生填写检查报告并打印，同时交付韩志敏及患者保存。

7）由韩志敏填写表格,记录疾病状况,装置状况(图像显示是否稳定,设备是否有故障等),患者反馈，并由医生对试验用设备做出使用评价及反馈。具体见附表1

8）由护士或韩志敏对电子内窥镜进行洗净消毒。

9）对于采集到的高光谱图像，由韩志敏进行后续分析。

4、后续工作：(Future work)

1)对比分析。对采集到的病变组织及不同部位的正常组织的高光谱数据进行对比分析，确定高光谱医用内窥镜光源及图像处理器的临床效果。

a）通过高光谱向量分类算法，在一幅图像上实现对病变组织和正常组织的自动分类和边沿标示，将此结果与由医生人工确定的疾病组织范围或者活检范围进行对比，确定高光谱系统对疾病组织的识别准确性和临床效果。

b）将病变组织与同部位正常组织的高光谱数据进行对比，寻找对于每种疾病组织敏感的波长。该波长可以用于针对这种疾病的实时窄带光成像，增强窄带光成像的敏感性和专一性。

c）若能发现对于每种疾病组织敏感的特殊波长，可以继续研究形成这种特殊波长的病理学原因。例如分离病变组织含有的对该波长有吸收或者反射作用的特殊物质，或者分析相关物质含量的变化，以及建立病变组织的生理结构的模型等。

d）将每种疾病的高光谱图像（真实光谱图像）与经过FICE系统恢复的图像（重建的图像）进行对比，确定FICE恢复的光谱图像的误差大小。

2)申请研究项目。对于高光谱图像数据分析获得的结果，如需进一步的临床研究或验证，将联合申请国家研究项目，获得研究支持。

3)发表研究论文。对于高光谱图像分析的新算法及基于临床高光谱图像数据获得的分析结果，将联合署名发表科研论文。

产品的操作方法：(Manipulation of the system)

将电源插头插入电源插座，将内窥镜导光插头部插入光源系统的连接孔内。使用信号连接线连接图像处理器和光源系统，工作站，打印机以及监视器。按下光源电源开关，接通电源，开通白光照明，然后按下图像处理器电源开关，内窥镜图像经过图像处理器处理后，在监视器上显示，供医生观察。此时系统处于白光照明的常规检查模式。

在监视器显示特定部位时，踩下踏板，白光图像传输给工作站，并在工作站电脑显示器上显示，供医生打印报告及后续分析。然后按下高光谱照明键，系统进入高光谱照明模式，该特定部位的高光谱图像经过图像处理器传输给工作站分析处理，供医生后续分析。每次高光谱图像采集需耗时8秒钟。

高光谱图像采集完毕，系统自动恢复到白光照明的常规检查模式。

临床试验例数：(Targeted capacity of trials)

预计试验患者及志愿者人数~100人,每人预计正常组织高光谱图像例数为2-3例，患者的疾病组织高光谱图像例数为2-3例。

自2015年7月开始至10月，可保证有足够参与试验的患者人数。

表 1 临床检查记录表（Table 1 Record）

病例号	日期时间	检查时长（分钟）	部位	疾病	装置状况	备注

REFERENCES

[1] Akbari, H., Kosugi, Y., Kojima, K., and Tanaka, N., "Wavelet-based compression and segmentation of hyperspectral images in surgery," *Medical Imaging and Augmented Reality, Proceedings*, vol. 5128, pp. 142–149, 2008.

[2] Akbari, H., Kosugi, Y., Kojima, K., and Tanaka, N., "Blood vessel detection and artery-vein differentiation using hyperspectral imaging," *2009 Annual International Conference of the Ieee Engineering in Medicine and Biology Society, Vols 1-20*, pp. 1461–1464, 2009.

[3] Akbari, H., Kosugi, Y., Kojima, K., and Tanaka, N., "Detection and analysis of the intestinal ischemia using visible and invisible hyperspectral imaging," *Ieee Transactions on Biomedical Engineering*, vol. 57, no. 8, pp. 2011–2017, 2010.

[4] Akbari, H., Uto, K., Kosugi, Y., Kojima, K., and Tanaka, N., "Cancer detection using infrared hyperspectral imaging," *Cancer Science*, vol. 102, no. 4, pp. 852–857, 2011.

[5] Bambery, K. R., Wood, B. R., Quinn, M. A., and McNaughton, D., "Fourier transform infrared imaging and unsupervised hierarchical clustering applied to cervical biopsies," *Australian Journal of Chemistry*, vol. 57, no. 12, pp. 1139–1143, 2004.

[6] Bautista, P. A. and Yagi, Y., "Digital simulation of staining in histopathology multispectral images: enhancement and linear transformation of spectral transmittance," *Journal of Biomedical Optics*, vol. 17, no. 5, pp. 0560131–05601310, 2012.

[7] Bellisola, G. and Sorio, C., "Infrared spectroscopy and microscopy in cancer research and diagnosis," *American Journal of Cancer Research*, vol. 2, no. 1, pp. 1–21, 2012.

[8] Benavides, J., Chang, S., Park, S., Richards-Kortum, R., Mackinnon, N., MacAulay, C., Milbourne, A., Malpica, A., and Follen, M., "Multispectral digital colposcopy for in vivo detection of cervical cancer," *Optics Express*, vol. 11, no. 10, pp. 1223–1236, 2003.

[9] Boas, D. A., Pitris, C., and Ramanujam, N., *Handbook of biomedical optics*. CRC press, 2012.

[10] Bochko, V., Tsumura, N., and Miyake, Y., "Spectral color imaging system for estimating spectral reflectance of paint," *Journal of Imaging Science and Technology*, vol. 51, no. 1, pp. 70–78, 2007.

[11] Bochko, V. A., Miyake, Y., and Alander, J. T., "Spectral reflectance estimation for electronic endoscope," *Optical Review*, vol. 21, no. 3, pp. 313–319, 2014.

[12] Brauers, J., Schulte, N., and Aach, T., "Multispectral filter-wheel cameras: Geometric distortion model and compensation algorithms," *Image Processing, IEEE Transactions on*, vol. 17, no. 12, pp. 2368–2380, 2008.

[13] Brown, L. G., "A survey of image registration techniques," *Computing Surveys*, vol. 24, no. 4, pp. 325–376, 1992.

[14] C, C. L., I, B. A., R, M. J., Svetlana, P., Katherin, H., David, M., RN, J. B. S., Brian, T., and E., F. J., "Hyperspectral imaging: A new approach to the diagnosis of hemorrhagic shock," *Journal of Trauma-Injury Infection & Critical Care*, vol. 60, no. 5, 2006.

[15] Cancio, L. C., "Application of novel hyperspectral imaging technologies in combat casualty care," in *Proceedings of SPIE*, 2010.

[16] Chang, I., "Acoustooptic devices and applications," *IEEE transactions on sonics and ultrasonics*, vol. 23, no. 1, p. p2, 1976.

[17] Chaudhuri, S., Chatterjee, S., Katz, N., Nelson, M., and Goldbaum, M., "Detection of blood-vessels in retinal images using two-dimensional matched-filters," *Ieee Transactions on Medical Imaging*, vol. 8, no. 3, pp. 263–269, 1989.

[18] Chen, Y., Lin, Z., Zhao, X., Wang, G., and Gu, Y., "Deep learning-based classification of hyperspectral data,"

[19] Choi, H., Wadduwage, D., Matsudaira, P. T., and So, P. T., "Depth resolved hyperspectral imaging spectrometer based on structured light illumination and fourier transform interferometry," *Biomedical Optics Express*, vol. 5, no. 10, pp. 3494–3507, 2014.

[20] Chung, S. J., Kim, D., Park, M. J., Song, J. H., Kim, Y. S., Kim, J. S., Jung, H. C., and Song, I. S., "Efficacy of computed virtual chromoendoscopy on colorectal cancer screening: A prospective randomized rack-to-back trial of fuji intelligent color enhancement vs conventional colonoscopy to compare adenoma miss rates," *Gastrointestinal Endoscopy*, vol. 71, no. 5, pp. Ab247–Ab247, 2010.

[21] Clancy, N. T., Stoyanov, D., James, D. R. C., Di Marco, A., Sauvage, V., Clark, J., Yang, G. Z., and Elson, D. S., "Multispectral image alignment using a three channel endoscope in vivo during minimally invasive surgery," *Biomedical Optics Express*, vol. 3, no. 10, pp. 2567–2578, 2012.

[22] Colarusso, P., Kidder, L. H., Levin, I. W., Fraser, J. C., Arens, J. F., and Lewis, E. N., "Infrared spectroscopic imaging: From planetary to cellular systems," *Applied Spectroscopy*, vol. 52, no. 3, pp. 106a–120a, 1998.

[23] Connell, W. R., Lennardjones, J. E., Williams, C. B., Talbot, I. C., Price, A. B., and Wilkinson, K. H., "Factors affecting the outcome of endoscopic surveillance for cancer in ulcerative-colitis," *Gastroenterology*, vol. 107, no. 4, pp. 934–944, 1994.

[24] Crum, W. R., Hartkens, T., and Hill, D. L. G., "Non-rigid image registration: theory and practice," *British Journal of Radiology*, vol. 77, pp. S140–S153, 2004.

[25] Dayyeh, B. K. A., Thosani, N., Konda, V., Wallace, M. B., Rex, D. K., Chauhan, S. S., Hwang, J. H., Komanduri, S., Manfredi, M., and Maple, J. T., "Asge technology committee systematic review and meta-analysis assessing the asge pivi thresholds for adopting real-time endoscopic assessment of the histology of diminutive colorectal polyps," *Gastrointestinal endoscopy*, 2015.

[26] Dicker, D. T., Lerner, J., Belle, P. V., Guerry, D., Herlyn, M., Elder, D. E., and El-Deiry, W. S., "Differentiation of normal skin and melanoma using high resolution hyperspectral imaging," *Cancer Biology & Therapy*, 2006.

[27] Dinesen, L., Chua, T. J., and Kaffes, A. J., "Meta-analysis of narrow-band imaging versus conventional colonoscopy for adenoma detection," *Gastrointestinal Endoscopy*, vol. 75, no. 3, pp. 604–611, 2012.

[28] Dohi, T., Matsumoto, K., and Shimoyama, I., "The micro fabry-perot interferometer for the spectral endoscope," *Mems 2005 Miami: Technical Digest*, pp. 830–833, 2005.

[29] Du, Q., "Band selection and its impact on target detection and classification in hyperspectral image analysis," *2003 Ieee Workshop on Advances in Techniques for Analysis of Remotely Sensed Data*, pp. 374–377, 2004.

[30] Du, Z., Jeong, M. K., and Kong, S. G., "Band selection of hyperspectral images for automatic detection of poultry skin tumors," *Ieee Transactions on Automation Science and Engineering*, vol. 4, no. 3, pp. 332–339, 2007.

[31] Elliott, A. D., Gao, L., Ustione, A., Bedard, N., Kester, R., Piston, D. W., and Tkaczyk, T. S., "Real-time hyperspectral fluorescence imaging of pancreatic beta-cell dynamics with the image mapping spectrometer," *Journal of Cell Science*, vol. 125, no. 20, pp. 4833–4840, 2012.

[32] Fawzi, A. A., Lee, N., Acton, J. H., Laine, A. F., and Smith, R. T., "Recovery of macular pigment spectrum in vivo using hyperspectral image analysis," *Journal of Biomedical Optics*, vol. 16, no. 10, 2011.

[33] Ferris, D. G., Lawhead, R. A., Dickman, E. D., Holtzapple, N., Miller, J. A., Grogan, S., Bambot, S., Agrawal, A., and Faupel, M. L., "Multimodal hyperspectral imaging for the noninvasive diagnosis of cervical neoplasia," *Journal of Lower Genital Tract Disease*, vol. 5, no. 2, pp. 65–72, 2001.

[34] Fong, Y. M., Cohen, A. M., Fortner, J. G., Enker, W. E., Turnbull, A. D., Coit, D. G., Marrero, A. M., Prasad, M., Blumgart, L. H., and Brennan, M. F., "Liver resection for colorectal metastases," *Journal of Clinical Oncology*, vol. 15, no. 3, pp. 938–946, 1997.

[35] Foody, G. M., "Status of land cover classification accuracy assessment," *Remote Sensing of Environment*, vol. 80, no. 1, pp. 185–201, 2002.

[36] Foracchia, M., Grisan, E., and Ruggeri, A., "Luminosity and contrast normalization in retinal images," *Medical Image Analysis*, vol. 9, no. 3, pp. 179–190, 2005.

[37] Freeberg, J. A., Benedet, J. L., MacAulay, C., West, L. A., and Follen, M., "The performance of fluorescence and reflectance spectroscopy for the in vivo diagnosis of cervical neoplasia; point probe versus multispectral approaches," *Gynecologic Oncology*, vol. 107, no. 1, pp. S248–S255, 2007.

[38] Furness, P. N., Taub, N., Assmann, K. J. M., Banfi, G., Cosyns, J. P., Dorman, A. M., Hill, C. M., Kapper, S. K., Waldherr, R., Laurinavicius, A., Marcussen, N., Martins, A. P., Nogueira, M., Regele, H., Seron, D., Carrera, M., Sund, S., Taskinen, E. I., Paavonen, T., Tihomirova, T., and Rosenthal, R., "International variation in histologic grading is large, and persistent feedback does not improve reproducibility," *American Journal of Surgical Pathology*, vol. 27, no. 6, pp. 805–810, 2003.

[39] Galloro, G., "High technology imaging in digestive endoscopy," *World journal of gastrointestinal endoscopy*, vol. 4, no. 2, p. 22, 2012.

[40] Gehm, M., John, R., Brady, D., Willett, R., and Schulz, T., "Single-shot compressive spectral imaging with a dual-disperser architecture," *Optics Express*, vol. 15, no. 21, pp. 14013–14027, 2007.

[41] Gerstner, A. O. H., Laffers, W., Bootz, F., Farkas, D. L., Martin, R., Bendix, J., and Thies, B., "Hyperspectral imaging of mucosal surfaces in patients," *Journal of Biophotonics*, vol. 5, no. 3, pp. 255–262, 2012.

[42] Gong, F., Swain, P., and Mills, T., "Wireless endoscopy," *Gastrointestinal Endoscopy*, vol. 51, no. 6, pp. 725–729, 2000.

[43] Gono, K., Obi, T., Yamaguchi, M., Ohyama, N., Machida, H., Sano, Y., Yoshida, S., Hamamoto, Y., and Endo, T., "Appearance of enhanced tissue features in narrow-band endoscopic imaging," *Journal of Biomedical Optics*, vol. 9, no. 3, pp. 568–577, 2004.

[44] Gono, K., Yamazaki, K., Doguchi, N., Nonami, T., Obi, T., Yamaguchi, M., Ohyama, N., Machida, H., Sano, Y., and Yoshida, S., "Endoscopic observation of tissue by narrowband illumination," *Optical Review*, vol. 10, no. 4, pp. 211–215, 2003.

[45] Greene, F. L. and Sobin, L. H., "The staging of cancer: a retrospective and prospective appraisal," *CA: a cancer journal for clinicians*, vol. 58, no. 3, pp. 180–190, 2008.

[46] Guan, Y. N., Li, Q. L., Wang, Y. T., Liu, H. Y., and Zhu, Z. Q., "Pathological leucocyte segmentation algorithm based on hyperspectral imaging technique," *Optical Engineering*, vol. 51, no. 5, 2012.

[47] Guo, B. F., Gunn, S. R., Damper, R. I., and Nelson, J. D. B., "Band, selection for hyperspectral image classification using mutual information," *Ieee Geoscience and Remote Sensing Letters*, vol. 3, no. 4, pp. 522–526, 2006.

[48] Hagen, N. and Kudenov, M. W., "Review of snapshot spectral imaging technologies," *Optical Engineering*, vol. 52, no. 9, pp. 090901–090901, 2013.

[49] Han, Z. M., Ma, S. H., Wang, X. G., Li, Z. Z., and Xie, T. Y., "New real-time endoscopy image processing technology of hemoglobin color enhancement," *International Symposium on Photoelectronic Detection and Imaging 2011: Laser Sensing and Imaging and Biological and Medical Applications of Photonics Sensing and Imaging*, vol. 8192, 2011.

[50] Haneishi, H., Hasegawa, T., Hosoi, A., Yokoyama, Y., Tsumura, N., and Miyake, Y., "System design for accurately estimating the spectral reflectance of art paintings," *Applied Optics*, vol. 39, no. 35, pp. 6621–6632, 2000.

[51] Hartke, J. and Dereniak, E. L., "Snapshot dual-band visible hyperspectral imaging spectrometer," *Optical Engineering*, vol. 46, no. 1, 2007.

[52] Hurlstone, D. P., McAlindon, M. E., Sanders, D. S., Keogh, R., Lobo, A. J., and Cross, S. S., "Further validation of high-magnification chromoscopic-colonoscopy for the detection of intraepithelial neoplasia and colon cancer in ulcerative colitis," *Gastroenterology*, vol. 126, no. 1, pp. 376–377, 2004.

[53] Imai, F. H. and Berns, R. S., "Spectral estimation using trichromatic digital cameras," in *Proceedings of the International Symposium on Multispectral Imaging and Color Reproduction for Digital Archives*, vol. 42, Wiley.

[54] Ishwaran, H., Blackstone, E. H., Apperson-Hansen, C., and Rice, T. W., "A novel approach to cancer staging: application to esophageal cancer," *Biostatistics*, 2009.

[55] Ismail, S. M., Colclough, A. B., Dinnen, J. S., Eakins, D., Evans, D. M. D., Gradwell, E., O'Sullivan, J. P., Summerell, J. M., and Newcombe, R. G., "Observer variation in histopathological diagnosis and grading of cervical intraepithelial neoplasia," *British Medical Journal*, 1989.

[56] JA Chin, EC Wang, M. K., "Evaluation of hyperspectral technology for assessing the presence and severity of peripheral artery disease," *Journal of vascular surgery*, 2011.

[57] Jing Xin, Yue Tianxin, Z. L., "A spectral reflectance reconstruction algorithm for color image using wiener estimation method," *Journal of Shenyang Jianzhu University*, vol. 30, no. 1, 2014.

[58] Johnson, W. R., Wilson, D. W., Fink, W., Humayun, M., and Bearman, G., "Snapshot hyperspectral imaging in ophthalmology," *Journal of Biomedical Optics*, vol. 12, no. 1, 2007.

[59] Jolivot, R., Vabres, P., and Marzani, F., "Reconstruction of hyperspectral cutaneous data from an artificial neural network-based multispectral imaging system," *Computerized Medical Imaging and Graphics*, vol. 35, no. 2, pp. 85–88, 2011.

[60] Katzka, P., "Aotf overview: past, present, and future," in *OE LASE'87 and EO Imaging Symp (January 1987, Los Angeles)*, pp. 22–28, International Society for Optics and Photonics.

[61] Kenyon, I., *The light fantastic: a modern introduction to classical and quantum optics*. Oxford University Press, Inc., 2008.

[62] Keshava, N., "Best bands selection for detection in hyperspectral processing," *2001 Ieee International Conference on Acoustics, Speech, and Signal Processing, Vols I-Vi, Proceedings*, pp. 3149–3152, 2001.

[63] Kester, R. T., Bedard, N., Gao, L., and Tkaczyk, T. S., "Real-time snapshot hyperspectral imaging endoscope," *Journal of Biomedical Optics*, vol. 16, no. 5, 2011.

[64] Kester, R. T., Bedard, N., and Tkaczyk, T. S., "Image mapping spectrometry - a novel hyperspectral platform for rapid snapshot imaging," *Algorithms and Technologies for Multispectral, Hyperspectral, and Ultraspectral Imagery Xvii*, vol. 8048, 2011.

[65] Kester, R. T., Gao, L. A., Bedard, N., and Tkaczyk, T. S., "Real-time hyperspectral endoscope for early cancer diagnostics," *Advanced Biomedical and Clinical Diagnostic Systems Viii*, vol. 7555, 2010.

[66] Kiesslich, R., Fritsch, J., Holtmann, M., Koehler, H. H., Stolte, M., Kanzler, S., Nafe, B., Jung, M., Galle, P. R., and Neurath,

M. F., "Methylene blue-aided chromoendoscopy for the detection of intraepithelial neoplasia and colon cancer in ulcerative colitis," *Gastroenterology*, vol. 124, no. 4, pp. 880–888, 2003.

[67] Kinkel, K., Lu, Y., Both, M., Warren, R. S., and Thoeni, R. F., "Detection of hepatic metastases from cancers of the gastrointestinal tract by using noninvasive imaging methods (us, ct, mr imaging, pet): A meta-analysis," *Radiology*, vol. 224, no. 3, pp. 748–756, 2002.

[68] Kiyotoki, S., Nishikawa, J., Okamoto, T., Hamabe, K., Saito, M., Goto, A., Fujita, Y., Hamamoto, Y., Takeuchi, Y., Satori, S., and Sakaida, I., "New method for detection of gastric cancer by hyperspectral imaging: a pilot study," *Journal of Biomedical Optics*, vol. 18, no. 2, 2013.

[69] Kong, S. G., Du, Z., Martin, M., and Vo-Dinh, T., "Hyperspectral fluorescence image analysis for use in medical diagnostics," *Advanced Biomedical and Clinical Diagnostic Systems III*, vol. 5692, pp. 21–28, 2005.

[70] Krizhevsky, A., Sutskever, I., and Hinton, G. E., "Imagenet classification with deep convolutional neural networks," in *Advances in neural information processing systems*, pp. 1097–1105.

[71] Kujan, O., Khattab, A., Oliver, R. J., Roberts, S. A., Thakker, N., and Sloan, P., "Why oral histopathology suffers inter-observer variability on grading oral epithelial dysplasia: An attempt to understand the sources of variation," *Oral Oncology*, vol. 43, no. 3, pp. 224–231, 2007.

[72] Kwon, R. S., Adler, D. G., Chand, B., Conway, J. D., Diehl, D. L., Kantsevoy, S. V., Mamula, P., Rodriguez, S. A., Shah, R. J., and Wong Kee Song, L. M., "High-resolution and high-magnification endoscopes," *Gastrointestinal Endoscopy*, vol. 69, no. 3, pp. 399–407, 2009.

[73] Kybic, J., *Elastic image registration using parametric deformation models*. Thesis, 2001.

[74] Landgrebe, D., "Hyperspectral image data analysis," *Ieee Signal Processing Magazine*, vol. 19, no. 1, pp. 17–28, 2002.

[75] Lange, H., Baker, R., Hakansson, J., and Gustafsson, U., "Reflectance and fluorescence hyperspectral elastic image registration," *Medical Imaging 2004: Image Processing, Pts 1-3*, vol. 5370, pp. 335–345, 2004.

[76] Larsen, E. L. P., Randeberg, L. L., Olstad, E., Haugen, O. A., Aksnes, A., and Svaasand, L. O., "Hyperspectral imaging of atherosclerotic plaques in vitro," *Journal of Biomedical Optics*, vol. 16, no. 2, 2011.

[77] Lawrence, R., Bunn, A., Powell, S., and Zambon, M., "Classification of remotely sensed imagery using stochastic gradient boosting as a refinement

of classification tree analysis," *Remote Sensing of Environment*, vol. 90, no. 3, pp. 331–336, 2004.

[78] Lawrence, S., Giles, C. L., Tsoi, A. C., and Back, A. D., "Face recognition: A convolutional neural-network approach," *Ieee Transactions on Neural Networks*, vol. 8, no. 1, pp. 98–113, 1997.

[79] Le, Q. V., "Building high-level features using large scale unsupervised learning," in *Acoustics, Speech and Signal Processing (ICASSP), 2013 IEEE International Conference on*, pp. 8595–8598, IEEE.

[80] Lehnert, T., Knaebel, H. P., Duck, M., Bulzebruck, H., and Herfarth, C., "Sequential hepatic and pulmonary resections for metastatic colorectal cancer," *British Journal of Surgery*, vol. 86, no. 2, pp. 241–243, 1999.

[81] Leitner, R., De Biasio, M., Arnold, T., Dinh, C. V., Loog, M., and Duin, R. P. W., "Multi-spectral video endoscopy system for the detection of cancerous tissue," *Pattern Recognition Letters*, vol. 34, no. 1, pp. 85–93, 2013.

[82] Li, F., Gurudu, S. R., De Petris, G., Sharma, V. K., Shiff, A. D., Heigh, R. I., Fleischer, D. E., Post, J., Erickson, P., and Leighton, J. A., "Retention of the capsule endoscope: a single-center experience of 1000 capsule endoscopy procedures," *Gastrointestinal Endoscopy*, vol. 68, no. 1, pp. 174–180, 2008.

[83] Lin, Z., Chen, Y., Zhao, X., and Wang, G., "Spectral-spatial classification of hyperspectral image using autoencoders," in *Information, Communications and Signal Processing (ICICS) 2013 9th International Conference on*, pp. 1–5, IEEE.

[84] Lindsley, E., Wachman, E. S., and Farkas, D. L., "The hyperspectral imaging endoscope: A new tool for in vivo cancer detection," *Imaging, Manipulation, and Analysis of Biomolecules, Cells, and Tissues Ii*, vol. 5322, pp. 75–82, 2004.

[85] Lowe, D. G., "Distinctive image features from scale-invariant keypoints," *International Journal of Computer Vision*, vol. 60, no. 2, pp. 91–110, 2004.

[86] Lu, D. and Weng, Q., "A survey of image classification methods and techniques for improving classification performance," *International journal of Remote sensing*, vol. 28, no. 5, pp. 823–870, 2007.

[87] Lu, G. L. and Fei, B. W., "Medical hyperspectral imaging: a review," *Journal of Biomedical Optics*, vol. 19, no. 1, 2014.

[88] M. A. Konerding, E. Fait, A. G. *British Journal of Cancer*, vol. 84, no. 1354, 2001.

[89] Machida, H., Sano, Y., Hamamoto, Y., Muto, M., Kozu, T., Tajiri, H., and Yoshida, S., "Narrow-band imaging in the diagnosis of colorectal mucosal lesions: A pilot study," *Endoscopy*, vol. 36, no. 12, pp. 1094–1098, 2004.

[90] Maji, S., Berg, A. C., and Malik, J., "Efficient classification for additive kernel svms," *Pattern Analysis and Machine Intelligence, IEEE Transactions on*, vol. 35, no. 1, pp. 66–77, 2013.

[91] Marin, D., Aquino, A., Gegundez-Arias, M. E., and Bravo, J. M., "A new supervised method for blood vessel segmentation in retinal images by using gray-level and moment invariants-based features," *Ieee Transactions on Medical Imaging*, vol. 30, no. 1, pp. 146–158, 2011.

[92] Martin, M. E., Wabuyele, M. B., Chen, K., Kasili, P., Panjehpour, M., Phan, M., Overholt, B., Cunningham, G., Wilson, D., DeNovo, R. C., and Vo-Dinh, T., "Development of an advanced hyperspectral imaging (hsi) system with applications for cancer detection," *Annals of Biomedical Engineering*, vol. 34, no. 6, pp. 1061–1068, 2006.

[93] Martin, R., Thies, B., and Gerstner, A. O. H., "Hyperspectral hybrid method classification for detecting altered mucosa of the human larynx," *International Journal of Health Geographics*, vol. 11, 2012.

[94] Masood, K., Rajpoot, N., Rajpoot, K., and Qureshi, H., "Hyperspectral colon tissue classification using morphological analysis," *Second International Conference on Emerging Technologies 2006, Proceedings*, pp. 735–741, 2006.

[95] McFee, C., "Noise sources in a ccd."

[96] McGill, S., Soetikno, R., and Kaltenbach, T., "Image-enhanced endoscopy in practice," *Canadian Journal of Gastroenterology*, vol. 23, no. 11, p. 741, 2009.

[97] Miyake, Y., Kouzu, T., Takeuchi, S., Yamataka, S., Nakaguchi, T., and Tsumura, N., "Development of new electronic endoscopes using the spectral images of an internal organ," *Thirteenth Color Imaging Conference, Final Program and Proceedings*, pp. 261–263, 2005.

[98] Miyake, Y., *Application of Spectral Imaging to Electronic Endoscopes*, pp. 485–497. Springer, 2013.

[99] Mobley, J. and Vo-Dinh, T., "Optical properties of tissue," *Biomedical photonics handbook*, vol. 2, pp. 1–2, 2003.

[100] Moser, G. and Serpico, S. B., "Combining support vector machines and markov random fields in an integrated framework for contextual image classification," *Geoscience and Remote Sensing, IEEE Transactions on*, vol. 51, no. 5, pp. 2734–2752, 2013.

[101] Nakamura, K., "Development of real-time endoscopic image processing technology: adaptive index of hemoglobin color enhancement processing," *Digestive Endoscopy*, vol. 14, pp. 40–47, 2002.

[102] Neumann, H., Neurath, M. F., and Mudter, J., "New endoscopic approaches in ibd," *World Journal of Gastroenterology*, vol. 17, no. 1, pp. 63–68, 2011.

[103] Nouvong, A., Davis, B., Hoogwerf, B., Tajaddini, A., Mohler, E., and Medenilla, E., "Evaluation of diabetic foot ulcer healing with hyperspectral imaging of oxyhemoglobin and deoxyhemoglobin," *Diabetes Care*, vol. 32, no. 11, pp. 2056–2061, 2009.

[104] Ntziachristos, V., "Going deeper than microscopy: the optical imaging frontier in biology," *Nature methods*, vol. 7, no. 8, 2010.

[105] Ohyama, N., Machida, H., Gono, K., Obi, T., Hamamoto, Y., Endo, T., Yamaguchi, M., Sano, Y., and Yoshida, S., "Appearance of enhanced tissue features in narrow-band endoscopic imaging," *Journal of Biomedical Optics*, vol. 9, no. 3, pp. 568–577, 2004.

[106] Palmer, C. A., Loewen, E. G., and Thermo, R., *Diffraction grating handbook*. Newport Corporation Springfield, OH, 2005.

[107] Pan, Z., Healey, G., Prasad, M., and Tromberg, B., "Face recognition in hyperspectral images," *Pattern Analysis and Machine Intelligence, IEEE Transactions on*, vol. 25, no. 12, pp. 1552–1560, 2003.

[108] Panasyuk, S. V., Yang, S., Faller, D. V., Ngo, D., Lew, R. A., Freeman, J. E., and Rogers, A. E., "Medical hyperspectral imaging to facilitate residual tumor identification during surgery," *Cancer Biology & Therapy*, vol. 6, no. 3, pp. 439–446, 2007.

[109] Patterson, M. S., Wilson, B. C., and Wyman, D. R., "The propagation of optical radiation in tissue i. models of radiation transport and their application," *Lasers in Medical Science*, vol. 6, no. 2, pp. 155–168, 1991.

[110] Pham, N.-A., Morrison, A., Schwock, J., Aviel-Ronen, S., Iakovlev, V., Tsao, M.-S., Ho, J., and Hedley, D. W., "Quantitative image analysis of immunohistochemical stains using a cmyk color model," *Diagnostic pathology*, vol. 2, no. 1, p. 8, 2007.

[111] Pu, Y., Achilefu, S., and Alfano, R. R., "Cancer detection/fluorescence imaging:'smart beacons' target cancer tumors,"

[112] Quantum Scientific Imaging, I., "Understanding ccd read noise."

[113] Qumseya, B. J., Wang, H. B., Badie, N., Uzomba, R. N., Parasa, S., White, D. L., Wolfsen, H., Sharma, P., and Wallace, M. B., "Advanced imaging technologies increase detection of dysplasia and neoplasia in patients with barrett's esophagus: A meta-analysis and systematic review," *Clinical Gastroenterology and Hepatology*, vol. 11, no. 12, pp. 1562–U221, 2013.

[114] Reddy, N. D., "Sparse acquisition and reconstruction for some computer vision problems," 2011.

[115] Renkoski, T. E., Hatch, K. D., and Utzinger, U., "Wide-field spectral imaging of human ovary autofluorescence and oncologic diagnosis via previously collected probe data," *Journal of Biomedical Optics*, vol. 17, no. 3, 2012.

[116] Rey, J., Kuznetsov, K., and Lambert, R., *Narrow band imaging: A wide field of possibilities*, vol. 13. 2007.

[117] Rodarmel, C. and Shan, J., "Principal component analysis for hyperspectral image classification," *Surveying and Land Information Science*, vol. 62, no. 2, pp. 115–122, 2002.

[118] Roggan, A., Drschel, K., Minet, O., Wolff, D., and Mller, G., "The optical properties of biological tissue in the near infrared wavelength range: review and measurements," in *LITT: laser-induced interstitial thermotherapy. Workshop*, pp. 10–44.

[119] Ruiz, P. D., Huntley, J. M., and Coupland, J. M., "Depth-resolved imaging and displacement measurement techniques viewed as linear filtering operations," *Experimental Mechanics*, vol. 51, no. 4, pp. 453–465, 2011.

[120] Schumann, L. W. and Lomheim, T. S., "Infrared hyperspectral imaging fourier transform and dispersive spectrometers: comparison of signal-to-noise based performance," *Imaging Spectrometry Vii*, vol. 4480, pp. 1–14, 2001.

[121] Sellar, R. G. and Boreman, G. D., "Classification of imaging spectrometers for remote sensing applications," *Optical Engineering*, vol. 44, no. 1, 2005.

[122] Shinya Kodashima, M. F., "Novel image-enhanced endoscopy with i-scan technology," *World Jour*, 2010.

[123] Siegel, R., Naishadham, D., and Jemal, A., "Cancer statistics, 2012," *Ca-a Cancer Journal for Clinicians*, vol. 62, no. 1, pp. 10–29, 2012.

[124] Skala, M. C., Hendargo, H., Fontanella, A., Dewhirst, M. W., and Izatt, J. A., "Combined hyperspectral and spectral domain optical coherence tomography microscope for non-invasive hemodynamic imaging," *Optical Tomography and Spectroscopy of Tissue Viii*, vol. 7174, 2009.

[125] Song, J., Zhang, J., Wang, J., Guo, X., Yu, S., Wang, J., Liu, Y., and Dong, W., "Meta-analysis of the effects of endoscopy with narrow band imaging in detecting dysplasia in barrett's esophagus," *Diseases of the Esophagus*, 2014.

[126] Song, L. M. W. K., Adler, D. G., Chand, B., Conway, J. D., Croffie, J. M. B., DiSario, J. A., Mishkin, D. S., Shah, R. J., Somogyi, L., Tierney, W. M., and Petersen, B. T., "Chromoendoscopy," *Gastrointestinal Endoscopy*, vol. 66, no. 4, pp. 639–649, 2007.

[127] Sotoca, J. M., Pla, F., and Klaren, A. C., "Unsupervised band selection for multispectral images using information theory," *Proceedings of the 17th International Conference on Pattern Recognition, Vol 3*, pp. 510–513, 2004.

[128] S.Prahl., "Optical absorption of hemoglobin."

[129] Stranneby, D., *Digital signal processing and applications*. Elsevier, 2004.

[130] Stubbs, C. W., Marshall, S. L., Cook, K. H., Hills, R., Noonan, J. P., Akerlof, C. W., Alcock, C. R., Axelrod, T. S., Bennett, D., and Dagley, K., "32-megapixel dual-color ccd imaging system," in *IS&T/SPIE's Symposium on Electronic Imaging: Science and Technology*, pp. 192–204, International Society for Optics and Photonics.

[131] Subramanian, V. and Ragunath, K., "Advanced endoscopic imaging: A review of commercially available technologies," *Clinical Gastroenterology And Hepatology*, vol. 12, no. 3, pp. 368–+, 2014.

[132] Sun, D.-W., *Hyperspectral imaging for food quality analysis and control*. Elsevier, 2010.

[133] Truesense Imaging, I., "Ccd image sensor noise sources."

[134] Tsuji, S., Sato, N., Kawano, S., and Kamada, T., "Functional imaging for the analysis of the mucosal blood hemoglobin distribution using electronic endoscopy," *Gastrointestinal Endoscopy*, vol. 34, no. 4, pp. 332–336, 1988.

[135] Tsumura, N., Haneishi, H., and Miyake, Y., "Estimation of spectral reflectance from multi-band images by multiple regression analysis," *Japanese Journal of Optics*, vol. 27, no. 7, pp. 384–391, 1998.

[136] Tsumura, N., Tanaka, T., Haneishi, H., and Miyake, Y., "Optimal design of mosaic color filters for the improvement of image quality in electronic endoscopes," *Optics Communications*, vol. 145, no. 27, p. 32, 1998.

[137] Tu, T. N., Chen, C. H., Wu, J. L., and Chang, C. I., "A fast two-stage classification method for high-dimensional remote sensing data," *Ieee Transactions on Geoscience and Remote Sensing*, vol. 36, no. 1, pp. 182–191, 1998.

[138] Tuchin, V. V., "Handbook of photonics for biomedical science preface," *Handbook of Photonics for Biomedical Science*, pp. Xix–Xxiii, 2010.

[139] Tuchin, V. V. and Tuchin, V., *Tissue optics: light scattering methods and instruments for medical diagnosis*, vol. 642. SPIE press Bellingham, 2007.

[140] Uhr, J. W., Huebschman, M. L., Frenkel, E. P., Lane, N. L., Ashfaq, R., Liu, H., Rana, D. R., Cheng, L., Lin, A. T., Hughes, G. A., Zhang, X. J., and Garner, H. R., "Molecular profiling of individual tumor cells by hyperspectral microscopic imaging," *Translational Research*, 2012.

[141] Unfried, G., Wieser, F., Albrecht, A., Kaider, A., and Nagele, F., "Flexible versus rigid endoscopes for outpatient hysteroscopy: a prospective randomized clinical trial," *Human Reproduction*, vol. 16, no. 1, pp. 168–171, 2001.

[142] Usenik, P., Brmena, M., Fidlerb, A., Pernua, F., and Likara, B., "Evaluation of cross-polarized near infrared hyperspectral imaging for early detection of dental caries," *Proceedings of SPIE*, 2012.

[143] Valiente, F. B. . M. L.-M. . S. S. . G. B. . J. H. . M., "Hyperspectral imaging based method for fast characterization of kidney stone types," *Journal of Biomedical Optics*, 2012.

[144] van Velden, F. H., van Beers, P., Nuyts, J., Velasquez, L. M., Hayes, W., Lammertsma, A. A., Boellaard, R., and Loeckx, D., "Effects of rigid and non-rigid image registration on test-retest variability of quantitative [18f] fdg pet/ct studies," *EJNMMI research*, vol. 2, no. 1, pp. 1–13, 2012.

[145] Vlachos, M. and Dermatas, E., "Multi-scale retinal vessel segmentation using line tracking," *Computerized Medical Imaging and Graphics*, vol. 34, no. 3, pp. 213–227, 2010.

[146] Vo-Dinh, T., "A hyperspectral imaging system for in vivo optical diagnostics," *Engineering in Medicine and Biology Magazine, IEEE*, vol. 23, no. 5, pp. 40–49, 2004.

[147] Wang, L. V. and Wu, H.-i., *Biomedical optics: principles and imaging*. John Wiley & Sons, 2012.

[148] Welch, A. J., van Gemert, M. J. C., and Star, W. M., "Definitions and overview of tissue optics," *Optical Thermal Response of Laser-Irradiated Tissue, Second Edition*, pp. 27–64, 2011.

[149] Wolfe, W. L., *Introduction to imaging spectrometers*, vol. 25. SPIE Press, 1997.

[150] Woodcock, C. E. and Gopal, S., "Fuzzy set theory and thematic maps: accuracy assessment and area estimation," *International Journal of Geographical Information Science*, vol. 14, no. 2, pp. 153–172, 2000.

[151] YANG, G.-w., ZHENG, Z.-r., CHEN, X.-x., LI, H.-f., and LIU, X., "Study of multiple-stage lyot liquid crystal tunable filter [j]," *Journal of Zhejiang University (Engineering Science)*, vol. 6, p. 035, 2009.

[152] Yasser Fawzy, Stephen Lam, H. Z., "Rapid multispectral endoscopic imaging system for near real-time mapping of the mucosa blood supply in the lung," *Biomedical Optics Express*, vol. 6, 7 2015.

[153] Yelin, D., White, W. M., Motz, J. T., Yun, S. H., Bouma, B. E., and Tearney, G. J., "Spectral-domain spectrally-encoded endoscopy," *Optics Express*, vol. 15, no. 5, pp. 2432–2444, 2007.

[154] Yoshida, N., Naito, Y., Kugai, M., Inoue, K., Uchiyama, K., Takagi, T., Ishikawa, T., Handa, O., Konishi, H., Wakabayashi, N., Kokura, S., Yagi, N., Morimoto, Y., Yanagisawa, A., and Yoshikawa, T., "Efficacy of magnifying endoscopy with flexible spectral imaging color enhancement in the diagnosis of colorectal tumors," *Journal of Gastroenterology*, vol. 46, no. 1, pp. 65–72, 2011.

[155] Zeiler, M. D. and Fergus, R., "Visualizing and understanding convolutional neural networks," *arXiv preprint arXiv:1311.2901*, 2013.

[156] Zhang, X. H. and Chen, C. H., "New independent component analysis method using higher order statistics with application to remote sensing images," *Optical Engineering*, vol. 41, no. 7, pp. 1717–1728, 2002.

[157] Zhang, Y., Chen, Y. J., Yu, Y., Xue, X. B., Tuchin, V. V., and Zhu, D., "Visible and near-infrared spectroscopy for distinguishing malignant tumor tissue from benign tumor and normal breast tissues in vitro," *Journal of Biomedical Optics*, vol. 18, no. 7, 2013.

[158] Zhi Liu, Hongjun Wang, Q. L., "Tongue tumor detection in medical hyperspectral images," *Sensors*, 2011.

[159] Zitova, B. and Flusser, J., "Image registration methods: a survey," *Image and Vision Computing*, vol. 21, no. 11, pp. 977–1000, 2003.

[160] Zuzak, K. J., Naik, S. C., Alexandrakis, G., Hawkins, D., Behbehani, K., and Livingston, E., "Intraoperative bile duct visualization using near-infrared hyperspectral video imaging," *American Journal of Surgery*, vol. 195, no. 4, pp. 491–497, 2008.

[161] Zuzak, K. J., Naik, S. C., Alexandrakis, G., Hawkins, D., Behbehani, K., and Livingston, E. H., "Characterization of a near-infrared laparoscopic

hyperspectral imaging system for minimally invasive surgery," *Analytical Chemistry*, vol. 79, no. 12, pp. 4709–4715, 2007.

VITA

Zhimin Han was born in Shandong Province, China, and received his early education till high school there. From 2006 to 2010, he joined Yuanpei Programme (Yuanpei College now) of Peking University, and majored in Electronic Engineering. After awarded Bachelor degree at 2010, he enrolled in PKU-GT-Emory joint PhD program, and majored in Biomedical Engineering. During 2014, he studied at Atlanta for one year.

Zhimin Han aspires to contribute to development and application of medical device. His research focuses on endoscope system development, biomedical optics, and biomedical image analysis.

Outside the lab, he prefers to spend his time in playing basketball and Mixed Martial Arts, reading history, and learning traditional culture and antiquities.